



Departament de Química, Facultat de Ciències  
Doctorat en Programa de Ciència de Materials  
Universitat Autònoma de Barcelona

Muling Zeng

**Bacterial cellulose: fabrication,  
characterization and biocompatibility studies**

Doctoral Thesis 2014

Supervised by Dr. Anna Roig Serra and Dr. Anna Laromaine Sagué

Tutor: Dr. Adelina Vallribera Massó

at “Institut de Ciència de Materials de Barcelona”



---

---

**Dra. Anna Roig Serra** (Investigadora Científica del CSIC), la **Dra. Anna Laromaine Sagué** Investigadora contractada Ramon y Cajal i **Dra. Adelina Vallribera Massó**, Titular d'universitat numerari, UAB

CERTIFIQUEN:

Que l'Muling Zeng, amb un Màster en Química per la "Universitat de Yunnan", Xina ha dut a terme aquesta tesis doctoral sota la seva direcció i que porta per títol "**Bacterial cellulose: fabrication, characterization and biocompatibility studies**", la qual queda recollida en aquesta memòria per optar al grau de Doctor en Química.

I perquè així consti, signen el present certificat

Dr. Anna Roig Serra Dr. Anna Laromaine Sagué Dr. Adelina Vallribera Massó

Muling Zeng

Bellaterra, 4 de Julio 2014

---

---

For beautiful eyes, look for the good in others; for beautiful lips, speak  
only words of kindness; and for poise, walk with the knowledge that you

are never alone.

**Audrey Hepburn**

---

---

## Acknowledgements

Thanks to my country and the grant from the China Scholarship Council (CSC) I had the opportunity to pursue the Ph.D. studies, and also experience a wonderful life in Barcelona. There are a number of people without whom this thesis might not have been written, and to whom I am greatly indebted.

First and foremost, I would like to express the deepest appreciation to my supervisors, Dr. Anna Roig and Dr. Anna Laromaine. Without their guidance and persistent help this thesis would not have been possible. Anna Roig, thanks for your support and trust all the time and your elegant personality, which give me great pleasure during these three years. Anna Laromaine, thanks for your guidance and for being always available for discussions. It has been an honour to be your first Ph.D. student.

I am also grateful to Dr. Alex Perálvarez and Pablo Doñate Macian, for their help and teaching in bacterial cellulose production. It was a great pleasure to learn from you.

In addition, I would like to thank “El servei de Llengües de la UAB” for the grant to support the writing of this thesis in English. My huge appreciation to Mrs. Helen McNally who was my assigned tutor.

Thanks to the members of our group, nanoparticles and nanocomposites: Elisa, Nerea, Martí, Elena, Oana, Maria, Laura, Ilargi, Siming, Pengfei and Wojtek: thanks for your company and your suggestions on my work. There are many good memories with you all, the parties inside and outside ICMAB, the dinners at different restaurants, the travels with the girls, the delicious homemade cakes...

My friends: Rafael, Paula, Ivy, Magda, Helan, Yang, Loxu, Lajia, Ping, Shuang, Dayuan, Eudald, Gina and Alex, thank you for your friendship. I am so happy for having you around.

Lastly, I would like to thank my family for all their love and encouragement. Dear Mom and Dad, thank you so much for understanding and supporting me in all my pursuits. And most of all for my loving, supportive and patient boyfriend Chengzhi for his staunch love, even geographically distant. Especially, I would like to dedicate this thesis to my dear brother: Chengde. You were brave, honest and always very kind to me. I do believe you have found the happiness and peace in heaven.

---



---

## Foreword and Scope of the thesis

My curiosity in material science was born from a “magic necktie” (nano self-cleaning necktie), which was presented in a course of nanotechnology during my Bachelor. It seemed amazing to me how powerfully science have changed our life, it somehow guided me in pursuing science.

In March 2011, I started the application of a scholarship from CSC (Chinese Scholarship Council), which cooperated with the Universitat Autònoma de Barcelona (UAB). After about half year, I secured the scholarship and began my doctoral thesis under the supervision of Dr. Anna Roca and Dr. Anna Laromaine. My project assignment was on bacterial cellulose: fabrication, characterization and biocompatibility studies. To start and expand a completely new project in our group was not easy; I had to spend quite an amount of time learning bio-chemistry and designing the initial experiments. Bacterial cellulose is a renewable polysaccharide, which is produced by some types of bacteria in nature. It presents remarkable chemical and physical properties, including high chemical purity and crystallinity, nano-scale fibre network, porosity, high water absorption capacity and mechanical strength. Bacterial cellulose is being used for a wide variety of commercial applications, for example textiles, cosmetics, food products and other technical areas. Furthermore, bacterial cellulose is also biocompatible with excellent biological affinity and biodegradability, which is drawing immense attention from the bio and medical area researchers.

The objective of my thesis was to learn how to produce bacterial cellulose films and find strategies to control their properties. A second objective was to develop methods to fabricate nanocomposites based on bacterial cellulose. The final objective was related to prove the biocompatibility of the in-house produced bacterial cellulose films and to be able to use them as three-dimensional scaffolds for cell in-growth. In this way setting up a platform that will allow us to study the interaction of cells and nanoparticles in a realistic 3D environment.

During the first year, a lab set-up was successfully built to produce bacterial cellulose from two bacterial strains and three methods of drying were accessed to dry the thin films; at room temperature, freeze drying and supercritical drying. Moreover, the full characterization of bacterial cellulose films was accomplished: their porosity, transparency, water absorption capacity and mechanical properties were tuned by selecting the bacterial strain and the drying method. In the second year, bacterial cellulose composited with nanoparticles as novel functional cellulose materials were synthesized by microwave-assisted method. This method is efficient and fast to form a homogenous conformal and controllable coating of nanoparticles on the bacterial cellulose films. By drying the cellulose films using different routes, the final amount of the nanoparticles content in the composites can be controlled. Furthermore, those films were patterned with hydrophobic/hydrophilic domains and selectively anchored

---

nanoparticles to create more complex and functional cellulose composites. During the last year, an investigation of the biocompatibility of the bacterial cellulose films *in vitro* was performed. Although bacterial cellulose is generally considered non-cytotoxic material, its biocompatibility as a major requirement for the use in biological and medical applications has not been fully evaluated. Furthermore, an improved 3D bacterial cellulose scaffold was fabricated.

The thesis is organized into six chapters.

**Chapter 1** provides an introduction to bacterial cellulose: bacteria types and pathway for producing cellulose, growth medium, polymorph structures information, and also the comparison with plant cellulose. The synthesis methods and applications of bacterial cellulose composites are included, especially, applications on the bacterial cellulose composites with nanoparticles.

**Chapter 2** describes a detailed description of the fabrication of bacterial cellulose films (BCFs) from two bacteria strains, and the methodology used to obtain clean, pure and uniform BCFs. Aiming to get different and controllable properties of BCFs, three different drying methods were used: room temperature, freeze and supercritical drying. Furthermore, the evaluation of their chemical structure, purity, crystallinity, microstructure, water absorption capacity, transparency and mechanical properties are included.

**Chapter 3** focuses on the synthesis of functional bacterial cellulose composites incorporating nanoparticles. Firstly, superparamagnetic Fe<sub>2</sub>O<sub>3</sub> and Au nanoparticles were successfully synthesized by one-step microwave-assisted thermal decomposition method. Later, the same microwave method was used to prepare functional BCF-NPs composites without the need for any post-synthesis treatment. Experimental details, structural, morphological, mechanism and functional characterizations are discussed. Furthermore, the preliminary results in a strategy to selectively pattern the bacterial cellulose films with iron oxide nanoparticles are also presented.

**Chapter 4** presents the studies of bacterial cellulose biocompatibility as 2D and 3D scaffold for cell studies *in vitro*. It starts with an evaluation of the stability and the behaviour of bacterial cellulose incubated in biological medium and cell culture medium. The biocompatibility investigation of bacterial cellulose with two cell lines is discussed. In order to provide 3D growth environment for cells, we improved the production of bacterial cellulose films and developed a new method to enlarge the pore size. Optical and confocal microscopes were used to visualize and characterize cell distributions.

**Chapter 5** lists the main conclusions derived from the present thesis and some suggestions for the future work.

**Chapter 6** gathers information about the author and the publications during the Ph.D. studies.

---

## Prólogo y alcance de la tesis

Mi curiosidad por la ciencia de materiales nació de una "corbata mágica" (una corbata que se autolimpiaba), que fue presentada en un curso de nanotecnología durante mi licenciatura. Me parecía increíble la fuerza con que la ciencia cambiaba nuestra vida, de alguna manera me inició en la ciencia de materiales.

En marzo de 2011, apliqué a una beca del CSC (Consejo de Becas de China), en cooperación con la Universitat Autònoma de Barcelona (UAB). Después de medio año, conseguí la beca y comencé mi tesis doctoral bajo la supervisión de la Dra. Anna Roig y la Dra. Anna Laroaine. Mi proyecto asignada era en celulosa bacteriana: su síntesis, caracterización y estudios de biocompatibilidad. Iniciar el proyecto no fue fácil, era un proyecto completamente nuevo en nuestro grupo. Estuve mucho tiempo aprendiendo la bioquímica de la celulosa y en el diseño de mis experimentos iniciales. La celulosa bacteriana es un polisacárido de fuente renovables, y puede ser producida por algunos tipos de bacterias en la naturaleza. Presenta propiedades químicas y físicas notables, incluyendo una alta pureza química y cristalinidad, una red de nanofibras, porosa, alta capacidad de absorción de agua y resistencia mecánica. La celulosa bacteriana se utiliza para una amplia variedad de aplicaciones comerciales, por ejemplo textiles, cosmética, productos alimenticios y otras áreas técnicas. Por otra parte, la celulosa bacteriana es biocompatible con afinidad biológica y biodegradabilidad, que suscita una gran atención de investigadores en la área de la biomedicina.

El primer objetivo de mi tesis fue aprender a producir películas de celulosa bacteriana y encontrar estrategias para controlar sus propiedades. Un segundo objetivo fue el desarrollo de métodos para la fabricación de nanocompuestos basados con celulosa bacteriana. El objetivo final estudia la biocompatibilidad de las capas de celulosa bacteriana que hemos producido y su utilidad como soportes tridimensionales para el crecimiento celular. Así se pretende establecer una plataforma para el estudio de la interacción de células y nanopartículas en un entorno 3D más realista.

Durante el primer año, se realizó la puesta a punto en el laboratorio del sistema para producir capas de celulosa bacteriana a partir de dos cepas bacterianas y secarlas a partir de tres métodos de secado: a temperatura ambiente, secado por liofilización y secado supercrítico. Por otra parte, se realizó la caracterización completa de las capas de celulosa bacteriana: su porosidad, la transparencia, la capacidad de absorción de agua y las propiedades mecánicas que se podían controlar seleccionando la cepa bacteriana y el método de secado. En el segundo año, se sintetizó la celulosa bacteriana compuesta con nanopartículas por el método asistida por microondas como materiales de celulosa funcionales novedosos. Este método es eficiente y rápido, forma un recubrimiento de las capas de celulosa bacteriana por nanopartículas de forma homogénea y controlable. Secando las capas de celulosa utilizando diferentes rutas, se puede

---

controlar la cantidad final del contenido de las nanopartículas en los materiales compuestos. Así capas con dominios hidrófobos / hidrófilos favorecían el anclaje de nanopartículas de forma selectiva para crear materiales de celulosa más complejos y funcionales. En este último año, se ha llevado a cabo el estudio de la biocompatibilidad de las capas de celulosa bacteriana *in vitro*. Aunque la celulosa bacteriana se considera generalmente un material no citotóxico, su biocompatibilidad es un requisito importante para su uso en aplicaciones biológicas y médicas y no ha sido evaluado completamente. Además se fabricó una estructura de celulosa bacteriana 3D mejorada.

La tesis se estructura en seis capítulos:

**Capítulo 1** proporciona una introducción a la celulosa bacteriana: tipos de bacterias y vía para la producción de celulosa, medio de cultivo, información de sus estructuras polimorfas, así como la comparación con la celulosa de origen vegetal. Se incluyen los métodos de síntesis y aplicaciones de materiales compuestos de celulosa bacteriana, especialmente, las aplicaciones de los materiales compuestos de celulosa bacteriana con nanopartículas.

**Capítulo 2** ofrece una descripción detallada de la fabricación de capas de celulosa bacteriana (BCF) de las dos cepas bacterianas, y la metodología utilizada para obtener los BCF limpios, puros y uniformes. Con el objetivo de obtener propiedades diferentes y controlables de BCF, se utilizaron tres diferentes métodos de secado: temperatura ambiente, la liofilización y el secado supercrítico. Se incluye la evaluación de su estructura química, la pureza, la cristalinidad, la microestructura, la capacidad de absorción de agua, la transparencia y sus propiedades mecánicas.

**Capítulo 3** se centra en la síntesis de compuestos de celulosa bacteriana funcionales que incorporan nanopartículas. En primer lugar, las nanopartículas superparamagnéticas  $Fe_2O_3$  y Au se sintetizaron con éxito por el método de descomposición térmica asistida por microondas en un solo paso. Posteriormente, se utilizó este método de microondas para preparar materiales compuestos BCF-NPs funcionales sin la necesidad de ningún tratamiento posterior a la síntesis. Se discuten los detalles experimentales, estructurales, morfológicos, los mecanismos y la caracterización funcional. Además, se presentan resultados preliminares para obtener capas de celulosa bacteriana con nanopartículas de óxido de hierro selectivamente localizadas.

**Capítulo 4** presenta estudios de biocompatibilidad de la celulosa bacteriana como estructura 2D y 3D para estudios celulares *in vitro*. Se inicia con una evaluación de la estabilidad y el comportamiento de la celulosa bacteriana incubada en medio biológico y en medio de cultivo celular. Se discute la biocompatibilidad de celulosa bacteriana con dos líneas celulares. Con el fin de proporcionar un entorno de crecimiento 3D de células, hemos mejorado la producción de capas de celulosa bacteriana y desarrollado un nuevo método

---

para aumentar el tamaño de poro de las estructuras. Se utiliza la microscopia óptica y confocal para visualizar y caracterizar las distribuciones de células en las estructuras.

**Capítulo 5** se enumeran las principales conclusiones derivadas de la presente tesis y algunas sugerencias para el trabajo futuro.

**Capítulo 6** recoge información sobre el autor y las publicaciones durante el doctorado.

---

---

## Attributions

I would like to thank you the people who contributed to this thesis.

- **Alex Perálvarez** and **Pablo Doñate Macian** (Departament de Bioquímica i Biologia Molecular, UAB) Dr. Alex guided me to the biological field. He tutored me in the bacterial culture and offered the use of the facilities in the lab. Pablo helped me whenever I had any problems with the bacterial culture experiment.
- **Maria Milla** (Group member, ICMAB-CSIC) who did *in vitro* cell culture experiment and biological assays investigating the bacterial cellulose biocompatibility with different cell lines. She taught me the basics for the manipulation of cell cultures and cytotoxicity assay. She also helped me with the writing of the Chapter 4.
- **Ilargi Napal** (Group member, ICMAB-CSIC) who contributed in the studies of bacterial cellulose degradability.
- **Raul Solanas** (MATGAS-Barcelona) who helped me in supercritical fluids technology for drying bacterial cellulose films.
- **Prof. Elies Molins** and **Toni Pons** (ICMAB-CSIC) for the use and advices in the use of the freeze drier.
- **Technical staff of the Nanoquim Platform at ICMAB-CSIC:** Neus Romà, Enrique Irisarri and Edgar León who helped me in microwave-assisted synthesis of nanoparticles and contact angle measurement of bacterial cellulose films.
- **Judit Oró** (ICMAB-CSIC) who performed TEM analysis of iron oxide and gold nanoparticles.
- **Anna Esther Carrillo** (ICMAB-CSIC) who taught me how to use the SEM equipment.
- **Bernat Bozzo** (ICMAB-CSIC) who performed the magnetic measurements for the characterization of iron oxide nanoparticles and magnetic bacterial cellulose films.
- **Roberta Ceravola** (ICMAB-CSIC) who performed the thermal gravimetric analysis of bacterial cellulose films and bacterial cellulose nanocomposites.
- **Anna Crespi** and **Joan B. Esquiú** (ICMAB-CSIC) who performed the X-ray Diffraction of bacterial cellulose films.
- **Oriol Osso** and **Abel Roige** (MATGAS-Barcelona) who helped me in mechanical properties investigation of bacterial cellulose films by performing Nanoindentation.
- **Josep Puigmartí** and **David Amabilino group** (ICMAB-CSIC) who allow us the use of their optical microscope.
- **Victor Puntès Group, Eudald Casals Mercadal** (ICN2-CSIC), to let us use their facilities and being available at any time.

- 
- **People of Servei de Cultius Cel·lulars, Producció d'Anticossos i Citometria** (SCAC-UAB) who offered their help in the cell culture facility.
  - **Núria Barba** (Servei de Microscòpia, UAB) who performed confocal microscopy images of bacterial cellulose with cells.



---

## List of Abbreviations

3D	Three dimensions
2D	Two dimensions
Au	Gold
BC	Bacterial cellulose
BC-NPs	Bacterial cellulose coated with nanoparticles
BCE	Bacterial cellulose from GE strain
BCX	Bacterial cellulose from GX strain
BCFs	Bacterial Cellulose Films
BCF-NPs	Bacterial cellulose films coated with nanoparticles
CSC	China Scholarship Council
CSIC	Consejo Superior de Investigación Científica
DI water	Deionized water
E	Young Modulus
Fe(acac) <sub>3</sub>	Iron acetylacetonate
γ-Fe <sub>2</sub> O <sub>3</sub>	Hematite
Fe <sub>2</sub> O <sub>3</sub>	Iron oxide
FBS	Fetal bovine serum
FD	Freeze drying
H	Hardness
ICMAB	Institut de Ciència de Materials de Barcelona
GX	Gluconacetobacter Xylinum
GE	Gluconacetobacter Europaeus
MTT assay	3-(4,5-dimethylthiazol-2-yl)- 2,5-diphenyltetrazolium bromide viability assay
MW	Microwave-assisted
NaOH	Sodium hydroxide
NPs	Nanoparticles
PDMS	Polydimethylsiloxane
PBS	Phosphate buffered saline
PFA	Paraformaldehyde
PI	Propidium iodide
RD	Room temperature drying
SCD	Supercritical drying
SCF	Supercritical fluid
SPIONs	Superparamagnetic iron oxide nanoparticles
TMAOH	Tetramethylammonium hydroxide
UAB	Universitat Autònoma de Barcelona

---

---

## Table of contents

- Acknowledgements
- Foreword and scope of the thesis
- Attributions
- List of Abbreviations
- Index

## Chapter 1 Introduction

<b>Chapter summary .....</b>	<b>3</b>
<b>1.1 Bacterial cellulose .....</b>	<b>4</b>
Brief introduction to polysaccharides.....	4
Bacterial cellulose and plant cellulose.....	4
Bacteria types for producing bacterial cellulose.....	7
<i>Gluconacetobacter Xylinum</i> and <i>Gluconacetobacter Europaeus</i> .....	7
Production methods of bacterial cellulose.....	8
Growth medium of bacteria.....	10
Pathway of bacterial cellulose production.....	11
Polymorphs of bacterial cellulose.....	12
Development and increasing publications of bacterial cellulose .....	13
<b>1.2 Bacterial cellulose-based composites.....</b>	<b>14</b>
Synthesis methods of bacterial cellulose-based composites.....	14
Classes of bacterial cellulose-based composites.....	15
<b>1.3 Bacterial cellulose composites with nanoparticles and their applications ....</b>	<b>16</b>
<b>1.4 References.....</b>	<b>19</b>

## Chapter 2 Bacterial cellulose: fabrication and characterization

<b>Chapter summary .....</b>	<b>27</b>
<b>2.1 Production of bacterial cellulose films.....</b>	<b>28</b>
Experimental set-up and methodology .....	28
<b>2.2 Cleaning process.....</b>	<b>32</b>
<b>2.3 Drying process .....</b>	<b>33</b>
Drying methodology.....	33
Three different drying methods .....	34
<b>2.4 Characterization of bacterial cellulose films.....</b>	<b>38</b>

---

Chemical structure and purity .....	38
Crystallinity .....	39
Microstructure .....	42
Water absorption capacity .....	44
Optical properties .....	46
Thermo-gravimetric Analysis.....	48
Mechanical properties .....	50
<b>2.5 Conclusions .....</b>	<b>54</b>
<b>2.6 References .....</b>	<b>55</b>

### **Chapter 3 Functional bacterial cellulose incorporating nanoparticles**

<b>Chapter summary .....</b>	<b>61</b>
<b>3.1 Synthesis of nanoparticles by microwave-assisted method.....</b>	<b>62</b>
Synthesis of Fe <sub>2</sub> O <sub>3</sub> nanoparticles .....	62
Synthesis of Au nanoparticles.....	65
<b>3.2 Synthesis of BCF-NPs composites by microwave-assisted method .....</b>	<b>66</b>
Synthesis of BCF-SPIONs composites .....	66
Characterization .....	69
Microstructure .....	70
Nanoparticles load.....	73
Magnetic properties.....	74
Stability of the nanoparticles.....	76
Mechanical properties .....	76
Water capacity ability.....	79
Conformal coating.....	80
Proposed mechanism.....	80
Synthesis of BCF-Au composites .....	81
<b>3.3 Synthesis of functional and complex BCF-NPs composites .....</b>	<b>83</b>
Synthesis of patterned BCF-SPIONs composites .....	83
Synthesis of BCF-Au-SPIONs composites.....	87
<b>3.4 Conclusions .....</b>	<b>90</b>
<b>3.5 References .....</b>	<b>91</b>

---

## **Chapter 4 Biocompatibility of bacterial cellulose films**

<b>Chapter summary .....</b>	<b>97</b>
<b>4.1 Biocompatibility of bacterial cellulose films .....</b>	<b>98</b>
Bacterial cellulose films in biological medium and cell culture medium.....	98
Bacterial cellulose films with cells.....	101
<b>4.2 3D bacterial cellulose scaffold.....</b>	<b>107</b>
Production of 3D bacterial cellulose scaffold.....	107
3D bacterial cellulose scaffold with cells.....	110
<b>4.3 Conclusions.....</b>	<b>113</b>
<b>4.4 References.....</b>	<b>114</b>

## **Chapter 5 Conclusions and future work**

5.1 General conclusions .....	118
5.2 Prospective for future work.....	121

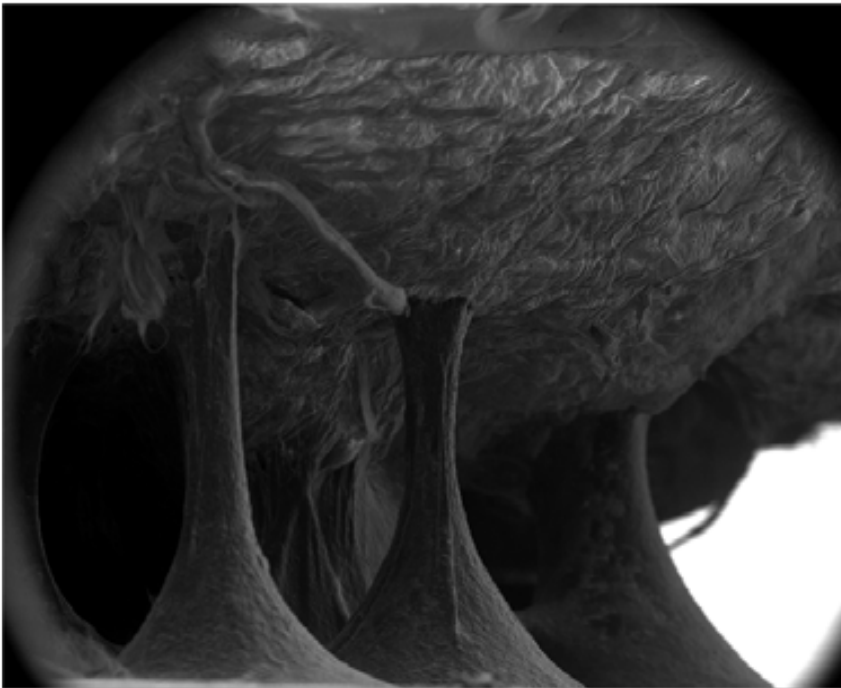
## **Chapter 6 Conclusions and future work**

6.1 Curriculum vitae of the author .....	124
6.2 List of publications.....	127

---

# Chapter 1

## Introduction



---

## Chapter Index

Chapter summary .....	3
1.1 Bacterial cellulose .....	4
Brief introduction to polysaccharides .....	4
Bacterial cellulose and plant cellulose .....	4
Bacteria types for producing bacterial cellulose .....	7
<i>Gluconacetobacter Xylinum</i> and <i>Gluconacetobacter Europaeus</i> .....	7
Production methods of bacterial cellulose .....	8
Growth medium of bacteria .....	10
Pathway of bacterial cellulose production .....	11
Polymorphs of bacterial cellulose .....	12
Development and increasing publications of bacterial cellulose .....	13
1.2 Bacterial cellulose-based composites .....	14
Synthesis methods of bacterial cellulose-based composites .....	14
Classes of bacterial cellulose-based composites .....	15
1.3 Bacterial cellulose composites with nanoparticles and their applications .....	16
1.4 References .....	19



---

## **Chapter summary**

Bacterial cellulose (BC) is a fascinating, abundant and renewable polysaccharide that has been reported in a large number of studies in the past few decades, due to its remarkable properties such as high chemical purity, large porosity with ultrafine 3D porous network, good mechanical properties, moldability, biocompatibility, biodegradability and biological affinity.

In this introductory chapter, firstly I will give a brief explanation of polysaccharides including the definition, the general formula and structures. Then I will present comprehensive information of BC, from the origin and discovery of BC to the details of bacteria types, polymorph structures information, growth medium and the methods of producing cellulose. Until now, three known methods have been widely used to produce BC suitable for industrial applications: submerged culture, rotating disk reactor and static culture. The comparison between BC and plant cellulose - main source of cellulose will also be included.

Furthermore, I will show the increasing number of publications of BC and BC-based composites. Depending on different desired applications, BC-based composite materials ranging from polymers to nanoparticles (NPs) can be synthesized and classified by two main approaches, which are chemical modification and particles deposition. Specially, BC composites with NPs (BC-NPs) have received increased interest. Here, some examples of these BC-NPs composites, their synthetic approaches and potential applications will be described.

---

## 1.1 Bacterial cellulose

### Brief introduction to polysaccharides

Polysaccharides are the most common natural polymers on earth, including starch, glycogen, pectin, cellulose and chitin. They are polymeric carbohydrate molecules consisting of long chains of repeating monosaccharide units with the general formula  $(C_6H_{10}O_5)_n$ , which is based on glucose bound together by glycosidic bonds. They range in structure from linear to highly branched, as shown in **Figure 1.1**. For instance, some polysaccharides such as cellulose are linear chains; others such as glycogen are branched. Natural polysaccharides offer a very promising future due to their biodegradability and compatibility with living tissues. Moreover, they are renewable and almost inexhaustible. Normally, they are classified as two main functional polysaccharides, including storage polysaccharides (e.g. starch and glycogen) and structural polysaccharides (e.g. chitin and cellulose). Cellulose is one of the best known and most widespread polysaccharide in nature, which can be produced in the biosphere with an annual production estimated to be over  $1.0 \times 10^{12}$  tons. (1, 2)

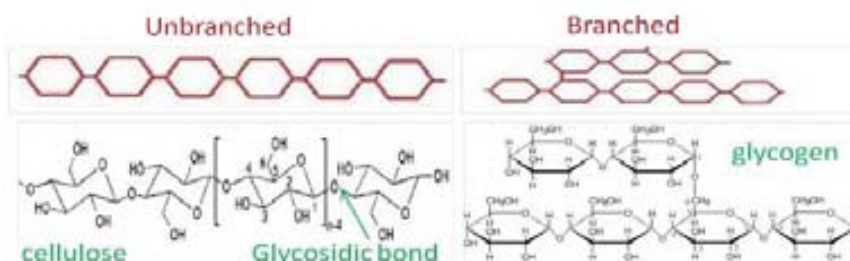


**Figure 1.1** Polysaccharides can be branched or unbranched but they have the same mono-saccharide unit as building block, which is bound together by glycosidic bonds. Cellulose is one example of linear chains; while glycogen is a branched polysaccharide.

### Bacterial cellulose and plant cellulose

Around 1838, the French chemist Anselme Payen discovered and named cellulose, which was isolated from various plant tissues. **Figure 1.2** shows the typical structure of cellulose from plants, which can be obtained from wood, cotton and other plant fibres. In plants, cellulose is found in a composite form composed of polymers of lignin, carbohydrates like hemicelluloses and cellulose, which are physically and chemically bound together.

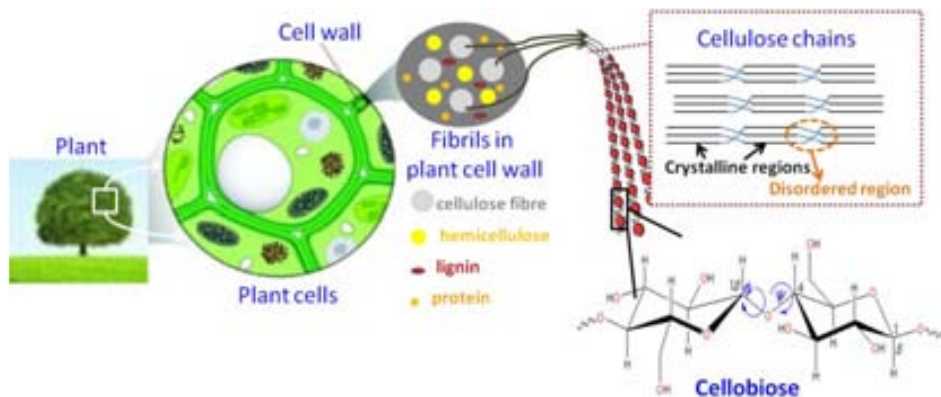


**Figure 1.2** The arrangement of cellulose and other polysaccharides in a plant cell wall. Cellulose fibrils come from the plant cell wall, which are combined with hemicelluloses, lignin and protein. Idealized cellulose fibril (cellulose chain) show one of the suggested configurations of the crystalline and amorphous regions. Every second AGU ring is rotated  $180^\circ$  in the cellulose chains.

In **Figure 1.1**, the structure of cellulose as a carbohydrate polymer is presented, it is generated from repeating  $\beta$ -D-glucopyranose molecules that are covalently linked between the equatorial OH group C4 and C1 carbon atom named  $\beta$ -1,4 glycosidic bonds. As a result, cellulose is an extensive, linear-chain polymer. Cellulose has three hydroxyl groups per anhydroglucose (AGU) unit. Every second AGU ring is rotated  $180^\circ$  in the plane. In this manner, two adjacent structural units define the disaccharide cellobiose, which is shown in **Figure 1.2**. The chain length of cellulose expressed in the number of constituent AGUs (degree of polymerization, DP) varies with the origin and treatment of the raw materials. In case of wood pulp, the values are typically 300 – 1700. Cotton and other plant fibres have DP values in the 800 – 10000 range depending on the treatment.

The main dominant pathway to obtain cellulose is from plants, although cellulose can be also synthesized by bacteria, algae and fungi.(3) The discovery of bacterial cellulose (BC) was first published by A.J. Brown in 1886. The paper described a synthesis of an extracellular gelatinous mat at the surface of an acetic fermentation.(4-6) Amongst the cellulose-forming bacteria, *Acetobacter* strains (also called *Gluconacetobacter*) are especially suitable for the production and investigation of cellulose. These are gram-negative and strictly aerobic bacteria with ellipsoidal, straight, or slightly bent rods shape.(2) *Gluconacetobacter xylinum* (GX) species produce extracellular cellulose that is easily isolated as fibre material. Under static immersed cultivation conditions, a bio-film of varying thickness is produced which helps the bacteria to maintain a high oxygen content near the surface, and protects them as a barrier against drying, natural enemies, and radiation. During the synthetic process, the glucose chains are produced inside the bacterial body and then extruded out through tiny pores present on the cell envelope of bacteria. The glucose chains then combine, to form nano-sized fibres that further aggregate to ribbons (less

than 100 nm wide) (**Figure 1.3**). These ribbons or micro-fibres subsequently generate a web shaped network structure with plenty of empty spaces between the fibres. The well separated nano-fibres of BC create an expanded surface area and highly porous matrix. The formation of cellulose by laboratory bacterial cultures is an interesting and attractive access to pure cellulose. By selecting the substrates, cultivation conditions, various additives, and finally the bacteria strains, it is possible to control the thickness, the shape and the microstructure, thus to control important structural properties, which are studied in Chapter 2.

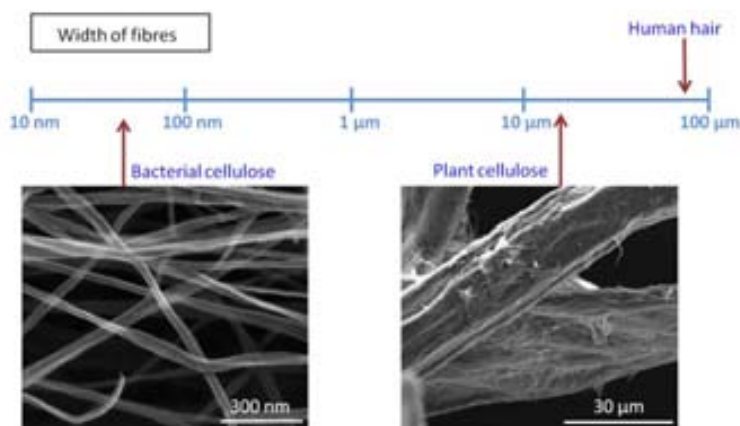


**Figure 1.3** Width scale for BC fibres, plant cellulose fibres and human hair. BC fibres are less than 100 nm that is much smaller than plant cellulose. SEM images of BC fibres of my sample and plant cellulose fibres of a chromatography paper.

Plant cellulose was isolated over 170 years ago, the study of this natural polymer still remains of interest to scientists because it is renewable, cheap, light-weight and biodegradable. Plant cellulose has versatile uses in many industries such as the pulp and paper industry, cosmetic, food and textile industries, as well as pharmaceutical applications. For instance, they can be used as excipient, bio-adhesives, extended and controlled release matrices and many other applications.(7)

However, in the plant cellulose coexist lignin and other polysaccharides (e.g. hemicelluloses), as shown in **Figure 1.2**. To get pure cellulose from plants is not easy; it has to be isolated by physical and chemical separation and some purification processes. Meanwhile, the purity of cellulose becomes increasingly important in biological-medical applications.

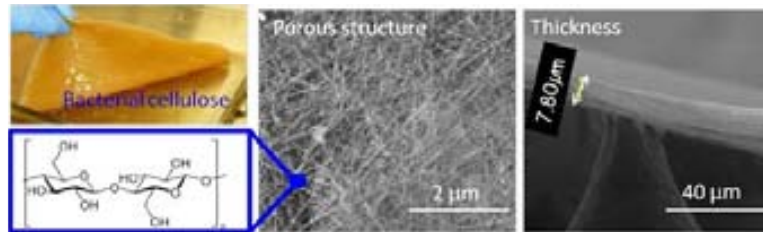


**Figure 1.4** Picture of one piece of wet BC pellicle. SEM images of one sample from my thesis of pure BC: 3-D porous structure.

In contrast to plant cellulose, BC is a pure biopolymer with a high degree of polymerization (DP values of 2000-8000). It is an outstanding biomaterial with unique properties that in some aspects are superior to those of the plant cellulose, including high purity and crystallinity (with values of 60-90 %<sup>(8)</sup>), high water capacity (extremely high water content close to 100 times their own weight<sup>(9)</sup>), ultrafine and porous 3-D network, great tensile strength.<sup>(10-19)</sup> BC is quite promising for modern medicine and biomedical applications where plant cellulose could not be used; this is mainly due to the high purity and the biological affinity of the BC.

Over the past few decades, the interest in commercial applications of BC has increased. Examples include supports for proteins, cell cultures and microorganisms, products for temporary skin and tissue replacement (Biofill, Bioprocess, and Gengiflex) and calorie-free food such as Coco de Nata. Moreover, BC is considered bio-compatible, which does not elicit chronic inflammatory responses *in vi vo*.<sup>(20)</sup> These properties also make BC very interesting for tissue engineering applications. In addition, because of its crystalline nano- and micro-fibril structure (**Figure 1.4**); BC has excellent mechanical properties which are evaluated in Chapter 2 of this thesis. It is therefore well-suited as a reinforcing agent for paper and fibres made from glass, carbon, phenol resin, and silicon in small quantities. Owing to the high modulus of elasticity in combination with a large internal loss factor, it is also a superior material for headphones and loud-speaker membranes (for example Sony Corp).<sup>(21)</sup>

## **Bacteria types for producing bacterial cellulose**

### *Gluconacetobacter Xylinum* and *Gluconacetobacter Europaeus*

BC can be synthesized by several bacteria including Gram-negative bacteria species such as *Acetobacter*, *Azotobacter*, *Rhizobium*, *Pseudomonas*, *Salmonella*, *Alcaligenes*, and also Gram-positive bacteria species such as *Sarcina ventriculi*. An overview of BC producers is presented in **Table 1.1**.<sup>(22)</sup> The most effective producers of cellulose are *A. xylinum*, *A. hansenii*, and *A. pasteurianus*. Of these, the most common used is *Acetobacter Xylinum* (also formerly known as *Gluconacetobacter Xylinum* (GX)), which is known to synthesize BC fibres and it is a model microorganism for basic and applied

studies on BC. GX is one of the two bacteria strains I have used in this thesis. It is aerobic and rod-shaped bacteria extensively studied due to its ability to produce a high amount of cellulose from a wide range of carbon and nitrogen sources.(23, 24) Furthermore, GX produces extracellular cellulose as a pure, ultra-fine random fibre network, with high crystallinity, high water absorption capacity and mechanical strength.(24-27)

**Table 1.1** Producers of Bacterial Cellulose (BC).

Genus	Cellulose structure	Biological role
<i>Acetobacter</i>	Extracellular pellicle, ribbons	Maintain aerobic environment
<i>Achromobacter</i>	Ribbons	Flocculation
<i>Aerobacter</i>	Fibrils	Flocculation
<i>Agrobacterium</i>	Short fibrils	Attachment to plants
<i>Alcaligenes</i>	Fibrils	Flocculation
<i>Pseudomonas</i>	Non-distinct	Flocculation
<i>Rhizobium</i>	Short fibrils	Attachment to plants
<i>Sarcina</i>	Amorphous	Unknown

The second strain of bacteria that I have used is *Gluconacetobacter europaeus* (GE) which is one of the most prominent acetic acid bacteria. GE plays an important role in multiple natural processes leading to the production of chemicals of industrial interest and high-value food and beverage products. (28, 29) These species derive their energy from the oxidation of ethanol to acetic acid during fermentation and can be isolated from industrial submerged vinegar fermenters, with high resistance to acetic acid. For instance, *Gluconacetobacter europaeus* V 3, previously isolated from industrial vinegar-producing bioreactors, tolerates extremely high acetic acid concentrations of up to 10% (v/v).(30-32) Especially interesting, GE is much less studied for cellulose production than GX bacteria.

## Production methods of bacterial cellulose

### Submerged culture method

Submerged culture method is a method for growing pure culture of aerobic bacteria in which microorganisms are incubated in a liquid medium subjected to continuous, vigorous agitation. Over the past hundred years, the submerged culture method of growing fungi and bacteria has been successfully applied to fermentation processes.

In this process, the organism is grown in a liquid medium, which is vigorously aerated and agitated in large tanks called fermentors. The fermentor could be

---

either an open tank or a closed tank and may be a batch or a continuous tank and they are generally made of non-corrosive metal, glass lined or wood. In batch fermentation, the organism is grown in a known amount of culture medium for a defined period of time and then the cell mass is separated from the liquid before further processing. However, in the continuous culture, the culture medium is withdrawn depending on the rate of product formation and the inflow of fresh medium. Most fermentation industries today use the submerged process for the production of microbial products.

#### Rotating disk reactor method (RDR)

This system consists of a tray with inoculated medium in which a disk assembly is introduced. The disk assembly is made from flat, circular disks mounted on a centred shaft and rotated with a motor. The cells adhere to the surface of the disks, most likely as a result of the extruding fibres and form a pellicle on the surface of the disks. BC pellicles can be produced in a rotating disk reactor. Normally after 12 hours nearly all cells are entrained on the disks leaving the medium clear. A schematic drawing of the method is shown in **Figure 1.5**. Solid disks are inferior to perforated or meshed disks, as the holes allow more medium hold-up on the disks, and therefore faster and stronger film formation.

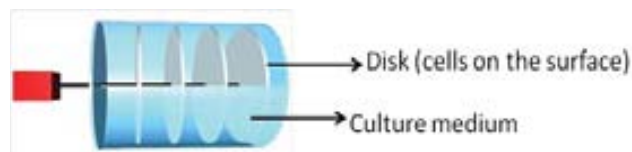


**Figure 1.5** Schematic diagram of a rotating disk reactor

#### Static culture method

The traditional method of static culture has been the growth of BC on the surface of the growth medium. One method of bacterial culture with the static condition is based on solid medium; they can be grown in petri dishes of different sizes that have a thin layer of agar-based growth medium. Then the petri dishes can be incubated at the best temperature for growing of the selected bacteria (usually around 25 °C for acetobacter bacteria).

Another method of bacterial culture is using liquid culture, in which the desired bacteria are suspended in a “liquid broth”. In this static production, an inoculated medium is poured into shallow trays, then covered and allowed to rest static for 5 to 20 days (depending on the desired thickness) until the pellicle nearly fills the tray. During the growth, once the pellicle has formed, the cellulose propagates from the surface of the culture. Several researches have been published showing that the uppermost layer of the pellicle is the only one growing,(8, 33) and the bacteria that are left further into the pellicle

become inactive or die from lack of oxygen. **Figure 1.6** shows the pellicle in a static tray with the active layer indicated.

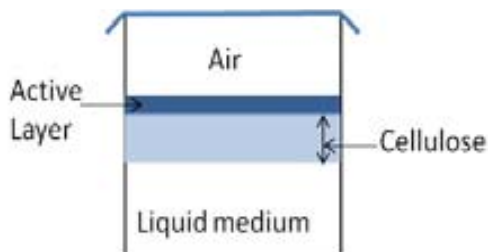


**Figure 1.6** Cellulose growing in static culture.

The static production is very simple, low-tech and it is widely utilized. The trays, once inoculated, cannot be disturbed until the harvesting time. After the required number of culture days, the pellicle can be removed and washed to eliminate the impurities (like medium, bacteria debris or other biological impurities); then it can be processed as desired.

### **Growth medium of bacteria**

It is known that the biosynthesis of BC can be affected by several factors such as environmental conditions, and the growth medium. It has been reported that the composition of culture media affects the various properties of BC (34), which might be due to different types of carbon sources. For instance, mannitol has been used as a carbon source for production of cellulose by the *Gluconacetobacter* bacteria, allowing high productivity when used as substrate.(35) It has also been reported that glucose is a ubiquitous monosaccharide commonly used as a carbon source in nutritious culture media for bacteria growth.(36, 37)

**Table 1.2** Composition medium proposed in previous studies.(38, 39)

Components of Medium	Concentration (% w/v)
Glucose	2.0
Bacto Peptone	0.5
Yeast Extract	0.5
Disodium Phosphate	0.27
Citric Acid	0.115

Following the discovery of Brown's membrane(40), several researchers have investigated the capability of GX and GE bacteria to grow in different mediums. Most of the researchers have concluded that a minimum set of conditions are required: a liquid environment, a 3 to 6 pH level and a carbon source. One of the most commonly utilized growth mediums for GX is the Schramm-Hestrin(39) medium presented in **Table 1.2**. The initial pH value of the medium is 6.0 and it utilizes disodium phosphate as a buffering agent.



## Pathway of bacterial cellulose production

As shown in *Table 1.1*, the structure of BC depends on the organism although the pathway of biosynthesis and mechanism of its regulation are probably common for the majority of BC for producing cellulose. (8, 33, 41) *Figure 1.7* presents two main pathways of production of cellulose including plant cellulose and bacterial cellulose, one is biosynthesis and another is *in vitro* synthesis, in total with four different methods by which cellulose is accessed today. In my case, it is very important to understand the mechanism of production and metabolism of BC.

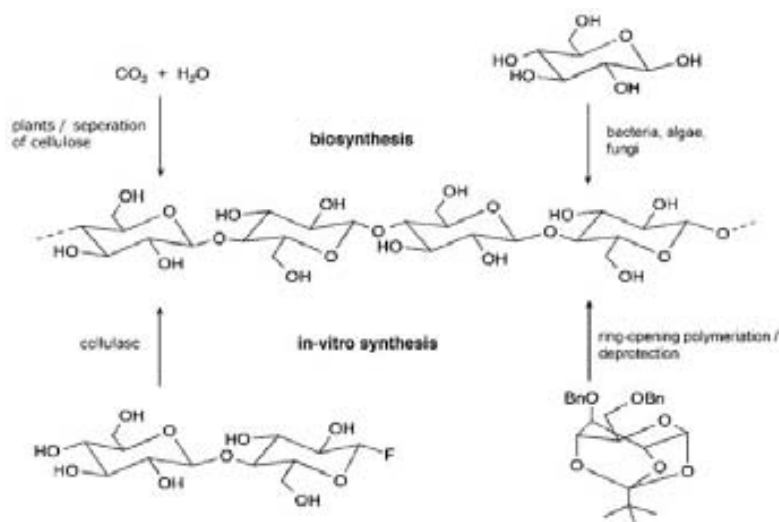


*Figure 1.7* Main pathways to cellulose (plant cellulose and bacterial cellulose) formation.(2)

The synthesis of BC is a multiple process that involves two main mechanisms: the synthesis of uridine diphosphoglucose (UDPGlc), followed by the polymerization of glucose into long and un-branched chains ( $\beta$ -1-4 glucan chain). BC is considered to be secondary metabolite and its synthesis starts with “bacteria food” (for instance glucose) that is catalyzed by enzymes. The pathway is believed to be as described in *Figure 1.8* (follow the black arrow): Glucose-- Glucose-6-Phosphate-- Glucose-1-Phosphate-- UDP-Glucose-- cellulose.(2, 42) The fabrication and extrusion of BC fibres is one part of the metabolism of glucose. In static culture medium, the BC fibres bundle together to form a mat or pellicle within which the bacteria are held. The pellicle floats on the surface of the medium allowing the bacteria to obtain plenty of oxygen, which they require for growth, multiplication and synthesis of more BC.

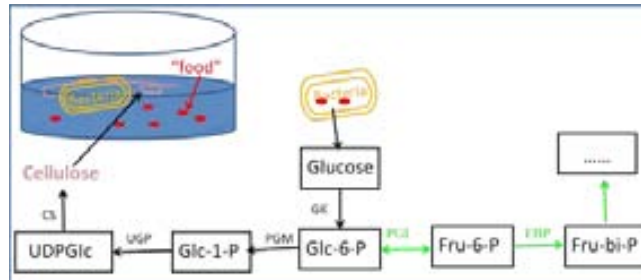


**Figure 1.8** Pathways of carbon metabolism in bacteria. To obtain more oxygen, bacteria live on the surface of the medium. They “eat” and “digest” glucose as food (Glucose to Glc-6-P and then to Fru-6-P ...) to enable growth and multiplication. At the same time, extrusion of cellulose fibrils is another part of the metabolism of glucose. The pathway is Glucose-- Glc-6-P-- Glc-1-P-- UDP-Glc-- Cellulose.

During a rapid growth period with enough food and oxygen, the thickness of the BC pellicle increases steadily. Fibrils appear to be not necessarily linear but contains some "three-way branching points" (**Figure 1.9**) along their length. This type of branching is produced by cell mitosis.(43) After a constant increasing thickness of cellulose, bacteria are trapped by cellulose fibres and begin to die due to insufficient oxygen.

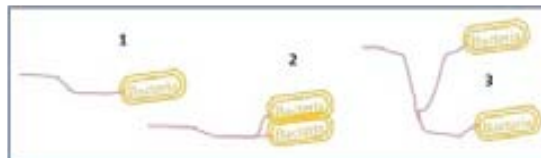


**Figure 1.9** Three-way of producing cellulose fibres.

### Polymorphs of bacterial cellulose

BC is a linear chain of ringed glucose molecules with a repeat unit of  $C_6H_{10}O_5$  (**Figure 1.10**), which are linked together through a  $\beta$  1-4 glucosidic bond. The molecular structure imparts BC with its characteristic properties, such as hydrophilicity, degradability, and broad chemical versatility, which can be initiated by the reactivity of the OH groups. It is the basis for an extensive hydrogen bond network, which plays a major role in directing the crystalline packing and governing its physical properties.(44)

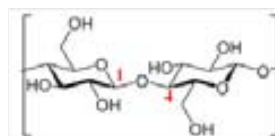


**Figure 1.10** Basic structure of BC showing the repeat unit, each monomer bears three hydroxyl groups.

It is acknowledged that cellulose (plant cellulose and bacterial cellulose) can exist as crystalline micro-fibrils with several polymorphs (cellulose I and II).

Cellulose I is the crystalline cellulose naturally produced by a variety of organisms (trees, plants, tunicates, algae, and bacteria); it is sometimes referred to as “natural” cellulose. Cellulose I has two polymorphs,  $I_\alpha$  and  $I_\beta$ , which coexist in various proportions depending on the cellulose source. The  $I_\alpha$  structure is the dominant polymorph for most algae and bacteria, whereas  $I_\beta$  is the dominant polymorph for tunicate cellulose. The  $I_\alpha$  polymorph is metastable and can be converted to  $I_\beta$  by hydrothermal treatments in alkaline solutions, or high temperature treatment in organic solvents. Typically,  $I_\alpha$ -rich algae and bacterial cellulose have been used in these conversion studies, and the extent of  $I_\alpha$  to  $I_\beta$  conversion can be controlled by adjusting the treatment parameters. However, complete conversion to  $I_\beta$  is typically not achieved.(45) Cellulose II has been the most stable structure of technical relevance with a monoclinic structure which is presented in **Figure 1.11**. Interestingly, cellulose II also can be produced by the process of mercerization.(45)

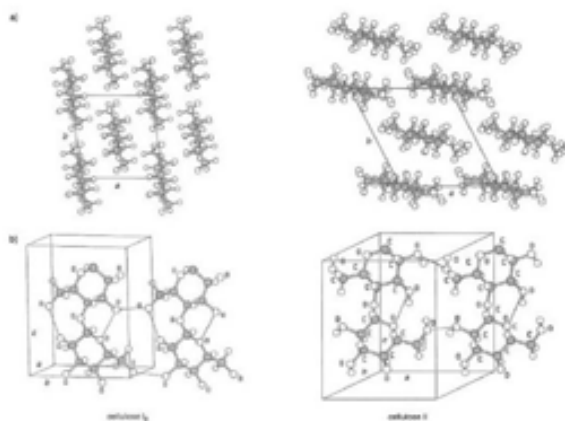


**Figure 1.11** Crystal structure of cellulose  $I_\beta$  and II, adapted from Klemm, D., et al.(2, 46)

### **Development and increasing publications of bacterial cellulose**

BC has been investigated as an attractive eco-friendly nano-material; meanwhile the functionalization of BC with organic or inorganic materials opens up new pathways for the fabrication of novel multifunctional nano-composites with promising performances. The production of BC and its applications in composite materials has gained increasing attention due to the combination of both properties.

**Figure 1.12** shows the increasing annual publication on BC since 2000. In recent years, the utilization and investigation of BC in functional materials have been the focus of research because they enable the creation of materials with improved or new properties, such as electronic, optical, catalytic and magnetic properties, scaffold for tissue engineering and cell culture

applications by mixing multiple constituents and exploiting synergistic effects.(12, 47-50)

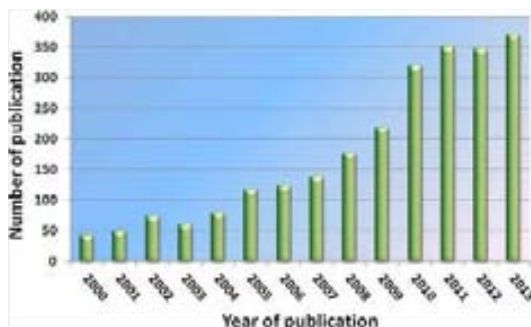


**Figure 1.12** The illustration of the annual number of publications on bacterial cellulose since 2000 (SciFinder Scholar search system, search term “bacterial cellulose”).(47)

## 1.2 Bacterial cellulose-based composites

### Synthesis methods of bacterial cellulose-based composites

Depending on the desired applications, BC-based composites can be synthesized by two main approaches: chemical modification and particles deposition. Chemical modification of BC can be carried out at the hydroxyl groups of the glucose units on the BC backbone structure. Previous works have accomplished several modifications, which are shown in **Figure 1.13**. Several possible routes have been listed: such as sulfonation, oxidation, cationization, grafting (via acid chloride, acid anhydride, or isocyanate) and silylation.(51-57)

On the other hand, particles deposition is an attractive direction for fabrication of BC-based composites. There are several reports on the use of BC as a stabilizing matrix for different particles.(58-63) In **Figure 1.13**, some examples are shown including BC-silver NPs (antimicrobial wound dressing application(63)), BC- ferrite NPs (loudspeaker application(64)) and BC-Montmorillonite (biomedical applications(49)). The combination of BC and different materials offer a wide range of applications.

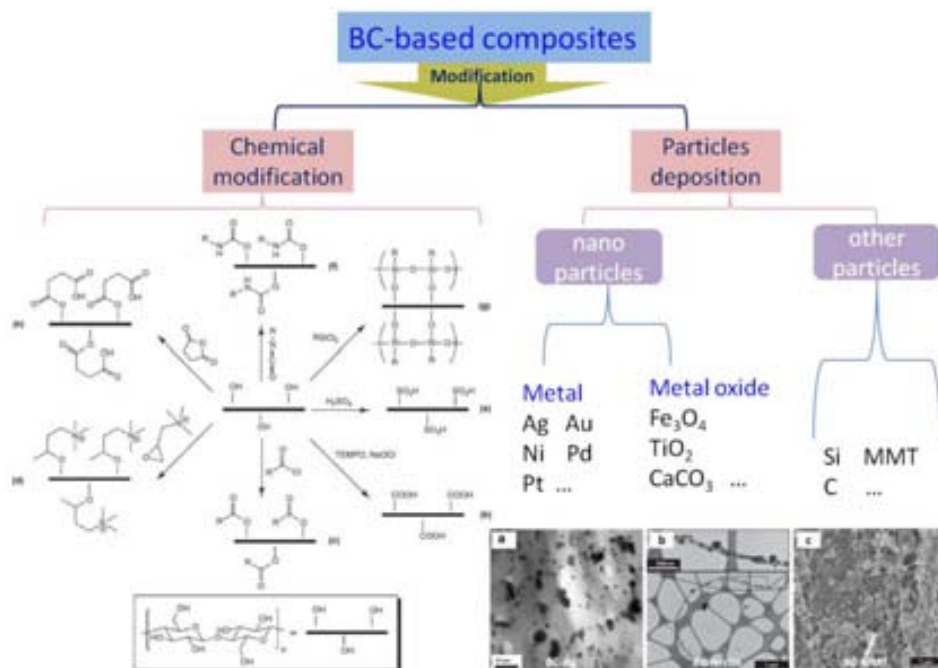


**Figure 1.13** Two main approaches of synthesis BC-based composites: chemical modification and particles deposition. Chemical modification part: some possible routes (clockwise from right) a) sulfonation; b) oxidation by TEMPO; c) ester linkages via acid chlorides; d) cationization via epoxides; e) ester linkages via acid anhydrides; f) urethane linkages via isocyanates; and g) silylation. Particles deposition part: a generalized classification of BC-based material prepared with NPs (metal, metal oxides) and other particles (e.g. Si and MMT). FE-SEM images of some samples of BC-based materials including BC-silver NPs (a), BC-ferrite NPs (b) and BC-MMT (c). This image was modified from the original images by N. Shah and E. Lam.(65, 66)

### Classes of bacterial cellulose-based composites

Based on the composite materials ranging from polymers to NPs, BC composites can be generally classified into organic materials and inorganic materials. These two main classes can be further divided into sub-classifications: polymers, particles including NPs (e.g. metal and metal oxide NPs) and other particles (e.g. clay and silica particles).(67)

Polymers are organic and most of them have specific hydrogen bonding sites. There are many examples of BC-based composites with different polymers that have led to improvements in medical applications, physic-mechanical properties and conducting capabilities of BC. For instance, the synthesis of BC-Chitosan (BC-Ch) composites for bio-medical applications(68, 69) such as wound healing effects, tissue engineering scaffold, and anti-viral properties. Moreover, the BC-Gelatin polymeric composites followed the same strategy as BC-Ch. Gelatins have been investigated to combine with scaffold such as BC due to their bio-medical properties including their enhanced cell adhesion and

---

proliferation activities. For example, Luo et al.(70) have synthesized novel BC-collagen composite for potential tissue engineering scaffolds. M. Phisalaphong and co workers(71) have prepared BC-Alginate blend membranes with improved water absorption capacity and water vapor transmission rate, which can be used in membrane separation processes. BC-based composites with some conducting polymers have been produced to impart conducting properties to BC, for example the high conductivity BC-Polyaniline composites were synthesized by Shi et al(72).

Additionally to polymers, particles deposition also is important in the synthesis of BC-based composites. Particles have been used to introduce electrical, optical, conducting and anti-microbial properties in BC. As I listed in **Figure I.13**, there are metals and metal oxide NPs used in the preparation of BC-based composites. Silver, gold, palladium and magnetic NPs have received much attention due to their potential for use in anti-bacterial materials, bio-sensors, catalysis, magnetic materials and several related fields. In addition to metal and metal oxide NPs, attempts have been made to combine other particles with BC to accelerate its efficiency and increase its applications. Here I will describe briefly two examples, such as clay and silica particles. Among clay materials, various clays have been utilized in BC-based composites as reinforcing materials. For example, montmorillonite (MMT) become popular owing to its bio-medical applications and polymer reinforcing properties.(73, 74) For instance, UI-Islam and co workers (74) prepared BC-MMT composites, which have higher mechanical and thermal properties than pristine BC. Recently, Ashori and colleagues(75) reported BC-Si composites prepared by immersing solid BC gels in an aqueous solution of tetraethoxysilane. The mechanical properties of the composites were increased with only 7 % loading of Si particles.

### **1.3 Bacterial cellulose composites with nanoparticles and their applications**

NPs are a special class of materials that have received considerable research interest due to their size effect, high specific surface area and unique properties.(76) BC can be composited with different NPs through a variety of synthetic approaches. Here, I will describe a few of these BC-NPs composites and their synthetic approaches and applications.

In 2007, BC-Ag nanocomposites were synthesized by Maneerung et al. (63). The metallic Ag NPs were produced into the BC sheets by reducing the  $\text{AgNO}_3$  in  $\text{NaBH}_4$  solution. BC-Ag nanocomposite showed strong antibacterial effects against gram positive and gram negative bacterial species, which can be used in antimicrobial applications such as wound care dressings. For instance, one of the similar following studies, Luiz C. S. Maria and co workers reported that they prepared BC-Ag nanocomposites for investigating the bactericidal effects against *Escherichia coli*.(77) Another example is that Sureshkumar and co

---

workers(78) prepared a magnetic BC-Ag nanocomposite by a facile method. They immersed the BC in a mixture of ferric and ferrous solution to precipitate the magnetic NPs on the surface of this matrix of BC by increasing the pH. Then a polydopamine layer was coated onto the magnetic BC, which helped to synthesize the Ag NPs from silver nitrate solution onto the magnetic BC surface. This magnetic BC-Ag nanocomposites presented impressive antimicrobial activity against the model microbial species.

BC-Au nanocomposites have also received attention due to the properties of gold NPs with potential use in sensors, catalysis, and several related fields.(79) For instance, Zhang et al.(80) have synthesized BC-Au nanocomposites using BC nano-fibres as robust biotemplates for the potential use in enzyme immobilization and in bioelectronic systems. BC-Pt nano-composites showed that they have significant conducting efficiency and can be used as fuel cells and bio-sensors.(81) BC-Pd nanocomposites reported by Evans et al.(82), were able to catalyze the generation of hydrogen when incubated with sodium dithionite.

Instead of metals NPs, some metallic oxides NPs have been composited with BC to enhance its biological and conducting activities. BC hybrid fibres coated with TiO<sub>2</sub> NPs were synthesized by Gutierrez et al.(83), and were shown to be an important conducting material. Moreover, BC-TiO<sub>2</sub> can be also used in drug delivery and photo-catalyst applications.(84) Normally, the TiO<sub>2</sub> NPs were prepared by the sol gel method which was deposited onto the BC membranes. Another approach for synthesis of TiO<sub>2</sub> NPs in the presence of BC was reported by Sun et al.(84) In their method, BC not only acts as a matrix to hold these NPs, but also affords sites for the nucleation of TiO<sub>2</sub> NPs from the medium. This BC- TiO<sub>2</sub> nanocomposite demonstrated higher photo-catalytic activity for a model pollutant (methyl orange) than that of the commercial photo-catalyst, P25.

Magnetically responsive BC composites, which are incorporated with magnetic NPs such as maghemite and hematite, have also attracted attentions due to their potential novel applications (e.g. electro-magnetic interference shielding materials, counterfeiting, catalysis and sensors) related to their extra magnetic properties. Preparation of magnetically responsive BC is similar to that of other filler-loaded network. One way is to prepare and characterize magnetic NPs separately and then to mix them with BC and the cross-linking takes place after mixing BC and the magnetic NPs solution, which is normally called the dip coating method. Another alternative method is in-situ co-precipitation method, which involves the synthesis of magnetic NPs within the BC by using the hydroxyl terminated porous structure of BC as reacting sites. The fibrous network structure, apart from providing high mechanical strength, offers macro/mesoporous spaces, which can be used as reaction chambers for precipitation of NPs with the fibres providing a support structure to hold the NPs. For instance, the magnetically responsive BC sheets containing Fe<sub>3</sub>O<sub>4</sub>

---

NPs were prepared by using an ammonia gas-enhancing in situ co-precipitation method.<sup>(85)</sup> The homogeneous dispersion of the magnetic NPs throughout the BC matrix could enhance the percentage of incorporated magnetic NPs into BC samples, leading to high and uniform magnetic properties. Zhang et al.<sup>(86)</sup> synthesized amphiphobic BC-Fe<sub>3</sub>O<sub>4</sub> membrane by using fluoroalkyl silane, which showed the highest water contact angle and oil contact angle. This fluorinated membrane with appropriate roughness and hydrophobic and lipophobic surface would show promise to be used in electronic actuators, magnetographic printing, information storage, electromagnetic shielding coating and anti-counterfeit applications. In addition, magnetically responsive BC can also be synthesized by precipitation of ferromagnetic Ni NPs of 10–60 nm by room temperature chemical reduction of Ni-chloride hexahydrate.<sup>(87, 88)</sup> They clearly showed that the Ni loaded BC can be used for both non-biological applications such as magnetic printing and biological applications such as magnetic tissue scaffolds. Recently, metallic magnetic particles have also been loaded into BC by precipitating from the respective salt solutions using NaBH<sub>4</sub>, KH<sub>2</sub>PO<sub>2</sub>, and NaH<sub>2</sub>PO<sub>2</sub> as reducing agents.

However, the precipitation reaction method of loading NPs in the BC matrix does not allow complete control of particles formation-nucleation, growth, aggregation, and density. As a result, the synthesized NPs may have a broad distribution of sizes and different inter-particle distances. The reaction methods, conditions, type of reducing agents and the reduction medium are found to influence the chemical composition, crystallinity, and NPs size. In Chapter 3, I will present an efficient and fast method to prepare BC-NPs composites with homogenous and controllable dispersion of NPs and their characterizations.



---

## 1.4 References

1. Y. Habibi, Key advances in the chemical modification of nanocelluloses, *Chemical Society reviews*, **43**, 1519, (2014).
2. D. Klemm, B. Heublein, H. P. Fink, A. Bohn, Cellulose: fascinating biopolymer and sustainable raw material, *Angewandte Chemie International Edition*, **44**, 3358, (2005).
3. E. J. Vandamme, S. De Baets, A. Vanbaelen, K. Joris, P. De Wulf, Improved production of bacterial cellulose and its application potential, *Polymer Degradation and Stability*, **59**, 93, (1998).
4. A. J. Brown, LXII.-Further notes on the chemical action of *Bacterium aceti*, *Journal of the Chemical Society, Transactions*, **51**, 638, (1887).
5. A. J. Brown, XIX.-The chemical action of pure cultivations of *Bacterium aceti*, *Journal of the Chemical Society, Transactions*, **49**, 172, (1886).
6. A. J. Brown, XLIII.-On an acetic ferment which forms cellulose, *Journal of the Chemical Society, Transactions*, **49**, 432, (1886).
7. J. Shokri, K. Adibkia, *Application of Cellulose and Cellulose Derivatives in Pharmaceutical Industries*. Cellulose - Medical, Pharmaceutical and Electronic Applications (2013).
8. W. Czaja, D. Romanovicz, R. m. Brown, Structural investigations of microbial cellulose produced in stationary and agitated culture, *Cellulose*, **11**, 403, (2004).
9. D. Klemm, D. Schumann, F. Kramer, N. Heßler, M. Hornung, H.-P. Schmauder, S. Marsch, in *Polysaccharides II*, D. Klemm, Ed. (Springer Berlin Heidelberg, 2006), vol. 205, pp. 49-96.
10. H. P. S. Abdul Khalil, A. H. Bhat, A. F. Ireana Yusra, Green composites from sustainable cellulose nanofibrils: A review, *Carbohydrate polymers*, **87**, 963, (2012).
11. A. Walther, J. V. Timonen, I. Diez, A. Laukkanen, O. Ikkala, Multifunctional high-performance biofibers based on wet-extrusion of renewable native cellulose nanofibrils, *Advanced Materials*, **23**, 2924, (2011).
12. S. Saska, H. S. Barud, A. M. Gaspar, R. Marchetto, S. J. Ribeiro, Y. Messaddeq, Bacterial cellulose-hydroxyapatite nanocomposites for bone regeneration, *International journal of biomaterials*, **2011**, 175362, (2011).
13. N. Petersen, P. Gatenholm, Bacterial cellulose-based materials and medical devices: current state and perspectives, *Applied microbiology and biotechnology*, **91**, 1277, (2011).
14. R. J. Moon, A. Martini, J. Nairn, J. Simonsen, J. Youngblood, Cellulose nanomaterials review: structure, properties and nanocomposites, *Chemical Society reviews*, **40**, 3941, (2011).
15. Y. K. Lin, K. H. Chen, K. L. Ou, L. Min, Effects of different extracellular matrices and growth factor immobilization on biodegradability and biocompatibility of macroporous bacterial cellulose, *Journal of Bioactive and Compatible Polymers*, **26**, 508, (2011).
16. D. Klemm, F. Kramer, S. Moritz, T. Lindstrom, M. Ankerfors, D. Gray, A. Dorris, Nanocelluloses: a new family of nature-based materials, *Angewandte Chemie International Edition*, **50**, 5438, (2011).
17. W. K. Czaja, D. J. Young, M. Kawecki, R. M. Brown, The future prospects of microbial cellulose in biomedical applications, *Biomacromolecules*, **8**, 1, (2007).

- 
18. R. M. Brown, Cellulose structure and biosynthesis: What is in store for the 21st century?, *Journal of Polymer Science Part A: Polymer Chemistry*, **42**, 487, (2004).
  19. S. Reiling, J. Brickmann, Theoretical investigations on the structure and physical properties of cellulose, *Macromolecular Theory and Simulations*, **4**, 725, (1995).
  20. G. Helenius, H. Backdahl, A. Bodin, U. Nannmark, P. Gatenholm, B. Risberg, In vivo biocompatibility of bacterial cellulose, *Journal of biomedical materials research. Part A*, **76**, 431, (2006).
  21. D. Fragouli, I. S. Bayer, R. Di Corato, R. Brescia, G. Bertoni, C. Innocenti, D. Gatteschi, T. Pellegrino, R. Cingolani, A. Athanassiou, Superparamagnetic cellulose fiber networks via nanocomposite functionalization, *Journal of Materials Chemistry*, **22**, 1662, (2012).
  22. M. Shoda, Y. Sugano, Recent advances in bacterial cellulose production, *Biotechnology and Bioprocess Engineering*, **10**, 1, (2005).
  23. W. Czaja, A. Krystynowicz, S. Bielecki, R. M. Brown Jr, Microbial cellulose—the natural power to heal wounds, *Biomaterials*, **27**, 145, (2006).
  24. B. H. A. Rehm, Bacterial polymers: biosynthesis, modifications and applications, *Nature Reviews Microbiology*, **8**, 578, (2010).
  25. B. McKenna, D. Mikkelsen, J. B. Wehr, M. Gidley, N. Menzies, Mechanical and structural properties of native and alkali-treated bacterial cellulose produced by *Gluconacetobacter xylinus* strain ATCC 53524, *Cellulose*, **16**, 1047, (2009).
  26. D. S. Dieter Klemm, Ulrike Udhardt, Silvia Marsch, Bacterial synthesized cellulose- artificial blood vessels for microsurgery, *Progress in Polymer Science*, **26**, 1561, (2001).
  27. M. A. Meyers, P.-Y. Chen, A. Y.-M. Lin, Y. Seki, Biological materials: Structure and mechanical properties, *Progress in Materials Science*, **53**, 1, (2008).
  28. Á. González, N. Hierro, M. Poblet, A. Mas, J. M. Guillamón, Application of molecular methods to demonstrate species and strain evolution of acetic acid bacteria population during wine production, *International Journal of Food Microbiology*, **102**, 295, (2005).
  29. P. Raspor, D. Goranovič, Biotechnological Applications of Acetic Acid Bacteria, *Critical Reviews in Biotechnology*, **28**, 101, (2008).
  30. J. Trcek, K. Jernejc, K. Matsushita, The highly tolerant acetic acid bacterium *Gluconacetobacter europaeus* adapts to the presence of acetic acid by changes in lipid composition, morphological properties and PQQ-dependent ADH expression, *Extremophiles: life under extreme conditions*, **11**, 627, (2007).
  31. C. Andres-Barrao, L. Falquet, S. P. Calderon-Copete, P. Descombes, R. Ortega Perez, F. Barja, Genome sequences of the high-acetic acid-resistant bacteria *Gluconacetobacter europaeus* LMG 18890T and *G. europaeus* LMG 18494 (reference strains), *G. europaeus* 5P3, and *Gluconacetobacter oboediens* 174Bp2 (isolated from vinegar), *Journal of bacteriology*, **193**, 2670, (2011).
  32. I. Cleenwerck, M. De Wachter, A. Gonzalez, L. De Vuyst, P. De Vos, Differentiation of species of the family Acetobacteraceae by AFLP DNA fingerprinting: *Gluconacetobacter kombuchae* is a later heterotypic synonym of *Gluconacetobacter hansenii*, *International journal of systematic and evolutionary microbiology*, **59**, 1771, (2009).

- 
33. W. Borzani, S. J. D. Souza, A simple method to control the bacterial production of cellulosic films in order to obtain dried pellicles presenting a desired average thickness, *World Journal of Microbiology and Biotechnology*, **14**, 59, (1997).
  34. O. Shezad, S. Khan, T. Khan, J. K. Park, Physicochemical and mechanical characterization of bacterial cellulose produced with an excellent productivity in static conditions using a simple fed-batch cultivation strategy, *Carbohydrate polymers*, **82**, 173, (2010).
  35. D. R. Ruka, G. P. Simon, K. M. Dean, Altering the growth conditions of *Glucanacetobacter xylinus* to maximize the yield of bacterial cellulose, *Carbohydrate polymers*, **89**, 613, (2012).
  36. W. Wang, H.-Y. Li, D.-W. Zhang, J. Jiang, Y.-R. Cui, S. Qiu, Y.-L. Zhou, X.-X. Zhang, Fabrication of Bionzymatic Glucose Biosensor Based on Novel Gold Nanoparticles-Bacteria Cellulose Nanofibers Nanocomposite, *Electroanalysis*, **22**, 2543, (2010).
  37. T. R. Stumpf, R. A. Pertile, C. R. Rambo, L. M. Porto, Enriched glucose and dextrin mannitol-based media modulates fibroblast behavior on bacterial cellulose membranes, *Materials science & engineering. C, Materials for biological applications*, **33**, 4739, (2013).
  38. F. Liebner, E. Haimer, M. Wendland, M. A. Neouze, K. Schluffer, P. Miethe, T. Heinze, A. Potthast, T. Rosenau, Aerogels from unaltered bacterial cellulose: application of scCO<sub>2</sub> drying for the preparation of shaped, ultra-lightweight cellulosic aerogels, *Macromolecular bioscience*, **10**, 349, (2010).
  39. S. Hestrin, M. Schramm, Synthesis of cellulose by *Acetobacter xylinum*. 2. Preparation of freeze-dried cells capable of polymerizing glucose to cellulose, *Biochemical Journal*, **58**, 345, (1954).
  40. R. M. Brown, J. H. Willison, C. L. Richardson, Cellulose biosynthesis in *Acetobacter xylinum*: visualization of the site of synthesis and direct measurement of the in vivo process, *Proceedings of the National Academy of Sciences*, **73**, 4565, (1976).
  41. S.-P. Lin, I. Loira Calvar, J. Catchmark, J.-R. Liu, A. Demirci, K.-C. Cheng, Biosynthesis, production and applications of bacterial cellulose, *Cellulose*, **20**, 2191, (2013).
  42. P. O'Neill Skinner, R. E. Cannon, *Acetobacter xylinum*: An Inquiry into Cellulose Biosynthesis, *The American Biology Teacher*, **62**, 442, (2000).
  43. Y. Nishi, M. Uryu, S. Yamanaka, K. Watanabe, N. Kitamura, M. Iguchi, S. Mitsuhashi, The structure and mechanical properties of sheets prepared from bacterial cellulose, *Journal of Materials Science*, **25**, 2997, (1990).
  44. M. J. John, S. Thomas, Biofibres and biocomposites, *Carbohydrate polymers*, **71**, 343, (2008).
  45. P. Mansikkamäki, M. Lahtinen, K. Rissanen, The conversion from cellulose I to cellulose II in NaOH mercerization performed in alcohol–water systems: An X-ray powder diffraction study, *Carbohydrate polymers*, **68**, 35, (2007).
  46. P. Zugenmaier, Conformation and packing of various crystalline cellulose fibers, *Progress in polymer science*, **26**, 1341, (2001).
  47. W. Hu, S. Chen, J. Yang, Z. Li, H. Wang, Functionalized bacterial cellulose derivatives and nanocomposites, *Carbohydrate polymers*, **101**, 1043, (2014).
  48. L. Fu, J. Zhang, G. Yang, Present status and applications of bacterial cellulose-based materials for skin tissue repair, *Carbohydrate polymers*, **92**, 1432, (2013).

- 
49. M. Ul-Islam, T. Khan, J. K. Park, Nanoreinforced bacterial cellulose-montmorillonite composites for biomedical applications, *Carbohydrate polymers*, **89**, 1189, (2012).
  50. R. Pertile, S. Moreira, F. Andrade, L. Domingues, M. Gama, Bacterial cellulose modified using recombinant proteins to improve neuronal and mesenchymal cell adhesion, *Biotechnology progress*, **28**, 526, (2012).
  51. Y. Habibi, H. Chanzy, M. R. Vignon, TEMPO-mediated surface oxidation of cellulose whiskers, *Cellulose*, **13**, 679, (2006).
  52. M. Hasani, E. D. Cranston, G. Westman, D. G. Gray, Cationic surface functionalization of cellulose nanocrystals, *Soft Matter*, **4**, 2238, (2008).
  53. Y. Habibi, A.-L. Goffin, N. Schiltz, E. Duquesne, P. Dubois, A. Dufresne, Bionanocomposites based on poly ( $\epsilon$ -caprolactone)-grafted cellulose nanocrystals by ring-opening polymerization, *Journal of Materials Chemistry*, **18**, 5002, (2008).
  54. A. Junior de Menezes, G. Siqueira, A. A. Curvelo, A. Dufresne, Extrusion and characterization of functionalized cellulose whiskers reinforced polyethylene nanocomposites, *Polymer*, **50**, 4552, (2009).
  55. J. Pandey, W. Chu, C. Kim, C. Lee, S. Ahn, Bio-nano reinforcement of environmentally degradable polymer matrix by cellulose whiskers from grass, *Composites Part B: Engineering*, **40**, 676, (2009).
  56. G. Siqueira, J. Bras, A. Dufresne, Cellulose whiskers versus microfibrils: influence of the nature of the nanoparticle and its surface functionalization on the thermal and mechanical properties of nanocomposites, *Biomacromolecules*, **10**, 425, (2008).
  57. C. Goussé, H. Chanzy, G. Excoffier, L. Soubeyrand, E. Fleury, Stable suspensions of partially silylated cellulose whiskers dispersed in organic solvents, *Polymer*, **43**, 2645, (2002).
  58. W. K. Son, J. H. Youk, W. H. Park, Antimicrobial cellulose acetate nanofibers containing silver nanoparticles, *Carbohydrate polymers*, **65**, 430, (2006).
  59. Y. Shin, I.-T. Bae, B. W. Arey, G. J. Exarhos, Facile stabilization of gold-silver alloy nanoparticles on cellulose nanocrystal, *The Journal of Physical Chemistry C*, **112**, 4844, (2008).
  60. Y. Shin, I.-T. Bae, B. W. Arey, G. J. Exarhos, Simple preparation and stabilization of nickel nanocrystals on cellulose nanocrystal, *Materials Letters*, **61**, 3215, (2007).
  61. J. Cai, S. Kimura, M. Wada, S. Kuga, Nanoporous cellulose as metal nanoparticles support, *Biomacromolecules*, **10**, 87, (2008).
  62. J. He, T. Kunitake, A. Nakao, Facile in situ synthesis of noble metal nanoparticles in porous cellulose fibers, *Chemistry of Materials*, **15**, 4401, (2003).
  63. T. Maneerung, S. Tokura, R. Rujiravanit, Impregnation of silver nanoparticles into bacterial cellulose for antimicrobial wound dressing, *Carbohydrate polymers*, **72**, 43, (2008).
  64. S. Galland, R. L. Andersson, M. Salajková, V. Ström, R. T. Olsson, L. A. Berglund, Cellulose nanofibers decorated with magnetic nanoparticles – synthesis, structure and use in magnetized high toughness membranes for a prototype loudspeaker, *Journal of Materials Chemistry C*, **1**, 7963, (2013).
  65. N. Shah, M. Ul-Islam, W. A. Khattak, J. K. Park, Overview of bacterial cellulose composites: a multipurpose advanced material, *Carbohydrate polymers*, **98**, 1585, (2013).

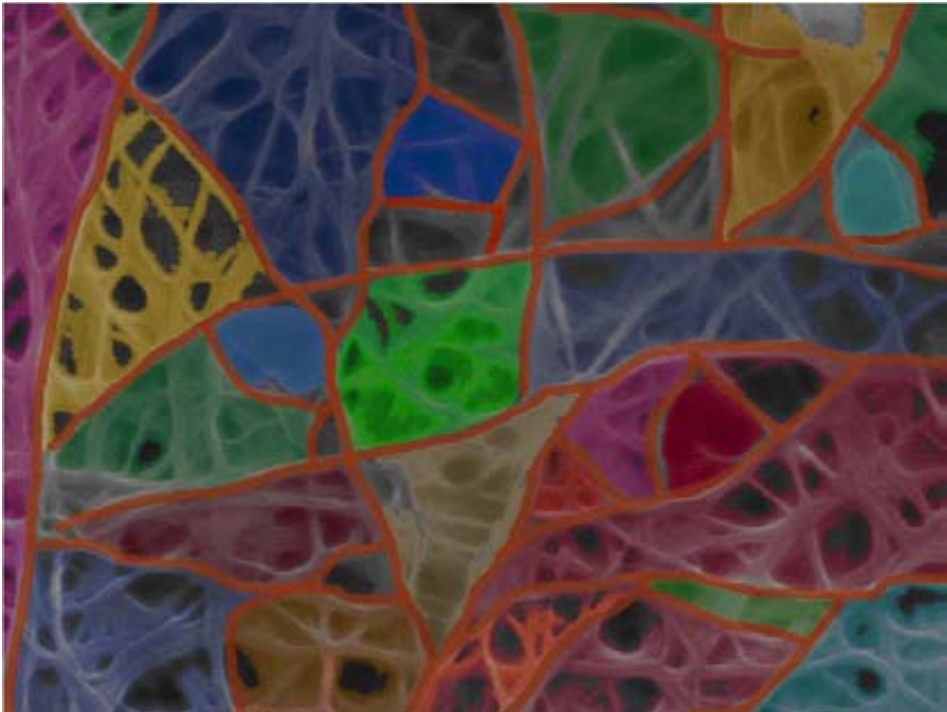
- 
66. E. Lam, K. B. Male, J. H. Chong, A. C. Leung, J. H. Luong, Applications of functionalized and nanoparticle-modified nanocrystalline cellulose, *Trends in biotechnology*, **30**, 283, (2012).
  67. N. Shah, M. Ul-Islam, W. A. Khattak, J. K. Park, Overview of bacterial cellulose composites: A multipurpose advanced material, *Carbohydrate polymers*, **98**, 1585, (2013).
  68. M. Ul-Islam, N. Shah, J. H. Ha, J. K. Park, Effect of chitosan penetration on physico-chemical and mechanical properties of bacterial cellulose, *Korean Journal of Chemical Engineering*, **28**, 1736, (2011).
  69. C. Zhijiang, H. Chengwei, Y. Guang, Retracted: Preparation and characterization of a bacterial cellulose/chitosan composite for potential biomedical application, *Journal of Applied Polymer Science*, **121**, 1488, (2011).
  70. H. Luo, G. Xiong, Y. Huang, F. He, Y. Wang, Y. Wan, Preparation and characterization of a novel COL/BC composite for potential tissue engineering scaffolds, *Materials Chemistry and Physics*, **110**, 193, (2008).
  71. M. Phisalaphong, T. Suwanmajo, P. Tammarate, Synthesis and characterization of bacterial cellulose/alginate blend membranes, *Journal of Applied Polymer Science*, **107**, 3419, (2008).
  72. Z. Shi, S. Zang, F. Jiang, L. Huang, D. Lu, Y. Ma, G. Yang, In situ nano-assembly of bacterial cellulose-polyaniline composites, *RSC Advances*, **2**, 1040, (2012).
  73. N. Meng, N. Zhou, S. Zhang, J. Shen, Synthesis and antimicrobial activities of polymer/montmorillonite–chlorhexidine acetate nanocomposite films, *Applied Clay Science*, **42**, 667, (2009).
  74. M. Ul-Islam, T. Khan, J. K. Park, Nanoreinforced bacterial cellulose–montmorillonite composites for biomedical applications, *Carbohydrate polymers*, **89**, 1189, (2012).
  75. A. Ashori, S. Sheykhnazari, T. Tabarsa, A. Shakeri, M. Gosalipour, Bacterial cellulose/silica nanocomposites: preparation and characterization, *Carbohydrate polymers*, **90**, 413, (2012).
  76. I. F. Nata, M. Sureshkumar, C.-K. Lee, One-pot preparation of amine-rich magnetite/bacterial cellulose nanocomposite and its application for arsenate removal, *RSC Advances*, **1**, 625, (2011).
  77. A. L. C. S. Luiz C. S. Maria, Philippe C. Oliveira, Aline S. S. Valle, Preparation and Antibacterial Activity of Silver Nanoparticles Impregnated in Bacterial Cellulose, *Polímeros: Ciência e Tecnologia*, **20**, 72, (2010).
  78. M. Sureshkumar, D. Y. Siswanto, C.-K. Lee, Magnetic antimicrobial nanocomposite based on bacterial cellulose and silver nanoparticles, *Journal of Materials Chemistry*, **20**, 6948, (2010).
  79. V. Berry, A. Gole, S. Kundu, C. J. Murphy, R. F. Saraf, Deposition of CTAB-terminated nanorods on bacteria to form highly conducting hybrid systems, *Journal of the American Chemical Society*, **127**, 17600, (2005).
  80. T. Zhang, W. Wang, D. Zhang, X. Zhang, Y. Ma, Y. Zhou, L. Qi, Biotemplated Synthesis of Gold Nanoparticle-Bacteria Cellulose Nanofiber Nanocomposites and Their Application in Biosensing, *Advanced Functional Materials*, **20**, 1152, (2010).
  81. J. Yang, D. Sun, J. Li, X. Yang, J. Yu, Q. Hao, W. Liu, J. Liu, Z. Zou, J. Gu, In situ deposition of platinum nanoparticles on bacterial cellulose membranes

- 
- and evaluation of PEM fuel cell performance, *Electrochimica Acta*, **54**, 6300, (2009).
82. B. R. Evans, H. M. O'Neill, V. P. Malyvanh, I. Lee, J. Woodward, Palladium-bacterial cellulose membranes for fuel cells, *Biosensors and Bioelectronics*, **18**, 917, (2003).
83. J. Gutierrez, A. Tercjak, I. Algar, A. Retegi, I. Mondragon, Conductive properties of TiO<sub>2</sub>/bacterial cellulose hybrid fibres, *Journal of colloid and interface science*, **377**, 88, (2012).
84. D. Sun, J. Yang, X. Wang, Bacterial cellulose/TiO<sub>2</sub> hybrid nanofibers prepared by the surface hydrolysis method with molecular precision, *Nanoscale*, **2**, 287, (2010).
85. C. Katepetch, R. Rujiravanit, Synthesis of magnetic nanoparticle into bacterial cellulose matrix by ammonia gas-enhancing in situ co-precipitation method, *Carbohydrate polymers*, **86**, 162, (2011).
86. W. Zhang, S. Chen, W. Hu, B. Zhou, Z. Yang, N. Yin, H. Wang, Facile fabrication of flexible magnetic nanohybrid membrane with amphiphobic surface based on bacterial cellulose, *Carbohydrate polymers*, **86**, 1760, (2011).
87. V. Thiruvengadam, S. Vitta, Ni-bacterial cellulose nanocomposite; a magnetically active inorganic-organic hybrid gel, *RSC Advances*, **3**, 12765, (2013).
88. S. Vitta, M. Drillon, A. Derory, Magnetically responsive bacterial cellulose: Synthesis and magnetic studies, *Journal of Applied Physics*, **108**, 053905, (2010).

# Chapter 2

Bacterial cellulose:

Fabrication and characterization



---

## Chapter Index

Chapter summary.....	27
2.1 Production of bacterial cellulose films .....	28
Experimental set-up and methodology .....	28
2.2 Cleaning process.....	32
2.3 Drying process.....	33
Drying methodology .....	33
Three different drying methods.....	34
2.4 Characterization of bacterial cellulose films.....	38
Chemical structure and purity .....	38
Crystallinity .....	39
Microstructure.....	42
Water absorption capacity.....	44
Optical properties.....	46
Thermo-gravimetric Analysis .....	48
Mechanical properties.....	50
2.5 Conclusions .....	54
2.6 References .....	55



---

## Chapter summary

As mentioned in the introductory chapter, cellulose is not only produced by plants, some fungi and bacteria also synthesize it. In my thesis, *Gluconacetobacter Xylinum* (GX) and *Gluconacetobacter E uropaeus* (GE) bacteria strains were chosen to produce bacterial cellulose (BC). BC can be harvested from the air/liquid interface of the culture medium by using the static culture method, which is simple, cheap and widely utilized.

In this chapter, I will present a detailed description of the production of GX and GE cellulose pellicles, and the methodology used to obtain clean, pure and uniform bacterial cellulose films (BCFs). The clean and wet BCFs were dried by three different drying processes: a) room temperature drying (RD), b) freeze drying (FD) and c) CO<sub>2</sub> supercritical drying (SCD). In order to understand the properties of BCFs I have evaluated their chemical structure, purity, crystallinity, microstructure, water adsorption capacity, transparency and mechanical properties.

---

## 2.1 Production of bacterial cellulose films

### Experimental set-up and methodology

The experiments related to bacteria culture presented in this section have been conducted at Departament de Bioquímica i Biologia Molecular/ Universitat Autònoma de Barcelona. I would like to thank here once more the group of Dr. Alex Perálvarez for the use of the facilities and their tutoring in bacterial culture.

#### Materials:

Bacterial strains *Gluconacetobacter Xylinum* (GX) (ATCC 11142) (1, 2) and *Gluconacetobacter Europeaus* (GE) (MF03) (2, 3) were purchased from CECT (Spain). Glucose, peptone, yeast extract and agar were purchased from Conda Lab. NaOH, Na<sub>2</sub>HPO<sub>4</sub>•12H<sub>2</sub>O and citric acid monohydrate were bought from Sigma Aldrich and used as received.

The laboratory system used is depicted in **Figure 2.1**, which is similar to the static culture approach mentioned in Chapter 1. I used an Erlenmeyer as a fermentor with a fixed amount of medium covered by an aluminium foil. The amount of medium can be changed depending on the different culture days. The aluminium foil prevents the system from being contaminated and also allows some oxygen in the fermentor.

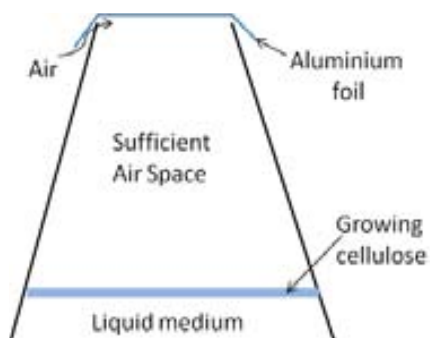


**Figure 2.1** Our laboratory culture system.

The growth medium for GX and GE are presented in **Table 2.1**. They are very similar except for a few changes which depend on the description of the bacteria company.

**Table 2.1** Reagents for GX and GE growth medium (Solid and Liquid Medium).

Components	Solid Medium (GX)	Liquid Medium (GX)	Solid Medium (GE)	Liquid Medium (GE)
Glucose (g/L)	20	20	50	50
Peptone (g/L)	5	5	0	0
Yeast extract (g/L)	5	5	10	10
Citric acid monohydrate (g/L)	1.15	1.15	0	0
Na <sub>2</sub> HPO <sub>4</sub> ·12H <sub>2</sub> O (g/L)	6.8	6.8	0	0
Agar (g/L)	15	0	15	0
Distilled water (L)	1	1	1	1

1 L sample culture media for GX consisted of 20 g glucose, 5 g peptone, 5 g yeast extract, 1.15 g citric acid monohydrate, 6.8 g Na<sub>2</sub>HPO<sub>4</sub>·12H<sub>2</sub>O and 15 g agar (only for solid medium).(4) Culture media for GE was composed of glucose 50 g, yeast extract 10 g and 15 g agar (only for solid medium).(4, 5) All bottles containing solid or liquid medium of GX and GE were then autoclaved (**Figure 2. 2, r ight**) at 120 °C for 30 min. After sterilization, the bottles containing liquid medium were allowed to cool down to room temperature for further use. The rest of the bottles containing solid medium with agar were immersed in warm water to prevent the medium becoming solid.



**Figure 2.2** Work place in a aseptic hood (left) and the autoclave for sterilization (right).

**Step 1:** Preparing culture plates containing agar medium and nutrients for GX and GE (**Figure 2.3**)

For short-term maintenance and use, it is best to grow bacteria on nutrient agar plates. The best place to successfully and safely grow bacteria are in specially shaped glass or plastic petri dishes. In our case, we were using pre-sterilized plastic petri dishes. All the experiments have been done in an aseptic environment see **Figure 2.2 (Left)**.

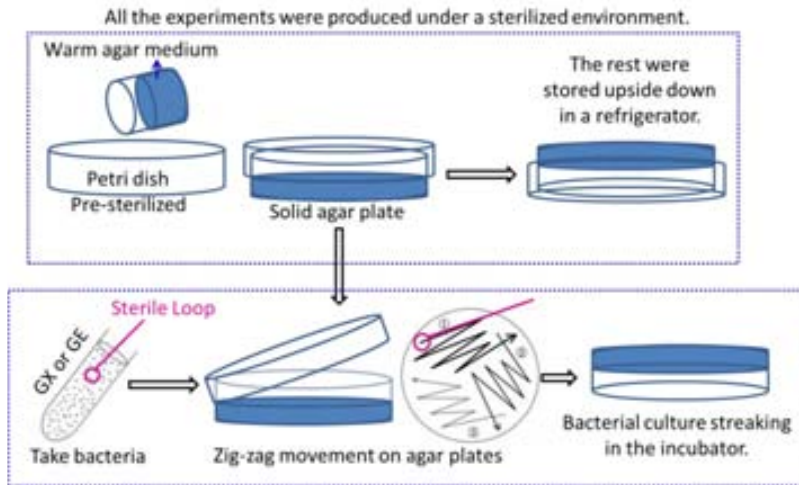


**Figure 2.3** Steps in preparing solid agar plates (top) and how to culture bacteria on the surface of the solid agar plate (bottom).

First of all, I poured the warm agar medium into a petri dish and tilted from side to side to coat the bottom. Then the lid was placed promptly to avoid bacteria and mold settling out of the air onto the growth medium and creating contamination. For the growth of bacteria on agar plate, only a thin layer is required. As soon as the agar plates were set to a hardness similar to Jell-O, they were ready to be used. Normally, I stored the agar plates in the refrigerator room overnight to get them fully hardened, which prevented surface tearing when I wiped or transferred the samples. The rest of the prepared agar plates were refrigerated until used and always stored upside down, **Figure 2.3**. This keeps condensation which forms in the lid from dropping onto the agar and disrupting the bacteria growing surface. (**Note:** If you store the agar plates in a refrigerator, be sure to allow your prepared agar plates to come back to room temperature before you add bacteria.)

Secondly, I used sterile plastic loops to take some bacteria from the tube (GX and GE bacteria from CECT company). Then using a prepared agar plate, I lifted the lid just enough to insert the sterile plastic loop. I streaked the loop containing the bacteria at the top end of the agar plates moving in a zig-zag horizontal pattern until 1/3 of the plate was covered. I rotated the plate about 60 degree and spread the bacteria from the end of the first streak into a second area using the same zig-zag motion. I rotated the plate 60 degree more and spread the bacteria from the end of the second streak into a new area in the same plate. Finally, I put all the agar plates containing bacteria in an incubator at 24 °C for about 3 days, with the plates upside down. This trick is regularly used by labs since it prevents the condensed water droplets to fall over the agar medium and initiate contamination. Bacterial culture streaking allows bacteria to reproduce and spread on the surface of the agar medium for a period of time. (**Note:** Incubate the plates only until good colonies have formed. Do not leave the

culture in the incubator beyond 3 days, or the bacteria will die on the plate. Store the plates in the refrigerator, and it will keep for about 2 months).

Long-term maintenance of bacteria is not easy and it is not generally recommended. After the first time of growing bacteria on the agar plates, the rest of the bacteria from the tubes were mixed with glycerol as a cryoprotectant and then frozen in  $-80\text{ }^{\circ}\text{C}$  refrigerator. In our case, we have confirmed they can be stored for 1-2 years. This is probably the best method for bacteria storage. (*Note:* If you need to refresh a new agar plate for bacteria, you have to pick a colony and scrape off a little of the bacteria from the old plate, and then streak them to the new agar plate.) The same process was used for GX and GE.

**Step 2:** Re-growth bacteria from the plates and transfer to an Erlenmeyer to produce cellulose

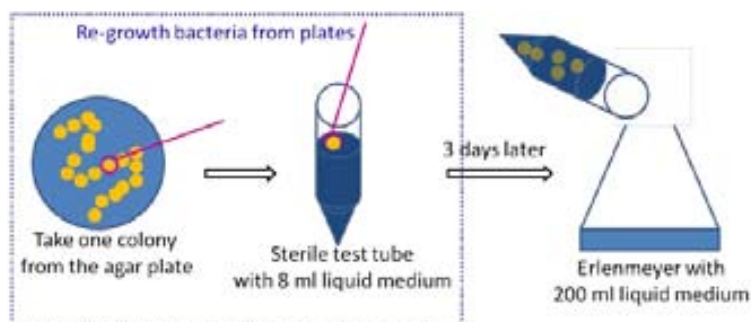


**Figure 2.4** Steps in re-growing bacteria from the solid agar plates and transfer to an Erlenmeyer.

After 3 days, I obtained isolated and pure bacterial colonies from a mixed population (**Figure 2.4**). It was, then, determined to be necessary to re-grow bacteria from the plates in a small amount medium, since I had failed to produce BC directly in an Erlenmeyer with a colony bacterium. This was done in order to prevent shocking the bacterial culture. In the case of re-growth from the agar plates, first 8 mL of liquid medium was poured off into a sterile test tube and seeded with a colony from the agar plate. After about 2 – 3 days of static culture in the incubator, the 8 mL liquid medium with more bacteria were transferred aseptically to an Erlenmeyer of 1 L with 200 mL liquid medium. Samples were then kept undisturbed using a plastic box as an incubator at  $26\text{ }^{\circ}\text{C}$  to produce the BC pellicle, for a minimum of 5 days and as long as 2 weeks. Growth of BC were found to work best if samples were allowed to sit in static culture. A 0.35 cm thick pellicle from the GX sample was achievable after 5 days. The pellicle from the GE sample grown during the same time was about 0.20 cm in thickness, which was thinner than GX pellicle, as can be clearly seen in **Figure 2.5**. In order to get the same pellicle thickness from both GX and GE bacteria, I kept the GE bacteria growing 5 days longer until the thickness was also around 0.35 cm.

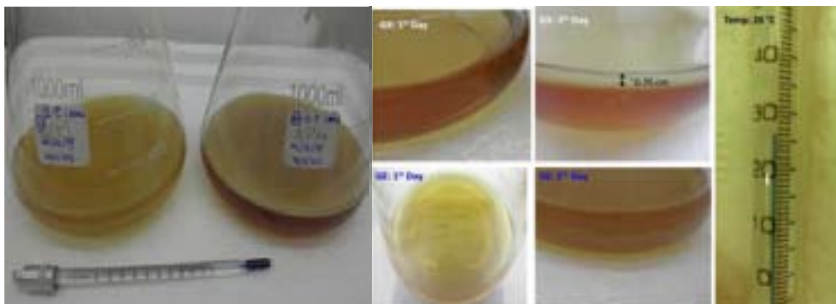


**Figure 2.5** GX and GE were growing in Erlenmeyer statically and inside a plastic box (not seen) at around 26 °C. After 5 days, the cellulose pellicles appeared on the top of the medium. GX produced a thick layer around 0.35 cm. GE produced a thin layer of cellulose, around 0.2 cm.

Once obtained, the pellicles were separated from the culture medium and kept in ethanol until the purification steps. (**Note:** Always dispose of the cultures properly when the culture process is completed. Pour a small amount of a strong disinfectant (household bleach in my case) over the colonies of the agar plates and also in the rest of the culture media to destroy the bacteria before disposing of them).

## 2.2 Cleaning process

When BC pellicles are harvested from the air/liquid interface, aside from the cellulose they contain a large amount of water, bacteria and other constituents of medium (**Figure 2.6** left). Thus, the pellicles have to be cleaned. Firstly, the pellicles were boiled with water, and then treated in alkali media.



**Figure 2.6** A harvested untreated pellicle of GX cellulose (left), compared with the one after clean treatment (right).

Pellicles of BC were immersed in ethanol. Subsequently, they were transferred to deionized (DI) water in an Erlenmeyer and boiled for 40 min with continuous stirring. After this cleaning, the pellicle changed colour from brownish yellow to milky white, indicating that most of the medium and bacteria were removed (**Figure 2.6** right). The alkaline treatment consists of soaking the pellicles in a NaOH solution. Several concentrations (from 0.1% to 5%) of NaOH solution have been described in literature but I have observed that the optimum conditions seem to be around NaOH 0.5 % and 90 °C in my case.(5, 6)

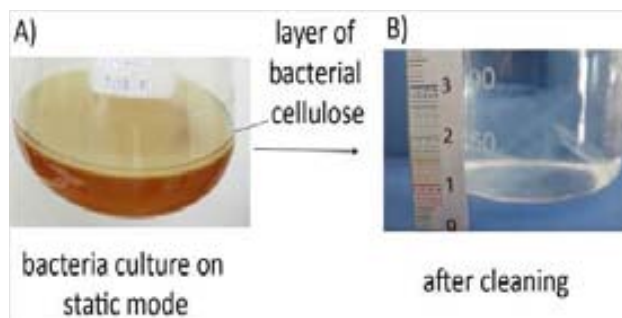


**Figure 2.7** Pellicles of A) uncleaned BC and B) cleaned BCFs.

The gel-like pellicles were boiled and cut into rectangular-shaped pieces, and then treated four times in 0.1 M aqueous NaOH at 90 °C for 20 min each time. After the alkali treatment, BCFs increased their transparency (**Figure 2. 7**). Finally, the BC pellicles were neutralized with DI water. They were shaken regularly and the water was refreshed every 6 hours until the pH reached a neutral value. After alkali treatment and washing in distilled water, the BC can be dried.

### 2.3 Drying process

After the cleaning process, I obtained pure, wet and gel-like BCFs in an Erlenmeyer with DI water. We target to study how the uses of different drying methods change the film properties and can enable us to tailor the properties of our BCFs.

#### Drying methodology

BCFs which had never been dried were cut into rectangular pieces of 1 □ 2 cm. Before drying, samples were placed over a sheet of chromatography paper and kept between two glass slides during the drying process. We created an accordion-like set-up; up to 10 wet BCFs were placed in the same setup. It was done to prevent bending during drying. (**Figure 2. 8** shows the schematics and picture of the drying setup).

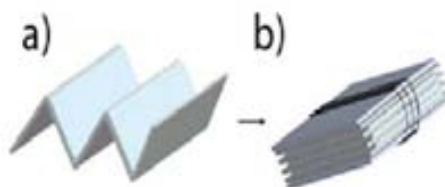


**Figure 2.8** a) Accordion-like set up made with a chromatography paper; b) folded set up containing the wet BCFs before drying.

---

### Three different drying methods

The selected drying methods provide different physical processes to evaporate the solvent content (water or ethanol) within the BCFs.

#### 1) Room temperature drying method (RD)

The room temperature drying method (RD) is the cheapest and easiest one, which is natural air drying. The process is slow and weather-dependent.

BCFs placed in the shown accordion-like setup were left in air and underwent a slow drying for 4 days until the BCFs were completely dried. When drying at room temperature, capillary pressures of the water meniscus exert a compressive force in the pores of the films that may induce the modification of the structure, and thus in the density and porosity of BCFs.

#### 2) Freeze drying method

The second method is freeze drying (FD), which is also known as lyophilization or cryodesiccation. It is a dehydration process typically used to preserve a perishable material or make the material more convenient for transport.

I froze the BCFs and then reduced the pressure to allow the frozen water in the material to sublime directly from the solid phase to the gas phase, **Figure 2.9**. There are two main steps in this drying process: freezing (step 1) and drying (step 2). This method avoids a large extent capillary stress in the pores which leads to a reduced shrinkage of the gel skeleton.

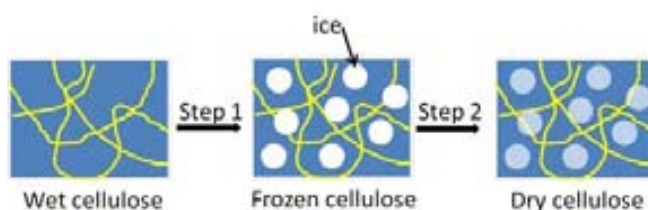


**Figure 2.9** Two steps of BCFs freeze drying process. Step 1: wet BCFs were frozen by liquid nitrogen (liquid phase to solid phase), step 2: solid water (ice) was sublimated from the BCFs.

#### Freezing (step 1: liquid phase to solid phase)

Usually freezing is done using a dedicated apparatus. In a lab, this can be also achieved by placing the material in a drying flask and rotating the flask in a bath, which is cooled by using dry ice and methanol, or liquid nitrogen. In this step, it is important to cool the material below its triple point, the lowest temperature at which the solid and liquid phases of the material can coexist. So I plunged -froze the BCFs in the setup with liquid nitrogen for 5 min in a 50 mL falcon tube.





**Figure 2.10** The frozen BCFs were placed in LYOQUEST- 85 freeze- drier/ Telstar (right).

Drying (step 2: solid phase to gas phase)

Frozen BCFs were subsequently placed in a LYOQUEST-85 freeze drier Telstar (**Figure 2.10**) at  $-80^{\circ}\text{C}$ , below 0.5 mbar for 12 h. During the drying phase, the pressure is lowered (to the range of a few millibars) for the solid water in the BCFs to sublime. This step should be slow (can be several days in the industry), because, if it is too fast, the BCFs structure could be altered. In this phase, pressure is controlled through the application of partial vacuum. The vacuum speeds up the sublimation, making it useful as a deliberate drying process. After the freeze-drying process is complete, the vacuum is slowly broken with an inert gas, such as nitrogen, before the BCFs are sealed.

### 3) Supercritical drying

Supercritical fluid (SCF) is defined as a single fluid phase which occurs when the temperature and pressure of a compound or mixture is above its critical temperature and pressure (critical point). This fluid exhibits similar physical properties to the liquid phase (density, thermal conductivity) and also to the gas phase (it fills its container, does not have surface tension). Under ambient conditions, during the evaporation of the solvent, a liquid-vapor interface is formed within the pores of the material. The surface tension of the liquid creates a concave meniscus in each capillary. Above the critical point (**Figure 2.11**) the two phases no longer exist and a single supercritical fluid phase is presented, so the liquid meniscus and its interfacial tension would not form in these conditions. The supercritical drying process is able to avoid the pore collapse and to keep the porous texture of the wet material intact.

The supercritical drying process consists of three important steps: 1) pressurization combined with heating to reach SCF conditions, (1-3 or 1-2-3 in **Figure 2.11**). 2) Continuous flushing with fresh SCF is used to remove any unreacted species, and 3) depressurization is used to remove the fluid phase (3-4 in **Figure 2.11**). In this way the interface of gas and liquid is circumvented. It should be noted that the heating in 1-3 or 2-3 and depressurization in 3-4 must be slow enough to avoid shear stress and consequent cracks in the nanostructure.

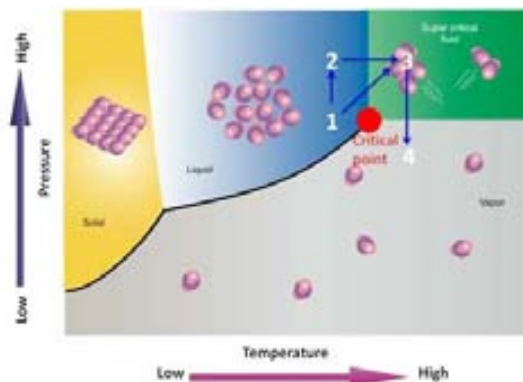


**Figure 2.11** Schematic representation of Supercritical Drying: the solvent is pressurized and heated beyond the critical point via one of two pathways either path 1-3 or path 1-2-3. Then this is followed by depressurization (path 3-4).

Fluids suitable for supercritical drying include carbon dioxide; CO<sub>2</sub> is of particular interest since it is non-flammable, non-toxic, abundant and inexpensive. Moreover, CO<sub>2</sub> has a relatively low critical temperature (304.2 K) and a moderate critical pressure (7.375 MPa). The relatively low temperature of the process and stability of CO<sub>2</sub> also allows most compounds to be extracted with little damage or denaturation. In addition, the solubility of many extracted compounds in CO<sub>2</sub> varies with pressure, permitting selective extractions. Furthermore, supercritical carbon dioxide has also been used as a multi-functional medium for processing of BC aerogels.(5, 7-11)

The supercritical drying process was performed on SCF 300 mL Plant (**Figure 2.12**) in MATGAS, Spain. scCO<sub>2</sub> involves the exchange of the water solvent within the BCFs by ethanol and further exchange of ethanol with liquid CO<sub>2</sub> in the reactor and the final evacuation of the CO<sub>2</sub> in the supercritical phase. First of all, the BCFs were subjected to the first solvent exchange step, which was performed by gently shaking the BCFs in absolute ethanol. After 6 and 12 h, the gels were transferred two times to a fresh ethanol bath without shaking. After another 6 h in ethanol, the resulting alcogels were placed in our homemade holder (**Figure 2.12D**) and loaded into a 300 mL autoclave vessel (**Figure 2.12A**) filled with ethanol. Secondly, the autoclave was pressurized to 100bars at room temperature. We exchanged the ethanol with liquid CO<sub>2</sub> at a flow rate of 1 kg/h for 1.5 h. Then we heated the reactor at 45 °C (**Figure 2.12B**) with a CO<sub>2</sub> flow of 1 kg/h for 1h. At 45°C and 100bar, the system was at the supercritical state. After drying transient period, the evacuation of solvents in supercritical conditions is very important and must be done slowly; this can prevent the pores collapsing. Finally, I slowly depressurized the autoclave and removed the dry BC aerogels.



**Figure 2.12** The CO<sub>2</sub> supercritical drying system from MATGAS, Spain. A and C) the vessel of SCF 300 mL plant, B) heater, D) our homemade sample holder.

After drying I labeled the obtained films as BCX or BCE depending on the bacteria types used and SCD for supercritical drying, FD for freeze drying, RD for room temperature drying, while for wet films they are labeled as BCX-Wet and BCE-Wet (**Figure 2.13**).

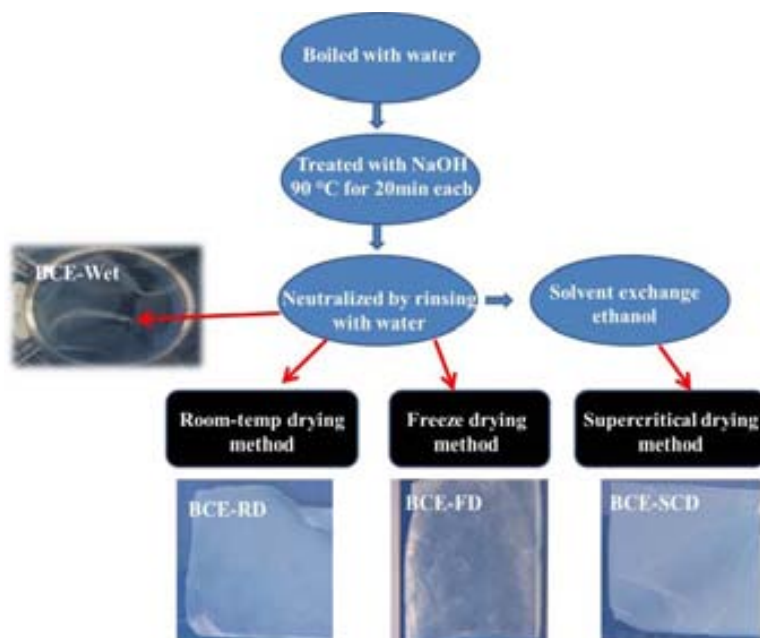


**Figure 2.13** After the cleaning and drying processes, I labelled the obtained films as BCE-RD, BCE-FD and BCE-SCD. (RD is room temperature drying, FD is freeze drying and SCD is supercritical drying). While BCE-Wet is the wet cellulose film without any drying processes. A similar labelling was followed for the GX strain.

## 2.4 Characterization of bacterial cellulose films

### Chemical structure and purity

BC is a biopolymer comprising of  $\beta$ -D-gluco-pyranose units linked through  $\beta$ -(1, 4) glucosidic linkages, which can be characterized by FTIR spectroscopy. Furthermore, FTIR can help us to check the purity of the BCFs after cleaning. I folded the BCFs 5 times and placed them onto the Universal diamond ATR top-plate (Perkin Elmer). IR spectra were acquired using a PerkinElmer FT-IR Spectrum One with U-ATR at  $4\text{ cm}^{-1}$  resolution, between  $4000$  to  $500\text{ cm}^{-1}$  using 4 scans and a pressure force between 80 % and 90 %.

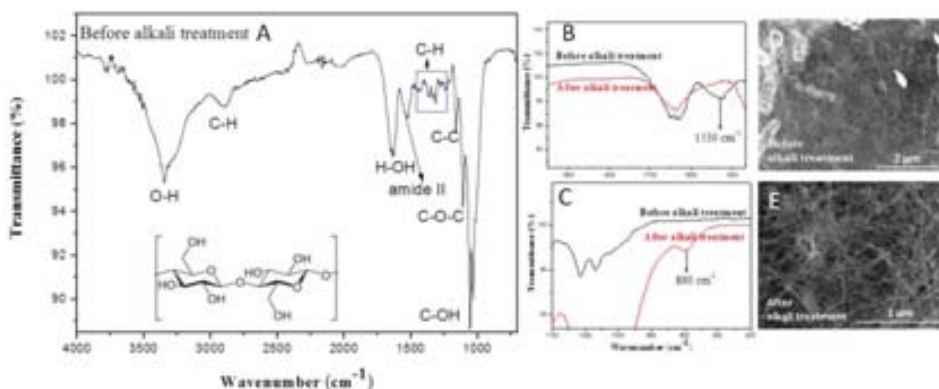


**Figure 2.14** A) FTIR spectrum of cellulose before alkali treatment (BCE), B) IR spectra of cellulose (before and after alkali treatment). After alkali treatment, the  $1530\text{ cm}^{-1}$  peak disappeared. This could be because of the removal of amide groups present in biological impurities during the alkali treatment, C) A new band appeared after alkali treatment, which was identified as the conversion of cellulose I to cellulose II structure. D) SEM image of BCE (before alkali treatment). It was clearly shown that there are still impurities in the cellulose, E) SEM image of BCE (after alkali treatment).

**Figure 2. 14-A** depicts the FTIR spectra of BC dried before the alkali treatment.(12, 13) A broad adsorbing band observed around  $3350\text{ cm}^{-1}$  corresponds to the  $-\text{OH}$  stretching vibrations of the BC ( $-\text{OH}$  groups).(14) The C-H stretching vibration bands of  $-\text{CH}_3$  and  $-\text{CH}_2$  groups are observed as a broad band centered at  $2890\text{ cm}^{-1}$ , while bending bands of these groups are noticed at  $1430$ ,  $1366$ ,  $1336$  and  $1314\text{ cm}^{-1}$ .(15, 16) The peak of  $1640\text{ cm}^{-1}$  is due to H-OH bending vibration of adsorbed water molecules in BC. The band at  $1160\text{ cm}^{-1}$  corresponds to the C-C stretching, which is the asymmetric ring breathing mode while at  $1108\text{ cm}^{-1}$  corresponds to glycosidic C-O-C stretching vibration. The two bands at  $1055\text{ cm}^{-1}$  and  $1028\text{ cm}^{-1}$  correspond to the C-OH stretching vibration of secondary and primary alcohols of BC, respectively. The peak around  $1530\text{ cm}^{-1}$  is the main difference observed in the spectra of native (before alkali treatment) and alkali treated BCFs (**Figure 2.14-B** and all spectra of BCX and BCE in **Figure 2.15**). This peak corresponds to amide II band of

proteins and other biological impurities in cellulose which were only cleaned by boiling water without NaOH treatment.

As I explained before, the first cleaning process (boiled cellulose in water) can remove the most medium and bacteria, but not all the biological impurities present in our BCFs. It was also supported by SEM image (**Figure 2.14-D**). After alkali treatment, a new band centered around  $890\text{ cm}^{-1}$  emerged (**Figure 2.14-C** and all the spectra of BCX and BCE in **Figure 2.15**). Dinand et al.(17) have assigned the band around  $895\text{ cm}^{-1}$  as the conversion of native cellulose (cellulose I) to cellulose II allomorph. A similar phenomenon was noticed with all the BCFs after alkali treatment.

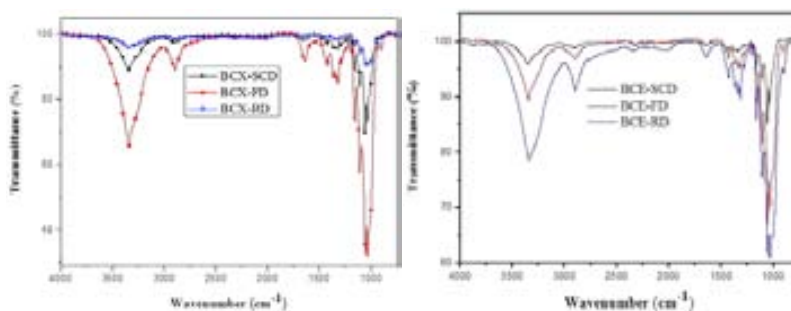


**Figure 2.15** FTIR spectra for BCX films (left) and for BCE films (right).

## Crystallinity

The crystallinity index of BC is an important parameter to establish because of the effect this property has on the utilization of BC as a material.(18) However, it has been reported that the crystallinity index varies significantly depending on the choice of instrument and data analysis technique applied to the measurement (For example: XRD or NMR).(19, 20) The most common method is X-ray Diffraction method, which has been described in literature.(18, 21-24)

BCX and BCE films were fixed flat on a silicon wafer to perform the XRD measurement. The XRD patterns of all the samples were recorded using an X-Ray Diffractometer (Siemens, Model D-5000 system), using a Cu anode with  $\lambda_{K\alpha 1}=1.540560\text{ \AA}$  and  $\lambda_{K\alpha 2}=1.544390\text{ \AA}$  in the  $2\theta$  range of  $3 - 60^\circ$  using a step of  $0.02^\circ/\text{min}$ . The crystallinity of our BCFs was calculated from the ratio between the intensity of the crystalline peaks ( $I_{200} - I_{am}$ ) and the total intensity ( $I_{200}$ ) after subtraction of the background signal measured without BC.(21, 25) The height of the peak at (200) represents the crystalline part  $I_{(200)}$  and the minimum height between (200) and (110) peaks the amorphous part,  $I_{(am)}$ . All the peaks were computed by Spectrum Viewer Basic 2.6.

Equation 1 
$$\text{CrI} = (I_{(200)} - I_{(am)}) / I_{(200)}$$

In addition to crystalline disorder (amorphous content), there are other intrinsic factors that influence peak broadening, such as non-uniform strain within the crystal and crystalline size. The crystal size can be calculated using the (200) peak, it was computed using Scherrer's equation: (22, 26)

$$\text{Equation 2} \quad L(hkl) = k \lambda / (B \cos\Theta)$$

Where  $L$  is the crystallite domain,  $\lambda$  is the X-ray wavelength,  $\Theta$  is diffraction angle in radians and  $B$  is the full width at half maximum of peak ( $B^2 = B_{\text{total}}^2 - B_{\text{instrument}}^2$ ),  $B_{\text{total}}$  is the integral breadth in radians of diffraction angle and  $B_{\text{instrument}}$  is the instrumental integral breadth in radians and  $k$  (Scherrer constant) is a dimensionless shape factor. The shape factor has a typical value of about 0.9, but varies with the actual shape of the crystal,  $k = 0.94$  was chosen in our case.(27, 28) Using Bragg equation, we calculated the inter-planar spacing between the atoms in the crystal ( $d$  spacing).

$$\text{Equation 3} \quad n \lambda = 2 d \sin\Theta$$

As mentioned in Chapter 1, BC is a semi crystalline material with a composite structure of cellulose  $I_\alpha$  and  $I_\beta$ , and produce broad diffraction peaks.  $I_\alpha$  polymorph predominates in cellulose from bacterial origin (29-31) although after alkaline treatment or hydrothermal annealing  $I_\alpha$  transforms to  $I_\beta$  and also cellulose I could convert to the stable crystalline form of cellulose II.(22, 32) These conversions complicate the elucidation of the polymorphs in the XRD powder characterization, this issue still raises controversies and a considerable amount of research.(23) We evaluated the XRD graphs for the two different strains and three different drying methods. **Figure 2.16** present the XRD graphs for the BCFs from two different origins dried using room temperature and it seems that BCX strains show XRD patterns at slightly higher angles than the BCE strain. After the alkali treatment all of our BCFs showed three main peaks at  $2\Theta$ , peak 1:  $14.5^\circ \pm 0.2^\circ$ , peak 2:  $16^\circ \pm 0.6^\circ$  and peak 3  $22.7^\circ \pm 0.2^\circ$ , (values averaged from all the BCFs, **Figure 2.17**). These peaks could be attributed to the two polymorphs of cellulose I and some contribution of cellulose II (FTIR also indicates the presence of cellulose II).

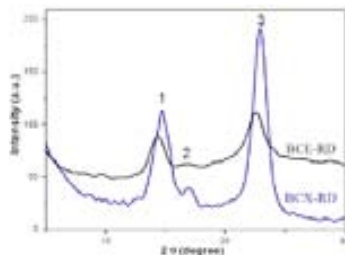


**Figure 2.16** XRD diffraction patterns for BCX-RD and BCE-RD film.

The diffraction peak at  $14.5^\circ \pm 0.2^\circ$  with  $d$ -spacing of  $0.61 \pm 0.01$  nm (mean values of all the BCFs) corresponds to the (100) plane of  $I_\alpha$  or to the (1-10)

plane of  $I_{\beta}$ . The peak at  $16 \bar{1} 0.6^{\circ}$  with d-spacing of  $0.55 \pm 0.02$  nm is ascribed to the (010) plane of cellulose  $I_{\alpha}$  or the (110) plane of cellulose  $I_{\beta}$ . The peak at  $22.7 \bar{1} 0.2^{\circ}$  corresponding to  $0.39 \pm 0.01$  nm d-spacing could be the contribution from the (110) plane of cellulose  $I_{\alpha}$  the (200) plane of cellulose  $I_{\beta}$  and also of the peak (200) plane of cellulose II. **Table 2.2** summarizes the main features computed from the XRD patterns of all the BCFs.

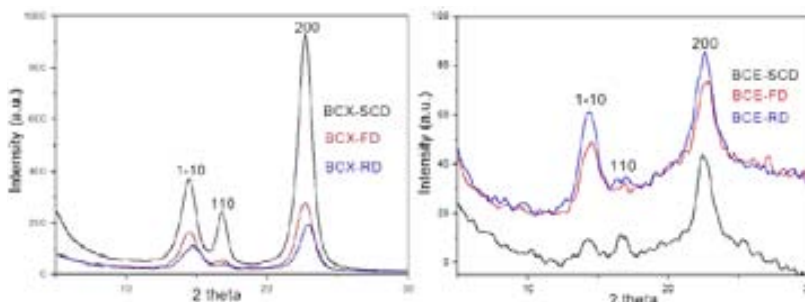


**Figure 2.17** X-ray diffraction pattern for BCX films and BCE films.

**Table 2.2** Summary of the main features from the XRD patterns for all the BCFs. d is the d-spacing, L crystallite size computed for each plane and CrI is the percentage of Crystallinity.

Samples	Peaks (2 $\theta$ ) <sup>a</sup>	d (nm)	L (nm)	CrI %	Samples	Peaks (2 $\theta$ ) <sup>a</sup>	d (nm)	L (nm)	CrI %
BCE-RD	14.2	0.62	5	72	BCX-RD	14.7	0.60	4	91
	16.0	0.55	6			16.1	0.52	8	
	22.6	0.40	5			22.9	0.39	5	
BCE-FD	14.6	0.61	5	76	BCX-FD	14.5	0.61	5	91
	16.0	0.55	6			16.1	0.55	8	
	22.8	0.39	5			22.7	0.39	5	
BCE-SCD	14.7	0.60	7	83	BCX-SCD	14.5	0.61	5	97
	15.4	0.58	7			16.9	0.52	8	
	22.4	0.40	6			22.7	0.39	6	

Relative crystallinity (CrI) of BCFs was calculated using the intensity of the (200) peak considering equation 1 and yielding  $91 \bar{1} 4 \%$  for BCX films,  $76 \bar{1} 6 \%$  for BCE films. It seems BCX strain offers higher crystalline films than BCE strain. It is noticeable that for each strain films dried using SCD present higher crystallinity. Since for each strain, all BCFs derive from the same initial sample, any variations in the crystallinity and crystal size are caused by the drying methods. The higher temperature of the drying with SCD,  $45^{\circ}\text{C}$ , could afford this small increase of crystallinity. Briefly, we have indentified some small changes in the XRD patterns and crystallite sizes and possibly in the  $I_{\alpha}/I_{\beta}$  ratio for the different strains and methods of drying used. As mentioned previously the exact determination of the  $I_{\alpha}/I_{\beta}$  ratio is a complicated measurement outside the scope of this thesis, although we believe it is an interesting feature which could be expanded in the future.

---

## Microstructure

BCFs present an open porous network formed by cellulose fibres confirmed by scanning electron microscopy (SEM), **Figure 2.18**. Similar to previous reports,(33, 34) BCFs show a hierarchical structure with pores of different sizes from macro to micro. For both strains, the SCD drying method offers the most open structure and a higher presence of individual fibrils than FD and RD films.

Individual BC fibrils measured by SEM are approximately  $18 \pm 2$  nm in thickness independently of the strain and the drying method used. Thus, the strain used or the drying methods do not seem to influence the fibril size which is somehow surprising considering the difference in the BC growth rate of the two strains. In contrast, a detailed observation of the images showed that the drying method, impacts on the fibre entangling. Analyzing in detail several SEM images, I computed that for both strains,  $85 \pm 2$  % of the fibres form bundles in the films dried at RD and FD whereas we detect just a  $38 \pm 2$  % of the fibres forming bundles in SCD films. Moreover, BCX-SCD is the material with the most differentiated microstructure since I distinguish a higher number of individual fibres, less entanglement and some degree of directionality of the fibres in comparison to the rest of the films. Some detailed studies to elucidate if fibre directionality induces anisotropic mechanical behaviour will be analyzed.

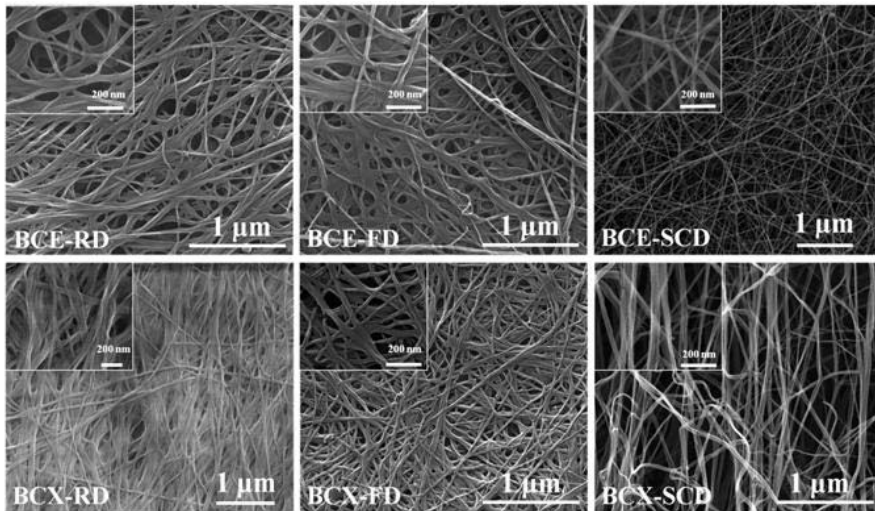


**Figure 2.18** SEM images of the BCFs obtained after different drying conditions. Inserts show higher magnification images of the films.

The thickness of wet BCFs and also the dry films were measured using an optical microscope (Olympus IX-71, program of Stream Essential 1.7) in differential interference contrast microscopy mode. The initial thickness of the wet BCFs was around  $200 \mu\text{m}$  (**Figure 2.19**) and after drying the computed thickness of all BCFs decreased, ranging from  $67 \mu\text{m}$  to  $24 \mu\text{m}$ , although these



values vary slightly from batch to batch. **Table 2.3** summarizes the film thicknesses of the dried films (n=10: the measurements were repeated 10 times.). For both strains (BCX and BCE), films dried in SCD conditions are thicker than films obtained by FD and RD. The elimination of the solvent meniscus during supercritical solvent evacuation, avoids the effects of the capillary forces, as previously described.

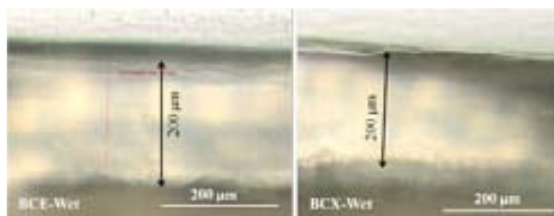


**Figure 2.19** Optical microscope images of the thickness of BCX-Wet and BCE-Wet films. n=12 means 12 time repeat.

Density values ( $\rho$ ) were determined from weighing the materials and measuring the BCFs volume. Films produced by GE are extremely light materials with densities around 0.08 - 0.05 g/cm<sup>3</sup> showing only a slight dependency of the density with the drying method. Densities of the BCX films are in the 0.16 - 0.6 g/cm<sup>3</sup> range and they strongly depend on the drying method used. BCX films dried by SCD are lighter than FD and RD ( $\rho_{BCX-RD} > \rho_{BCX-FD} > \rho_{BCX-SCD}$ ), although they are still two times denser than any BCE film ( $\rho_{BCX} > \rho_{BCE}$ ), see **Table 2.3**.

**Table 2.3** Summary of the structure values obtained for the BCX and BCE films.

Drying method	RD		FD		SCD	
Strain	BCE	BCX	BCE	BCX	BCE	BCX
Film Thickness ( $\mu\text{m}$ )	24 $\pm$ 2	37 $\pm$ 2	34 $\pm$ 2	40 $\pm$ 4	58 $\pm$ 3	67 $\pm$ 2
Density (g/mL)	0.08 $\pm$ 0.01	0.59 $\pm$ 0.03	0.06 $\pm$ 0.01	0.32 $\pm$ 0.02	0.05 $\pm$ 0.01	0.16 $\pm$ 0.01
Total Porosity (%)	94 $\pm$ 2	60 $\pm$ 2	95 $\pm$ 2	79 $\pm$ 2	96 $\pm$ 2	89 $\pm$ 2
Fibers diameter (nm)	17 $\pm$ 2	19 $\pm$ 3	20 $\pm$ 4	19 $\pm$ 3	16 $\pm$ 2	20 $\pm$ 4

From the density values one can evaluate the total porosity of the films from the equation:

$$\text{Total porosity } (\phi) = 1 - (\rho_{BCF} / \rho_{\text{cellulose}})$$

We have assumed a  $\rho_{\text{cellulose}} = 1.5 \text{ g/cm}^3$  for both strains, which may be an over-assumption knowing that crystallinity is slightly dependent on the strain.(35-37) Following the same trend as for the density, we observed that BCE films have porosity larger than 94 % for the three drying methods. On the other hand, BCX films are less porous and their porosity strongly depends on

the drying method used. We believe that the slow formation of the cellulose fibrils in GE influences the microstructure of the film, forming fibrils more resistant to compact and finally affording a more spongy structure.(35-37)

### Water absorption capacity

BC was described by Louis Pasteur as “a sort of moist skin, swollen, gelatinous and slippery”. The topical applications of BC are effective due to the water holding ability of cellulose or water absorption capacity. The use of BC as temporary skin is already patented and commercialized as BioFill®. This is because the high water holding ability provides a moist atmosphere at the injury site, which is critical in healing. BC materials are good absorbents, this property also identifies them as excellent candidates, for instance, for organic pollutants, absorbents and catalysts (improved efficiency of enzyme loading).(38, 39) This property is also exploited in order to create BC composites with a high yield of the different components, for instance in anti-bactericidal BC patches that need a homogeneous and high loading of Ag nano-particles.(40, 41)

Absorption tests start by immersing the two strains of BCFs in the same distilled water at room temperature, followed by periodically weighing them. Before the experiment, all the BCFs have been weighed and recorded. I immersed them in distilled water for 1h, 2h, 48h and 72h. Excess water was removed at each time and the weight was measured again. The water absorption capacity was measured using:

$$\text{Equation 3} \quad \text{WAC} = (W_{\text{wet}} - W_o)/W_o$$

Where  $W_{\text{wet}}$  is the weight of wet BCFs and  $W_o$  is the initial weight of the dried BCFs.

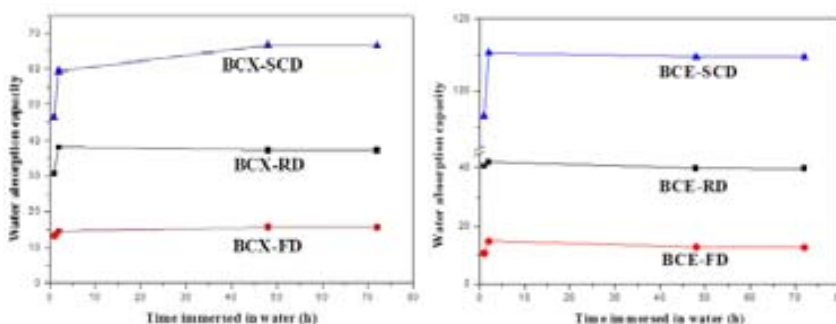


**Figure 2.20** Water absorption capacity (WAC) of BCX films (left) and BCE films (right) over time.

I measured the water absorption capacity and evaluated how the different drying methods (**Figure 2.20**) and therefore, the microstructure influence the water absorption capacity (WAC). WAC shows a strong influence of the drying method used. Supercritical dried films present the highest water absorbance

capability of all the films, obtaining water absorption capacities of up to 110 times its own weight for BCE-SCD films, **Figure 2.20** and **Figure 2.21**. FD films showed lower water absorption than RD for both strains. SCD drying method emerges as an ideal methodology to improve WAC in native BCFs. I also calculated different times immersed in water and concluded that around 48 hours is enough to reach the equilibrium.

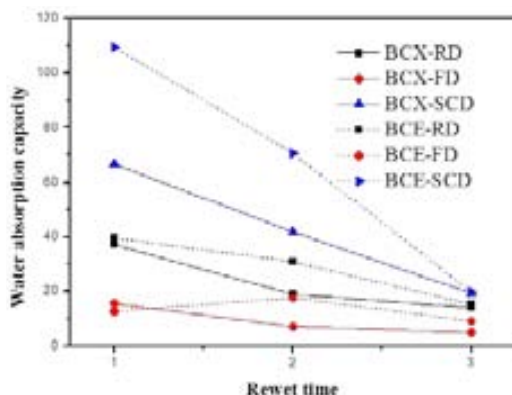


**Figure 2.21** WAC of mass of the water absorbed per mass of BCFs after three wetting-drying cycles.

The ability of the films to converge the WAC capacity after drying at room temperature was evaluated performing some wetting-drying cycles. I dried and weighed BCFs, upon immersion in distilled water at room temperature for two days (48 hours) they were weighed again. WAC quantifies the percentage of water absorbed in each film. I repeated two times the water absorption cycle drying them at room temperature. The weight of the dry films at the start of each WAC cycles did not change. After three wetting-drying cycles, the WAC values converged for all the drying methods and the BCFs still held up to 20 times their weight of water after 3 cycles, **Figure 2.21** and **Table 2.4**. We hypothesized, since in the WAC cycles we dry the films at room temperature, we compact the tridimensional structure of the film in each cycle until they all become similar.

**Table 2.4** Water Adsorption Capacity (WAC) results after 3 cycles.

Drying method	RD		FD		SCD	
Strain	BCE	BCX	BCE	BCX	BCE	BCX
1 <sup>st</sup> cycle	39.5	37.3	15.8	15.8	109.4	66.6
after 3 cycles	15.3	14.2	9.2	5.0	19.8	19.4
Decrease (%)	61	62	42	68	82	71

---

## Optical properties

Transparency is one of the interesting properties of BC. For instance, the applications of electronics(42) could also be expanded in water-based applications, in cell-based membranes, in skin-patches with flexible electronics since they could help to monitor wound healing, in sensors devices where we could envisage the transport of the liquid without the need of external power, we could image its reactivity from the change in transparency. Evaluation of the water absorption capacity also revealed that the films increased their transparency upon wetting (**Figure 2.22**).



**Figure 2.22** Pictures of BCs before and after WAC test.

Pictures depicting the qualitative measurement of the transparency for the BCs before and after WAC cycles are shown in **Figure 2.22**. Films are placed in contact with the paper below. In order to see the difference, the paper was marked by the blue “aerogel”. Here, I present BCE-SCD film that was getting more and more transparent when it was immersed in distilled water (**Figure 2.23**). After one WAC cycle, this BCE-SCD film was rewetted and dried again. It became more transparent than the chromatography paper. This is likely to be related to the collapse of pores in the size range with larger visible wavelengths scattering effect.



**Figure 2.23** Optical image of one sample (BCE-SCD film) immersed in a petri dish with water. The red line on the Petri dish surface is clearly distinguishable through the BCF.

Quantification of the transparency using ultraviolet visible spectroscopy (Shimadzu UV/VIS UV-2102 spectrometer) was performed for BCFs. Samples were carefully cut into the rectangle shapes to fit one side of the cuvette; they were placed in front of the Uv-vis spectroscopy in order to take the spectrum from 250 nm to 800 nm. Before the test experiment, I measured one piece of regular chromatography paper (named Paper 1) of 200  $\mu\text{m}$  thickness and one piece of lens paper (named Paper 2) of 35  $\mu\text{m}$  as comparison, **Figure 2. 24**. Before and after the WAC cycle, paper 1 and paper 2 almost kept the same transparency.

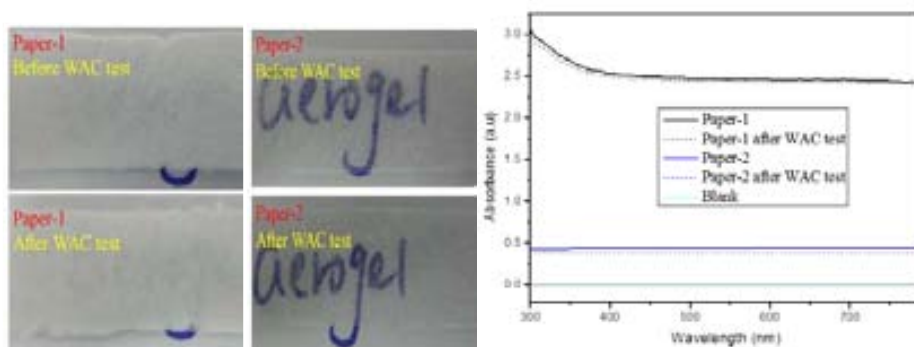


**Figure 2.24** Pictures of paper 1 and paper 2 before and after WAC (left); Uv-vis spectra of paper 1 and paper 2 before and after WAC test (right).

The results of all the BCFs are gathered in **Figure 2.25**. BCFs do not absorb above 500 nm before and after WAC showing a higher optical transmittance compared to Paper 1 and Paper 2. Also from the **Figure 2.22**, it is clear that initially BCE films are more transparent than BCX films that could indicate the existence of different light scattering effects in the films and they could reveal different surface roughness.(43) After the different WAC cycles, all the BCFs improved their transparency. High transparency of BCFs at visible wavelengths and the biological origin of the cellulose could appoint this material as a

suitable matrix to biological applications where the optical visualization through the material is necessary as for instance in cell culture surfaces.

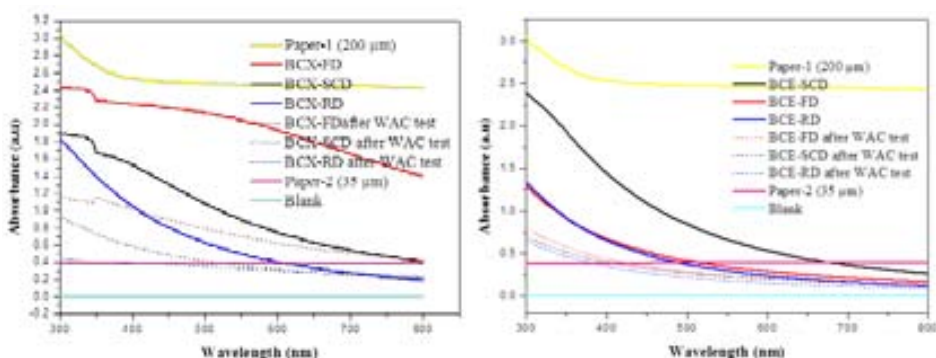


**Figure 2.25** UV-vis spectra of BCX (left) and BCE (right) films before and after WAC.

Furthermore, I also have evaluated the transparency after WAC by choosing the best wavelength of 555 nm, **Table 2.5**. A typical human eye can respond to wavelengths from about 390 to 750 nm. The light-adapted eye generally has its maximum sensitivity at around 555 nm, in the green region of the optical spectrum. Paper 1 and paper 2 almost kept the same transparency before and after rewetting. By contrast, the BCFs have all improved their optical transmittance. BCFs dried at room temperature increased about 40 %, and the BC-SCD films even more than 60 %.

**Table 2.5** The increase transparency of BCFs after WAC was calculated by UV-vis spectra on the wavelength of 555 nm.

Transparency /UV-vis	Before WAC test (Abs at 555nm)	After WAC test (Abs at 555nm)	Increase of the transparency (%)
BCX-SCD	0.8795	0.35368	59.8%
BCX-FD	2.04032	0.69212	66.1%
BCX-RD	0.48829	0.32389	33.7%
Paper-1	2.46782	2.43331	1%
Paper-2	0.43842	0.38735	1%
BCE-SCD	0.64907	0.22695	65.0%
BCE-FD	0.33365	0.23605	29.3%
BCE-RD	0.28563	0.17784	37.7%

### Thermo-gravimetric Analysis

Thermal stability of BC is of prime importance for its applications involving higher temperatures. Thermal decomposition of BC involves both dehydration and de-polymerization that results in the formation of solid residues, high

boiling volatiles, and gaseous products.(44) It can be effectively studied by Thermal Gravimetric Analysis, (13, 45) which is a thermal weight change analysis instrument that was used in conjunction with a thermal analysis controller. TGA measurement is a continuous process, measuring the amount and rate of change in weight of the material, either as a function of increasing temperature or time, in a controlled atmosphere. TGA measurement of the BCFs was performed with a TGA-DSC/DTA analyzer (NETZSCH STA 449 F1 Jupiter, ICMAB) with a heating rate of 10 °C/ min from room temperature to 800 °C in air.

TGA can help us to characterize the BCFs that exhibit the weight change on heating and to detect the phase changes due to decomposition and oxidation. The TGA curves (**Figure 2. 26**) were obtained by plotting percentage mass remaining against temperature and then showed the typical single step thermal degradation profile. It indicated that the commercial BC fibres (Sigma Aldrich 435236) started degradation around 280 °C, while the BCE films were stable up to a higher temperature (BCE-SCD is around 320 °C). The percentage weight loss for the BCE films over 550 degree was around 2 %, which is the same as the commercial cellulose and it is an indication of the high purity of the materials.

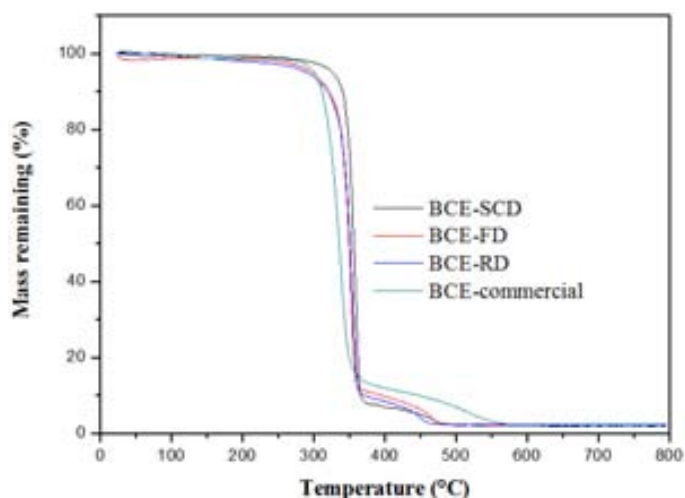


**Figure 2.26** Derivative TGA traces of commercial cellulose films and BCE films.

Thermogravimetric analysis of BCFs of the three different drying methods show a slight increase, of a few degrees, of the decomposition temperature of the samples, around 350°C, native cellulose 312, and alkali treated 340. These values agree to previously TGA analysis reported for BC materials after alkali treatment, **Table 2.6**. BCX films showed similar values.

**Table 2.6** Decomposition temperature and temperature at 20% weight loss of native cellulose, alkali treated cellulose and BCE films.

Sample	Decomposition Temperature °C	Temperature at 20% weight loss
Native cellulose (Int J. Bio I Mole 37, 2005, 189)	312.2 ± 2.2	285.0 ± 1.4
Alkali treated (Int J. Bio I Mole 37, 2005, 189)	351.0 ± 2.4	328.8 ± 0.8
BCE-RD	357 ± 1.5 (0.9)	321 ± 1.5 (0.8)
BCE-FD	358 ± 1.5 (0.9)	338 ± 1.5 (0.85)
BCE-SCD	362 ± 1.5 (0.91)	347 ± 1.5 (0.87)

## Mechanical properties

Mechanical properties are a key property for BCFs to be used in applications as reinforcing materials, sensors or scaffolds.(43) In particular, for cell studies, the possibility of tuning the mechanical properties of the scaffold for each cell type is very attractive. Biological tissues are soft and elastic and they show a broad range of Young modulus from  $1.5 \times 10^4 - 3 \times 10^4$  MPa are found in bones to  $10^4 - 10^3$  MPa in softer tissues such as brain tissue. (46) Numerous studies have revealed that cells have the ability to probe and respond to the rigidity of the substrates they are grown upon.(47-50) The cellular tensegrity model attempts to suggest that the homeostatic balance of forces governs the reciprocal relationship between cells and the physical properties of their microenvironment.(51)

When investigating mechanical properties of a material, it is important - in order to choose the most suitable method for testing - to predict the material's ultimate behaviour. Firstly, I tried to bend the BCFs to check their elastic and plastic properties. The bending test method is an easy and fast method that has also been described in some studies.(52, 53)

### 1) Bending Test

Firstly, I evaluated qualitatively the elastic behaviour of the films by bending them with a tweezer. **Figure 2.27** shows a series of images of the bending test performed. We clearly see that BCE-RD and BCE-FD films fully recovered and a flat sheet was recorded again. SCD films did not recover fully and some creasing was imaged after bending, although it did not break. After wetting-drying cycles, the BCFs do not break, indicating that the films keep their elasticity even after a WAC cycle. Films produced by GX followed the same trend, therefore the bacterial strain do not modify their film's elasticity. Unlike silica aerogels that are brittle and fragile materials, BC aerogels have a high degree of elasticity.(43)



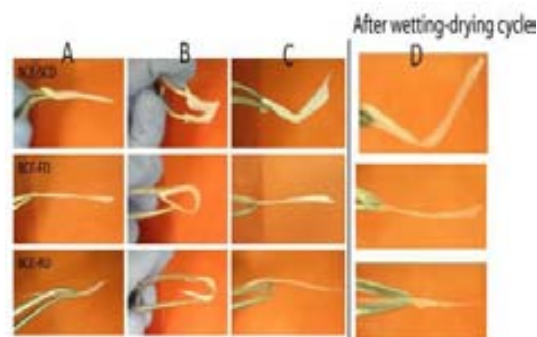


**Figure 2.27** (BCE) Pictures of the bending test performed: (A) BCE films before the bending test from the different drying methods, (B) process of the bending test, (C) the resulting shapes of the BCE films after the test and (D) the shape of the films obtained on a BCE film that was wetted-dried (WAC cycle).



**Figure 2.27** (BCX) Pictures of the bending test performed.

## 2) Nano-indentation

To measure the mechanical behaviour of the BCFs I have used nanoindentation. For the indentation cycles I used a constant maximum load of 0.4 mN to ensure that the penetration depth of the tip into the films was smaller than their thickness. Smaller loads from 0.05 – 0.1 mN did not give us reproducible results. Moreover, I evaluated the effect of the adhesive tape underneath the sample (presence and not presence) and the results did not change, therefore we conclude the adhesive under the sample did not affect the measurements.

**Figure 2.28** and **Table 2.7** gather the load-displacement curves and the values obtained for the penetration depth at maximum load, "Young Modulus,  $E$ ", "Hardness,  $H$ " and "elastic parameter,  $EP$ " for two samples (I have repeated 14 times for both BCX films and BCE films.). The load-displacement curves obtained are representative of a material with elastoplastic properties. BCFs show similar load-displacement curves except for BCX-RD and BCX-FD that show lower penetration depths and steeper unloading curves.

**Table 2.7** Mechanical properties of BCX and BCE films.

Drying method		RD		FD		SCD	
Strain		BCE	BCX	BCE	BCX	BCE	BCX
Mechanical Properties	Penetration depth at 0.4mN load ( $\mu\text{m}$ )	$3.9 \pm 0.4$	$1.1 \pm 0.1$	$4.1 \pm 0.4$	$1.4 \pm 0.3$	$3.2 \pm 0.5$	$4.3 \pm 1.5$
	Young modulus ("E")(MPa)	$196 \pm 46$	$659 \pm 85$	$204 \pm 46$	$601 \pm 155$	$238 \pm 25$	$198 \pm 34$
	Hardness ("H")(MPa)	$34 \pm 22$	$39 \pm 9$	$20 \pm 8$	$26 \pm 12$	$20 \pm 5$	$19 \pm 21$
	EP (%)	$59 \pm 7$	$39 \pm 3$	$53 \pm 4$	$33 \pm 3$	$52 \pm 5$	$48 \pm 13$

The analysis of the load-displacement curves shows that the BCFs creep and some literatures review this property as very desirable for scaffolds that interact with cells.(51) Although we used the slope of the curve to calculate the "Young Modulus", ("E") we have to notice that this estimation is not completely correct as the material has a strong elastoplastic behaviour, as it happens in soft tissues. The analysis of "E" shows that GE affords less stiff films than GX and they are independent of the drying method, while BCX films are more sensitive to the drying method obtaining stiffer BCFs than if we dry them by RD or FD.

The "E" values obtained are around 200 MPa except for BCX-RD and BCX-FD that we observed E of 600 MPa, suggesting that their stiffness could be comparable to tissues such as bone ( $1.5 \times 10^4 - 3 \times 10^4$  MPa) and of soft arteries (0.1 – 1 MPa).(46)

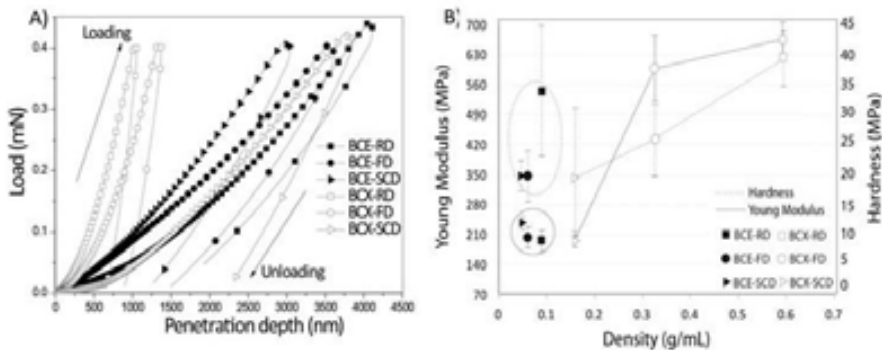


**Figure 2.28** (A) Representative loading-unloading curve for each BCF obtained using the nanoindenter under a load of 0.4 mN. (B) Mean values of "Young Modulus", ("E") and Hardness ("H") obtained for each BCF as a function of their density (n=14). We circled the "E" and "H" for BCE for clarity.

The averaged measured Hardness values ("H") of BC samples are around 20 – 34 MPa, which indicates the resistance of BCFs to the nanoindenter, BC-RD films shows higher "H" values than the other BCFs. The elastic component of the BCFs was analyzed using the *elastic parameter* ("EP").(54) BCFs presenting large "Young modulus" (BCX-RD and BCX-FD) also exhibit a low

elastic character. On the other side, " $E$ " and penetration depth at 0.4 mN values for BCE films are similar to the values found for BCX-SCD film even though they present a much smaller density (0.05- 0.08 g/cm<sup>3</sup> for BCE and 0.16 g/cm<sup>3</sup> for BCX-SCD) possibly pointing to a different mechanical strength of the cellulose microfibrils for each strain. The evaluation of the mechanical parameters with the density shows that the combination of BCX and the drying method used allow us to obtain a broader range of mechanical properties for BCX films than for the BCE films.

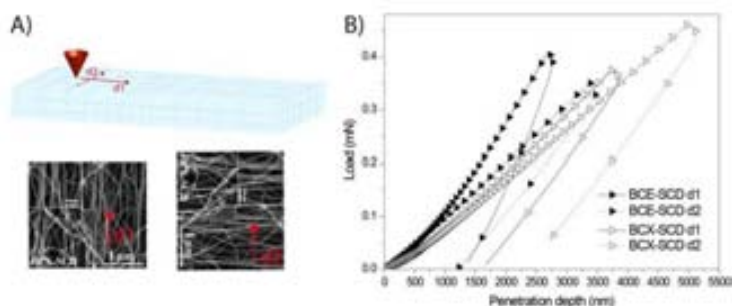


**Figure 2.29** A) Schematic representation of the mechanical measurements performed over two different directions. B) Load- displacement curves for BCFs dried on SCD conditions for the two bacterial strains.

BC-SCD films show in SEM images some anisotropy and possible directionality of the fibres therefore we evaluated " $E$ " and penetration depth if we placed the sample in two opposite directions. The load-displacement curves show different profiles as a function of the direction of the measurement, **Figure 2.29**. The evaluation of " $E$ " of BC-SCD shows some anisotropy in the measurements although the penetration depth remains unchanged. We found a difference in " $E$ " for BCX-SCD and BCE-SCD as a function of the direction where we performed the nanoindentation measurements. These results confirm the SEM images in that we observed some directionality of the fibres in BCX-SCD; we also found some directionality in BCE-SCD even though we could not detect it in SEM, **Table 2.8**. We believe these are interesting results that deserve a further and deeper analysis of the mechanical properties of the BC-SCD films that will be continued with extensive loads, time and different humidity conditions, since BC-SCD films also offer high absorption capacity.

**Table 2.8** Values of "*Young Modulus*" (MPa) and penetration depth at 0.4mN (µm) from BCFs dried in SCD conditions measured in two directions of the BCFs.

Mechanical	BCE-d1	BCE-d2	BCX-d1	BCX-d2
" <i>Young modulus, E</i> " MPa	233 ± 50	300 ± 50	150 ± 40	242 ± 100
Penetration depth at 0.4 mN (µm)	3.1 ± 0.5	3.5 ± 0.9	4.9 ± 0.8	4.4 ± 0.7

---

## 2.5 Conclusions

We have succeeded in fabricating BCFs from two types of bacteria (GX and GE). Moreover, we have completed a systematic characterization of BC thin films, including chemical and physical properties.

The use of two strains and three drying methods allowed us to obtain different BC thin films with different properties, which could be used in different applications. Room temperature drying, freeze-drying, and supercritical drying methods make an impact on the porosity, mechanical properties and water absorption capability of the BCFs expanding their range of properties.

Even after 10 days of culturing, BCE films are more transparent and lighter independently of the drying methods used in comparison to BCX films, harvested for 5 days. BCE-SCD shows the highest water absorbance capacity that allows us to suggest BCE films as suitable candidates for applications such as absorbents, removal of contaminants or wound healing dressings.<sup>(55)</sup> Although the manipulation of wet BCE films proved to be more difficult than the BCX films. Additionally, we have observed that the use of SCD drying improves the crystallinity of the cellulose fibres for both strains.

BCFs from GX source offer a more versatile platform since we can vary the porosity, mechanical properties and water absorption capacity, selecting the appropriate drying method. Additionally, GX strain offers the advantage of faster production of BCX films. We hypothesize that these films could be good candidates to interface with tissues since their mechanical properties could be tailored to mimic the final tissue replacement and their mechanical properties are not hampered in aqueous media.

---

## 2.6 References

1. T. Kouda, H. Yano, F. Yoshinaga, Effect of agitator configuration on bacterial cellulose productivity in aerated and agitated culture, *Journal of Fermentation and Bioengineering*, **83**, 371, (1997).
2. Y. Yamada, K. Hoshino, T. Ishikawa, The phylogeny of acetic acid bacteria based on the partial sequences of 16S ribosomal RNA: the elevation of the subgenus *Gluconoacetobacter* to the generic level, *Bioscience, biotechnology, and biochemistry*, **61**, 1244, (1997).
3. O. Adachi, D. Moonmangmee, H. Toyama, M. Yamada, E. Shinagawa, K. Matsushita, New developments in oxidative fermentation, *Applied microbiology and biotechnology*, **60**, 643, (2003).
4. S. Hestrin, M. Schramm, Synthesis of cellulose by *Acetobacter xylinum*. 2. Preparation of freeze-dried cells capable of polymerizing glucose to cellulose, *Biochemical Journal*, **58**, 345, (1954).
5. F. Liebner, E. Haimer, M. Wendland, M. A. Neouze, K. Schluffer, P. Miethe, T. Heinze, A. Potthast, T. Rosenau, Aerogels from unaltered bacterial cellulose: application of scCO<sub>2</sub> drying for the preparation of shaped, ultra-lightweight cellulosic aerogels, *Macromolecular bioscience*, **10**, 349, (2010).
6. S. Kim, H. J. Kim, N. L. Jeon, Biological applications of microfluidic gradient devices, *Integrative biology : quantitative biosciences from nano to macro*, **2**, 584, (2010).
7. A. Russler, M. Wieland, M. Bacher, U. Henniges, P. Miethe, F. Liebner, A. Potthast, T. Rosenau, AKD-Modification of bacterial cellulose aerogels in supercritical CO<sub>2</sub>, *Cellulose*, **19**, 1337, (2012).
8. J. Trygg, P. Fardim, M. Gericke, E. Makila, J. Salonen, Physicochemical design of the morphology and ultrastructure of cellulose beads, *Carbohydrate polymers*, **93**, 291, (2013).
9. H. Sehaqui, Q. Zhou, O. Ikkala, L. A. Berglund, Strong and tough cellulose nanopaper with high specific surface area and porosity, *Biomacromolecules*, **12**, 3638, (2011).
10. N. Yin, S. Chen, Z. Li, Y. Ouyang, W. Hu, L. Tang, W. Zhang, B. Zhou, J. Yang, Q. Xu, H. Wang, Porous bacterial cellulose prepared by a facile surfactant-assisted foaming method in azodicarbonamide-NaOH aqueous solution, *Materials Letters*, **81**, 131, (2012).
11. R. Sescousse, R. Gavillon, T. Budtova, Aerocellulose from cellulose-ionic liquid solutions: Preparation, properties and comparison with cellulose-NaOH and cellulose-NMMO routes, *Carbohydrate polymers*, **83**, 1766, (2011).
12. D. Klemm, D. Schumann, U. Udhardt, S. Marsch, Bacterial synthesized cellulose - artificial blood vessels for microsurgery., *Progress in Polymer Science*, **26**, 1561, (2001).
13. J. George, V. A. Sajeevkumar, R. Kumar, K. V. Ramana, S. N. Sabapathy, A. S. Bawa, Enhancement of thermal stability associated with the chemical treatment of bacterial (*Gluconoacetobacter xylinus*) cellulose, *Journal of Applied Polymer Science*, **108**, 1845, (2008).
14. T. Łojewski, K. Zięba, A. Knapik, J. Bagniak, A. Lubańska, J. Łojewska, Evaluating paper degradation progress. Cross-linking between chromatographic, spectroscopic and chemical results, *Applied Physics A*, **100**, 809, (2010).

- 
15. Y. Maréchal, H. Chanzy, The hydrogen bond network in cellulose as observed by infrared spectrometry, *Journal of Molecular Structure*, **523**, 183, (2000).
  16. M. Ali, A. M. Emsley, H. Herman, R. J. Heywood, Spectroscopic studies of the ageing of cellulosic paper, *Polymer*, **42**, 2893, (2001).
  17. M. V. Elizabeth Dinand, Henri Chanzy and Laurent Heux, Mercerization of primary wall cellulose and its implication for the conversion of cellulose I→cellulose II, *Cellulose*, **9**, (2002).
  18. S. Park, J. O. Baker, M. E. Himmel, P. A. Parilla, D. K. Johnson, Cellulose crystallinity index: measurement techniques and their impact on interpreting cellulase performance, *Biotechnology for biofuels*, **3**, 10, (2010).
  19. S. Park, D. K. Johnson, C. I. Ishizawa, P. A. Parilla, M. F. Davis, Measuring the crystallinity index of cellulose by solid state <sup>13</sup>C nuclear magnetic resonance, *Cellulose*, **16**, 641, (2009).
  20. H. Zhao, J. Kwak, Z. Conradzhang, H. Brown, B. Arey, J. Holladay, Studying cellulose fiber structure by SEM, XRD, NMR and acid hydrolysis, *Carbohydrate polymers*, **68**, 235, (2007).
  21. Y. Wang, Y. Zhao, Y. Deng, Effect of enzymatic treatment on cotton fiber dissolution in NaOH/urea solution at cold temperature, *Carbohydrate polymers*, **72**, 178, (2008).
  22. P. Mansikkamaki, M. Lahtinen, K. Rissanen, The conversion from cellulose I to cellulose II in NaOH mercerization performed in alcohol–water systems: An X-ray powder diffraction study, *Carbohydrate polymers*, **68**, 35, (2007).
  23. A. D. French, Idealized powder diffraction patterns for cellulose polymorphs, *Cellulose*, **21**, 885, (2013).
  24. M. W. A. T. OKANO, Synchrotron-radiated X-ray and neutron diffraction study of native cellulose, *Cellulose*, **4**, 221, (1997).
  25. L. Segal, J. J. Creely, A. E. Martin, C. M. Conrad, An Empirical Method for Estimating the Degree of Crystallinity of Native Cellulose Using the X-Ray Diffractometer, *Textile Research Journal*, **29**, 786, (1959).
  26. L. Zhang, D. Ruan, J. Zhou, Structure and Properties of Regenerated Cellulose Films Prepared from Cotton Linters in NaOH/Urea Aqueous Solution, *Industrial & Engineering Chemistry Research*, **40**, 5923, (2001).
  27. K. Das, D. Ray, N. R. Bandyopadhyay, S. Sengupta, Study of the Properties of Microcrystalline Cellulose Particles from Different Renewable Resources by XRD, FTIR, Nanoindentation, TGA and SEM, *Journal of Polymers and the Environment*, **18**, 355, (2010).
  28. A. Dietrich, D. A. I. Goring, J. F. Revol, Effect of mercerization on the crystallite size and crystallinity index in cellulose from different sources, *Canadian Journal of Chemistry*, **65**, 1724, (1987).
  29. R. J. Moon, A. Martini, J. Nairn, J. Simonsen, J. Youngblood, Cellulose nanomaterials review: structure, properties and nanocomposites, *Chemical Society reviews*, **40**, 3941, (2011).
  30. G. Siqueira, J. Bras, A. Dufresne, Cellulosic Bionanocomposites: A Review of Preparation, Properties and Applications, *Polymers*, **2**, 728, (2010).
  31. D. Klemm, B. Heublein, H. P. Fink, A. Bohn, Cellulose: fascinating biopolymer and sustainable raw material, *Angewandte Chemie*, **44**, 3358, (2005).
  32. K. Kobayashi, S. Kimura, E. Togawa, M. Wada, Crystal transition from cellulose II hydrate to cellulose II, *Carbohydrate polymers*, **86**, 975, (2011).

- 
33. I. Siro, D. Plackett, Microfibrillated cellulose and new nanocomposite materials: a review, *Cellulose*, **17**, 459, (2010).
  34. C. Schutz, J. Sort, Z. Bacsik, V. Oliynyk, E. Pellicer, A. Fall, L. Wagberg, L. Berglund, L. Bergstrom, G. Salazar-Alvarez, Hard and Transparent Films Formed by Nanocellulose-TiO<sub>2</sub> Nanoparticle Hybrids, *Plos One*, **7**, (2012).
  35. L. Y. Mwaikambo, M. P. Ansell, The determination of porosity and cellulose content of plant fibers by density methods, *Journal of Materials Science Letters*, **20**, 2095, (2001).
  36. H. Sehaqui, Q. Zhou, O. Ikkala, L. A. Berglund, Strong and Tough Cellulose Nanopaper with High Specific Surface Area and Porosity, *Biomacromolecules*, **12**, 3638, (2011).
  37. C. C. Sun, True density of microcrystalline cellulose, *Journal of pharmaceutical sciences*, **94**, 2132, (2005).
  38. Z.-Y. Wu, C. Li, H.-W. Liang, J.-F. Chen, S.-H. Yu, Ultralight, Flexible, and Fire-Resistant Carbon Nanofiber Aerogels from Bacterial Cellulose, *Angewandte Chemie International Edition*, **52**, 2925, (2013).
  39. O. Shezad, S. Khan, T. Khan, J. K. Park, Physicochemical and mechanical characterization of bacterial cellulose produced with an excellent productivity in static conditions using a simple fed-batch cultivation strategy, *Carbohydrate Polymers*, **82**, 173, (2010).
  40. M. Ul-Islam, T. Khan, J. K. Park, Nanoreinforced bacterial cellulose–montmorillonite composites for biomedical applications, *Carbohydrate Polymers*, **89**, 1189, (2012).
  41. M. Ul-Islam, N. Shah, J. H. Ha, J. K. Park, Effect of chitosan penetration on physico-chemical and mechanical properties of bacterial cellulose, *Korean Journal of Chemical Engineering*, **28**, 1736, (2011).
  42. M. Nogi, H. Yano, Transparent Nanocomposites Based on Cellulose Produced by Bacteria Offer Potential Innovation in the Electronics Device Industry, *Advanced Materials*, **20**, 1849, (2008).
  43. H. Yano, J. Sugiyama, A. N. Nakagaito, M. Nogi, T. Matsuura, M. Hikita, K. Handa, Optically transparent composites reinforced with networks of bacterial nanofibers, *Advanced Materials*, **17**, 153, (2005).
  44. A. van Der Kaaden, J. Haverkamp, J. J. Boon, J. W. De Leeuw, Analytical pyrolysis of carbohydrates: I. Chemical interpretation of matrix influences on pyrolysis-mass spectra of amylose using pyrolysis-gas chromatography-mass spectrometry, *Journal of Analytical and Applied Pyrolysis*, **5**, 199, (1983).
  45. J. George, K. V. Ramana, S. N. Sabapathy, J. H. Jagannath, A. S. Bawa, Characterization of chemically treated bacterial (*Acetobacter xylinum*) biopolymer: some thermo-mechanical properties, *International journal of biological macromolecules*, **37**, 189, (2005).
  46. S. W. Moore, P. Roca-Cusachs, M. P. Sheetz, Stretchy Proteins on Stretchy Substrates: The Important Elements of Integrin-Mediated Rigidity Sensing, *Developmental Cell*, **19**, 194, (2010).
  47. R. J. Pelham, Y.-I. Wang, Cell locomotion and focal adhesions are regulated by substrate flexibility, *Proceedings of the National Academy of Sciences*, **94**, 13661, (1997).
  48. A. S. Rowlands, P. A. George, J. J. Cooper-White, Directing osteogenic and myogenic differentiation of MSCs: interplay of stiffness and adhesive ligand presentation, *American Journal of Physiology - Cell Physiology*, **295**, C1037, (2008).

- 
49. A. Engler, L. Bacakova, C. Newman, A. Hategan, M. Griffin, D. Discher, Substrate Compliance versus Ligand Density in Cell on Gel Responses, *Biophysical Journal*, **86**, 617, (2004).
  50. W.-h. Guo, M. T. Frey, N. A. Burnham, Y.-l. Wang, Substrate Rigidity Regulates the Formation and Maintenance of Tissues, *Biophysical Journal*, **90**, 2213, (2006).
  51. A. R. Cameron, J. E. Frith, J. J. Cooper-White, The influence of substrate creep on mesenchymal stem cell behaviour and phenotype, *Biomaterials*, **32**, 5979, (2011).
  52. J.-H. Jeon, I.-K. Oh, C.-D. Kee, S.-J. Kim, Bacterial cellulose actuator with electrically driven bending deformation in hydrated condition, *Sensors and Actuators B: Chemical*, **146**, 307, (2010).
  53. A. N. Nakagaito, S. Iwamoto, H. Yano, Bacterial cellulose: the ultimate nano-scalar cellulose morphology for the production of high-strength composites, *Applied Physics A*, **80**, 93, (2005).
  54. M. Moner-Girona, E. Martínez, J. Esteve, A. Roig, R. Solanas, E. Molins, Micromechanical properties of carbon–silica aerogel composites, *Applied Physics A*, **74**, 119, (2014).
  55. H. Jin, M. Kettunen, A. Laiho, H. Pynnonen, J. Paltakari, A. Marmur, O. Ikkala, R. H. A. Ras, Superhydrophobic and Superoleophobic Nanocellulose Aerogel Membranes as Bioinspired Cargo Carriers on Water and Oil, *Langmuir*, **27**, 1930, (2011).



# Chapter 3

Functional bacterial cellulose  
incorporating nanoparticles



---

## Chapter Index

Chapter summary.....	61
3.1 Synthesis of nanoparticles by microwave-assisted method .....	62
Synthesis of Fe <sub>2</sub> O <sub>3</sub> nanoparticles .....	62
Synthesis of Au nanoparticles .....	65
3.2 Synthesis of BCF-NPs composites by microwave-assisted method .....	66
Synthesis of BCF-SPIONs composites .....	66
Characterization .....	69
Microstructure .....	70
Nanoparticles load .....	73
Magnetic properties .....	74
Stability of the nanoparticles .....	76
Mechanical properties.....	76
Water capacity ability .....	79
Conformal coating .....	80
Proposed mechanism .....	80
Synthesis of BCF-Au composites .....	81
3.3 Synthesis of functional and complex BCF-NPs composites.....	83
Synthesis of patterned BCF-SPIONs composites.....	83
Synthesis of BCF-Au-SPIONs composites .....	87
3.4 Conclusions .....	90
3.5 References .....	91

---

## Chapter summary

Bacterial cellulose composited with nanoparticles (BC-NPs) as novel functional cellulose materials are receiving interest for a variety of applications. (1, 2) Their synthesis methods are usually multi-step in-situ reduction of metal salts or the dip coating of BC in nanoparticles (NPs) suspension, both methods offer low coverage and non-homogeneous distribution of NPs.(3, 4) Therefore some of the challenges of this field are to achieve control of NPs loading in a sufficient and homogeneous way, avoiding NPs heterogeneous agglomerations and NPs leaching during the *in-operando* conditions and if possible developing it using an economical and environmentally friendly method.

I will show here that microwave-assisted (MW) thermal decomposition of metal precursors is an efficient and fast method (within minutes) suitable to form a homogenous, conformal and controllable coating on our bacterial cellulose films (BCFs). We will present the coating of BC films, with different types of NPs, including superparamagnetic crystalline Fe<sub>2</sub>O<sub>3</sub> NPs, Au NPs and two of them (Fe<sub>2</sub>O<sub>3</sub> NPs and Au NPs).

Firstly, Fe<sub>2</sub>O<sub>3</sub> NPs and Au NPs were prepared by the MW method in only five minutes. Later, the same in-situ thermal decomposition method was used to prepare BCF-NPs composites without the need for any post-synthesis treatment. By drying the BCFs using different routes, we were able to tune the final amount of the NPs content in the BCF-NPs composites. The NPs fraction could also be controlled, although to a lesser extent, with the initial precursor concentration. Detailed experiments and analysis of structural, magnetic and mechanical characterization of the materials are included in this chapter.

Subsequently, BCFs were patterned with hydrophobic/hydrophilic domains allowing to selectively anchoring the magnetic NPs and creating magnetic patterns in the BCFs.

---

### 3.1 Synthesis of nanoparticles by microwave-assisted method

#### Synthesis of Fe<sub>2</sub>O<sub>3</sub> nanoparticles

##### Materials

Iron (III) acetylacetonate (Fe(acac)<sub>3</sub>, 97%), benzyl alcohol, acetone, water solution (25 wt%) of trimethylammonium hydroxide (TMAOH) were purchased from Sigma-Aldrich and were used as-received.

The use of microwave irradiation as a non-traditional energy source is becoming very attractive in the preparation of NPs due to efficient microwave heating. It is faster and easier to operate than the thermal decomposition set-up. Moreover, it is environmentally friendly and it can produce high yield of NPs. Microwave irradiation is an electromagnetic radiation that can be divided into electric and magnetic components.(5) The electric part is responsible for dielectric heating. When an oscillating field is applied, the dipoles molecules attempt to realign themselves in the electric field by rotation. Their ability to align with the field is influenced by the irradiation frequency and the liquid viscosity. At high frequencies (2.45 GHz in our microwave reactor) the dipoles have time to respond to the field, therefore rotate, but do not have sufficient time for completing the rotation due to the faster change of the field, generating a phase difference between the field and dipole orientations. It results in an energy lost in the form of heat through molecular friction and collision producing dielectric heating. The amount of heat generated is directly related to the ability of dipoles to align themselves with the frequency of the applied field.(6)

The preparation and characterization of iron oxide NPs by microwave-assisted method have been extensively studied in our group.(7) Experiments were carried out using a CEM Discover reactor (Explorer 12-Hybrid) operating at a frequency of 2.45 GHz. The reaction temperature ( $T_{set}$ ), the time at the constant temperature and the maximum power input used for the heating step can be controlled. The microwave reactor is connected to a computer. The power is automatically adjusted to heat the sample to the set reaction parameters (temperature and time). Temperature and pressure are monitored by a volume-independent infrared sensor (**Figure 3.1**). For typical NPs synthesis, the following procedure was used (**Figure 3.2**):

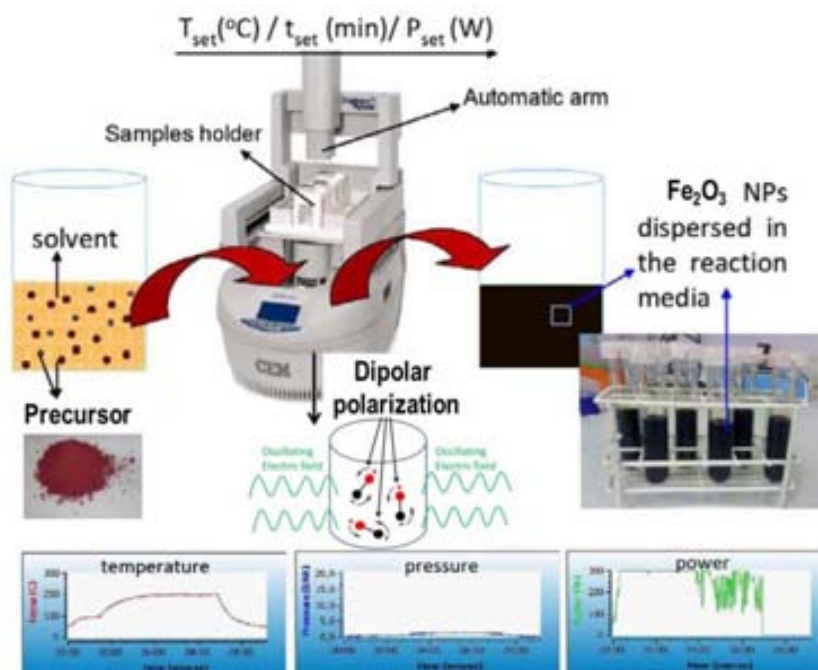


**Figure 3.1** Laboratory microwave reactor setup used for the synthesis of iron oxide NPs and BCF-NPs composites (ICMAB-Nanostructuring platform, Lab 4). (8)

1. Mixture preparation: 0.35 mmol (123.6 mg)  $Fe(acac)_3$  as the iron precursor were dissolved in 4.5 mL benzyl alcohol in a MW tube.
2. MW reaction: MW tube was pre-heated at 60 °C for 5 min in the microwave reactor, and then 5 min more in the same reactor to 200 °C with a maximum power of 300 W. After that, the solution was automatically cooled down to 50 °C by compressed nitrogen (being a built-in cooling feature of the apparatus) lasting approximately 3 min.
3. Cleaning process: the black precipitate in suspension was separated by adding 40 mL acetone with 20  $\mu$ L TMAOH (used as electrostatic stabilizer) and centrifuged at 6000 rpm during 20 min. The supernatant from this first centrifugation was discarded; the precipitate was re-dispersed in the same amount of acetone with TMAOH and centrifuged again. The magnetic precipitate, after drying it overnight in an oven at 70 °C, was re-dispersed in 2 mL distilled water containing 10  $\mu$ L of TMAOH yielding a time-stable magnetic colloidal dispersion to be used for further characterization.

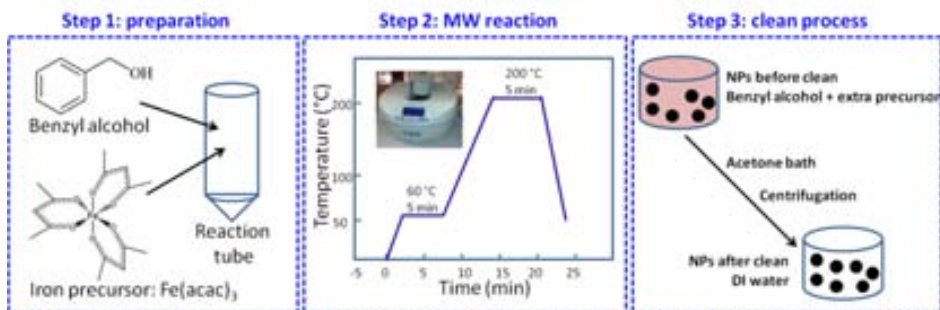


**Figure 3.2** Three steps of iron oxide NPs synthesis by microwave-assisted method. Step 1: iron precursor is dissolved in benzyl alcohol solvent; step 2: setup the microwave conditions (preheating for 5 min at 60 °C, and then 5 min at 200 °C for nucleation and growth of the NPs); step 3: NPs are cleaned with acetone and then kept in distilled water with TMAOH as electrostatic stabilizer.

## Results and discussion

The iron oxide NPs synthesized by microwave heating and stabilized using an electrostatic stabilizer (TMAOH) in water are displayed in **Figure 3.3** left. The structural and size characterizations were performed using Transmission Electron Microscopy (TEM). The samples were prepared by depositing a drop of diluted NPs dispersion onto a copper grid and evaporating the water. TEM images were obtained with a JEOL JEM-1210 electron microscope, operating at 120 kV. The NPs mean size was calculated by fitting a size histogram of the at least 200 NPs to a Gaussian function. The standard deviation ( $\sigma$ ) is defined as the square root of the average of squared differences of from their mean size, and the polydispersity of the distribution ( $P$ ) is defined as the percentage of the standard deviation ( $\sigma$ ) related to the mean size ( $P = \frac{\sigma}{\text{mean-value}} \times 100$ ). Electron diffraction (**Figure 3.3** right) confirmed that these are  $\gamma\text{-Fe}_2\text{O}_3$  NPs.(7)

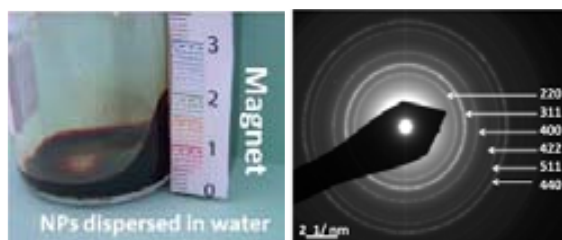


**Figure 3.3** Iron oxide NPs attracted by a magnet, which were dispersed in water after the cleaning process (left). Selected area electron diffraction pattern of the  $\gamma\text{-Fe}_2\text{O}_3$  NPs (right).

The iron oxide NPs are presented by the corresponding TEM micrographs in **Figure 3.4** (left) and the mean size ( $6 \pm 1$  nm) was calculated from the size histogram fitted to a Gaussian function.

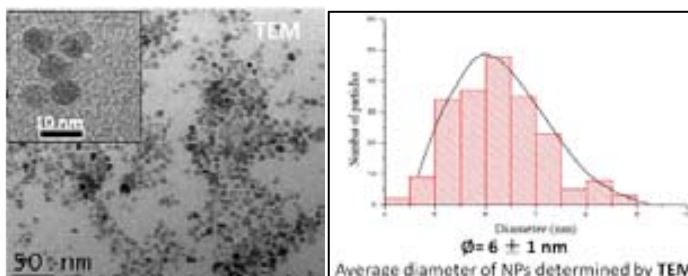


**Figure 3.4** TEM images showing iron oxide NPs synthesized by microwave-assisted method (left). NPs size distribution by Gaussian fitting (right), the average diameter of Fe<sub>2</sub>O<sub>3</sub> NPs is 6 nm.

The magnetic properties of iron oxide NPs were evaluated by SQUID (Superconducting Quantum Interference Device) measurements. Their magnetizations were tested by evaluating their magnetization vs magnetic field measurements at 300 K and zero-field-cooled (ZFC), field-cooled (FC) temperature dependent magnetization curves using a 50 Oe field. The result shows the typical magnetization loop of superparamagnetic nanoparticles (SPIONs) in which neither remnant magnetization nor coercivity at room temperature was observed. The saturation magnetization is high, with a value of approximately 60 emu/g  $\gamma$ -Fe<sub>2</sub>O<sub>3</sub> pointing to the high degree of crystallinity of the NPs. Superparamagnetism is also confirmed by the ZFC-FC magnetization curves, **Figure 3.5** (right). The ZFC magnetization increases with the temperature until reaching a maximum value corresponding to the blocking temperature (TB) at 55 K for this particular sample.

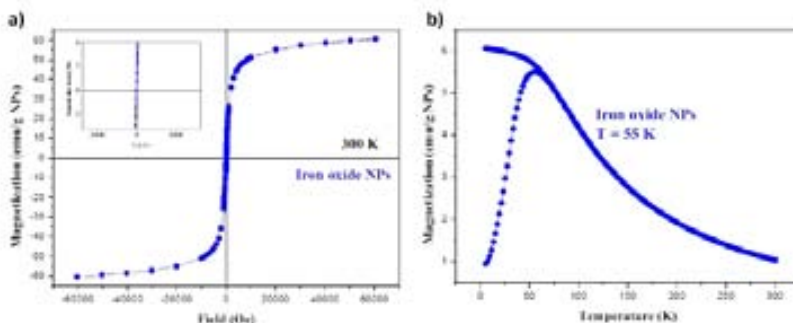


**Figure 3.5** Magnetic characterization of the SPIONs. M (H) at 300 K and ZFC-FC with 50 Oe applied field (right).

## Synthesis of Au nanoparticles

### Materials

Gold (III) chloride tri-hydrate and sodium citrate were purchased from Sigma-Aldrich and were used as-received.

The synthesis of Au NPs was done by reduction of  $[\text{AuCl}_4]^-$  using sodium citrate. Typically, 400  $\mu\text{L}$  of an aqueous solution of sodium citrate (10 %) was added to 2 mL of 1 mM  $\text{HAuCl}_4$  aqueous solution, at 80  $^{\circ}\text{C}$  for 2 min under the maximum microwave power of 300 W. A deep-red gold colloid was formed (**Figure 3. 6**), which indicates the formation of Au NPs with a typical band centered at approximately 526 nm in the UV-vis spectrum.

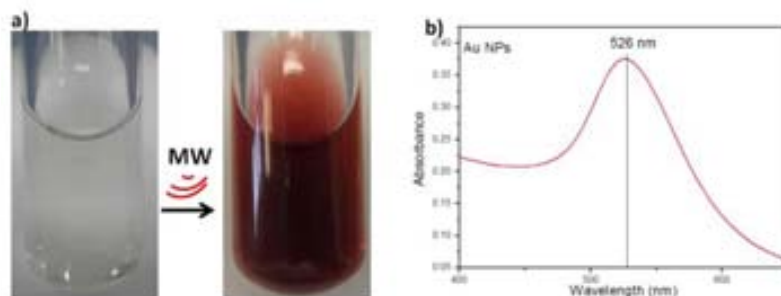


**Figure 3.6** a) Pictures of a reaction tube before and after MW. Au NPs were synthesized by MW method. b) Absorption spectrum obtained from the Au NPs, showing an absorption peak at 526 nm.

As explained in Chapter 1, Au NPs exhibit rich optical and electronic properties in addition to their biocompatibility, which therefore has a wide range of applications from catalysis to sensing and biological tagging.(9-11) The excellent properties of BCF and Au NPs inspired us to combine them into a nanocomposite.

### 3.2 Synthesis of BCF-NPs composites by microwave-assisted method

Different examples of BC-NPs can be found in the literature, some of them were already mentioned in Chapter 1. Maneerung et al. synthesized BC-Ag composites, where Ag NPs confers to the BC antibacterial properties against gram positive and gram negative bacteria species.(12) Zhang and co workers prepared BC-Au composites by using BC fibres for bio-sensor applications.(10) Magnetic BC composites have been prepared by Fragouli et al.(4), modifying cellulose sheets in a post-production step by dip coating the cellulose in a magnetic NPs solution. The above-mentioned examples used common synthetic method, and as far as I know, only few papers have been reported on the use of microwave heating for the synthesis of BC-NPs composites (calcium carbonate and silver nanoparticles). (13-15)

#### Synthesis of BCF-SPIONs composites

##### Materials

Iron (III) acetylacetonate ( $\text{Fe}(\text{acac})_3$ ), 97%), benzyl alcohol, acetone, water solution (25 wt%) of trimethylammonium hydroxide (TMAOH) were purchased



from Sigma-Aldrich and were used as-received. BCX films including BCX-SCD, BCX-FD, BCX-RD and BCX-Wet films were cut into rectangular shaped pieces (~ 2 x 1 cm).

Two approaches to fabricate magnetic responsive cellulose will be described. First one is to dip coat the cellulose films in a NPs stable dispersion and the second approach is to synthesize NPs in-situ on the BCFs using microwave-assisted process already described. (16, 17)

### Dip coating method

Using the dip coating, the magnetic NPs are entrapped on either the surface or around the BC fibres from which magnetically responsive cellulose can be prepared. The process (*Figure 3. 7*) proceeds in three steps. First of all, a concentrated suspension of iron oxide NPs was prepared, and it was vigorously agitated in a glass beaker. Secondly, one piece of BCX-RD films was immersed in the solution for about 1 hour, followed by a washing step to remove all the unbound-magnetic particles.

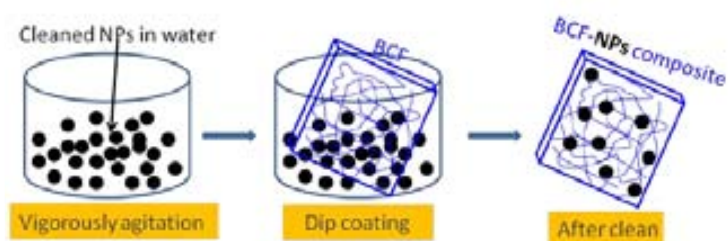


*Figure 3.7* Three steps of dip coating method.

The resulting materials are depicted in *Figure 3. 8*. This method is a physical approach, and the diffusion kinetics is mainly limited by the transport of the magnetic particles through the pores of the BCFs.

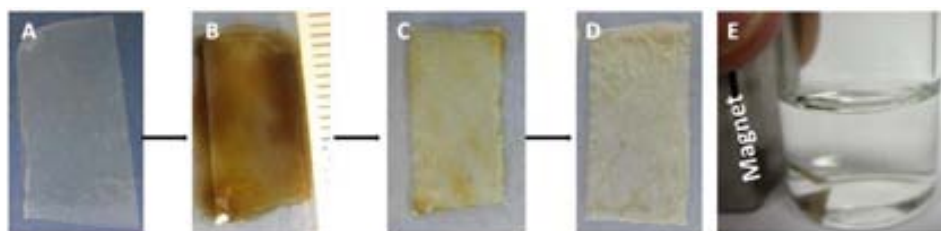


*Figure 3. 8* Dip coating experiment: A) pristine BCX-RD film; B) wet BCX-RD-SPIONs film after dip coating; C) wet BCX-RD-SPIONs film after cleaning process; D) dry BCX-RD-SPIONs film; E) BCX-RD-SPIONs film immersed in distilled water attracted by a magnet.

Even though the dip coating method has been widely used,(4, 18) it often results in a heterogeneous composite with NPs aggregation. As shown in *Figure 3.8D*, the colour of the dry magnetic cellulose is not homogeneous. This film was also

visualized using SEM. In **Figure 3.9**, few NPs were observed on the surface of the cellulose films. Moreover, it is difficult to achieve loads of more than 5 % in iron oxide in this way and the NPs are not chemically bonded to the BCFs.

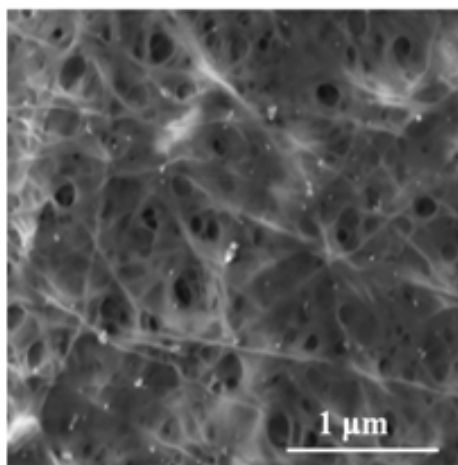


**Figure 3.9** SEM images of magnetic BCX-RD film, which was synthesized by the dip coating method.

### **In-situ synthesis by microwave-assisted thermal decomposition**

Another approach I have used to prepare BCF-SPIONs composites involves the in-situ synthesis of iron oxide NPs within the BCFs themselves by microwave-assisted thermal decomposition.<sup>(1, 19-25)</sup> The preparation relies on the in-situ precipitation of metal ions onto the cellulose fibres in the BCFs from a premixed precursor and the formation of the NPs (**Figure 3.10**). As shown in Chapter 2, our BCFs are micro and nano porous 3D networks, which can facilitate the penetration of iron ions into the interior. This in-situ thermal decomposition method offers more homogeneous and uniform magnetic BCF composites.

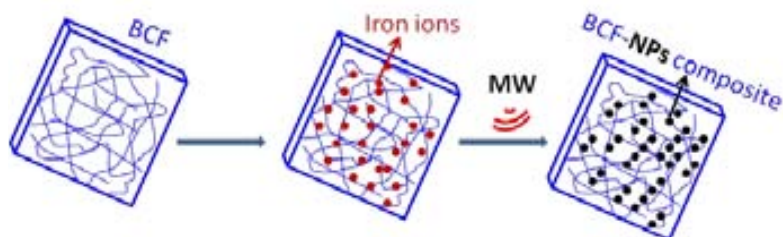


**Figure 3.10** Schematic diagram of the in-situ thermal decomposition of BCF-NPs composites.

Keeping the same synthetic conditions as in the synthesis of pure iron oxide NPs. Magnetic cellulose films were fabricated by in-situ thermal decomposition

of Fe(acac)<sub>3</sub> under microwave irradiation as follows: 0.35 mmol Fe(acac)<sub>3</sub> as iron precursor were dissolved in 4.5 mL benzyl alcohol.(7) In a first set of experiments, four type of BCX films with different properties (BCX-RD, BCX-FD, BCX-SCD and BCX-Wet films) were selected and immersed in the solution for 30 min to ensure a homogeneous diffusion of the iron precursor inside the cellulose network. Prior to that, the BCX-Wet film was subjected to a solvent exchange by immersing it in benzyl alcohol for 12 hours. Magnetic cellulose films were obtained after five minutes reaction at 200 °C in the microwave oven. They were collected from the solution and cleaned in a 10 mL acetone bath and sonicated for 3 minutes. The remaining NPs in suspension from their mother solutions were cleaned and stabilized in water following the same protocol described previously on the synthesis pure of Fe<sub>2</sub>O<sub>3</sub> NPs.

In a second set of experiments, BCX-RD films were treated using different Fe(acac)<sub>3</sub> concentrations: 0.156 M, 0.078M, 0.039M and 0.02M labeled as BCX-RD-A, BCX-RD-B, BCX-RD-C, BCX-RD-D respectively (*Table 3.1*).

**Table 3.1** Two set of microwave-assisted experiment for BC films.

BC films	Iron precursor (mmol)	Benzyl alcohol (ml)	BC films	Iron precursor (mmol)	Benzyl alcohol (ml)
BCX-SCD	0.35	4.5	BCX-RD-A	0.35	4.5
BCX-FD	0.35	4.5	BCX-RD-B	0.175	4.5
BCX-RD	0.35	4.5	BCX-RD-C	0.088	4.5
BCX-Wet	0.35	4.5	BCX-RD-D	0.044	4.5

## Characterization

The pristine BCX (before MW reaction) and the magnetic BCX films (after MW reaction) are shown in *Figure 3.11*. Films were not damaged during the microwave synthesis and present a homogenous coverage of the magnetic coating. Moreover, the series BCX-RD-A, B, C, and D also show a large degree of transparency. BCX-RD-A film presents a slight damage which occurred during the film cleaning. All the magnetic films readily respond to an externally applied permanent magnet. *Figure 3.12* also shows the Fe<sub>2</sub>O<sub>3</sub> NPs recovered from the mother solution after coating the films, which also readily respond to an external magnet. Moreover, some interesting videos of the quick response of the magnetic films to an external magnetic field have been made, which can be seen on the ICMAB webpage (<http://icmab.es/biomaterials-and-materials-for-drug-delivery-therapy-diagnostics-and-sensing/1775-origami-magnetic-cellulose-controlled-magnetic-fraction-and-patterning-of-flexible-bacterial-cellulose>).<sup>(25)</sup>

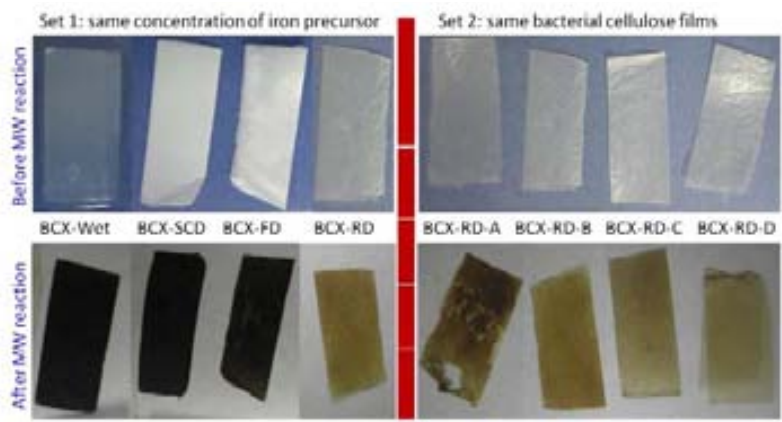


**Figure 3.11** Digital images of BCFs before and after microwave reaction. Magnetic responsive cellulose films from BCX-Wet, BCX-SCD, BCX-FD and BCX-RD synthesized using the same concentration 78 mM of iron precursor (left); Magnetic responsive cellulose films from the BCX-RD films and using decreasing amount of iron precursor concentration (right).

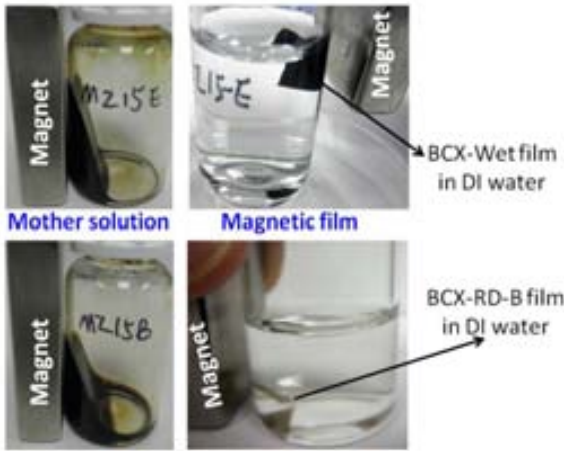


**Figure 3.12** Magnetic films and mother solutions attracted by an external magnet. Two samples (BCX-Wet and BCX-RD-B) are shown in this picture; the rest of the samples presented the same behaviour.

**Microstructure**

The resulting BCF-SPIONs composites presented a fibrous porous structure with good dispersed NPs. Scanning (SEM) and transmission (TEM) electron microscopy were used to characterize the decorated BCFs. Samples placed on an SEM aluminium substrate over a carbon-tape adhesive were imaged with a scanning electron microscope (QUANTA FEI 200 FEG-ESEM) under high-vacuum conditions, an acceleration voltage of 10-30 kV, an electron beam spot of 3.0, a pressure of 2 to 9  $\square 10^{-4}$  Pa, and a distance of 4 - 4.5 mm. SEM images

are shown in **Figure 3.13**, which allow us to identify the BC fibres and the NPs as well as the homogeneous conformal distribution of the NPs on cellulose fibres.

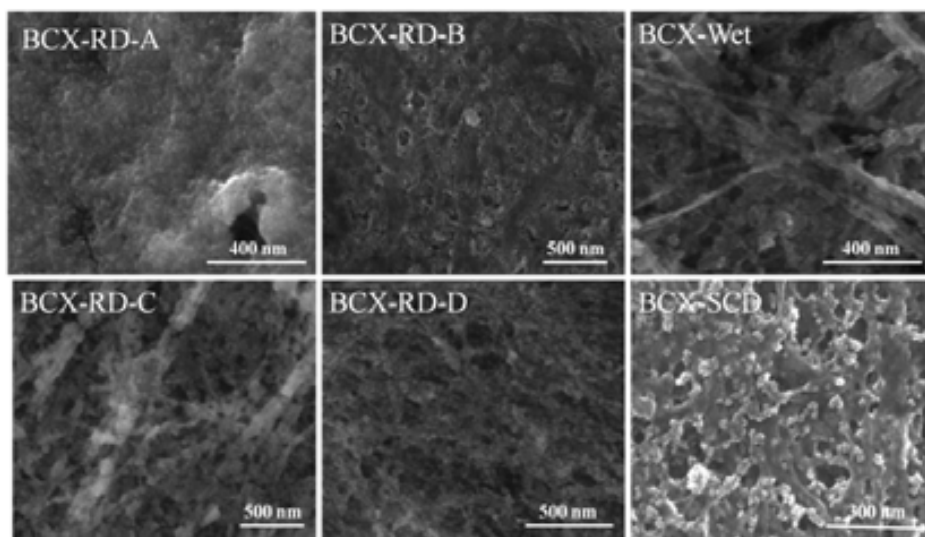


**Figure 3.13** SEM images of the magnetic BCX-RD-A, B, C, D, BCX-Wet and BCX-SCD films. Cellulose fibres can be distinguished from the NPs, homogeneity and conformal distribution of the magnetic load can be inferred for these images.

TEM was used to evaluating NPs size distribution and the identification of iron oxide NPs both in the BCFs and in the solution. TEM images were obtained with a JEOL JEM-1210 electron microscope, operating at 120 kV. **Figure 3.14a**, b and c contains TEM images, the selected area electrons patterns and size distribution of BCX-RD-B film. It can be seen that the particles are placed over the cellulose fibres and not within the pores; transmission mode was possible due to film thickness (under 100 microns) and the relatively low magnetic load for this sample. In this case, BC fibres are more clearly seen and the magnetic NPs are individually distinguishable allowing us to compute the particles size histogram, with a mean size of 5.8 nm. **Figure 3.14d** and f present the TEM image of the NPs from the mother solution and the size histogram with also a mean size of 5.8 nm. Thus, the nano-crystals in solution and those attached to the cellulose have the same size. The electron diffraction patterns of selected areas (figure **Figure 3.14b** and e) were used to identify the iron oxide phase and they were indexed with the maghemite diffraction planes for both synthesis.

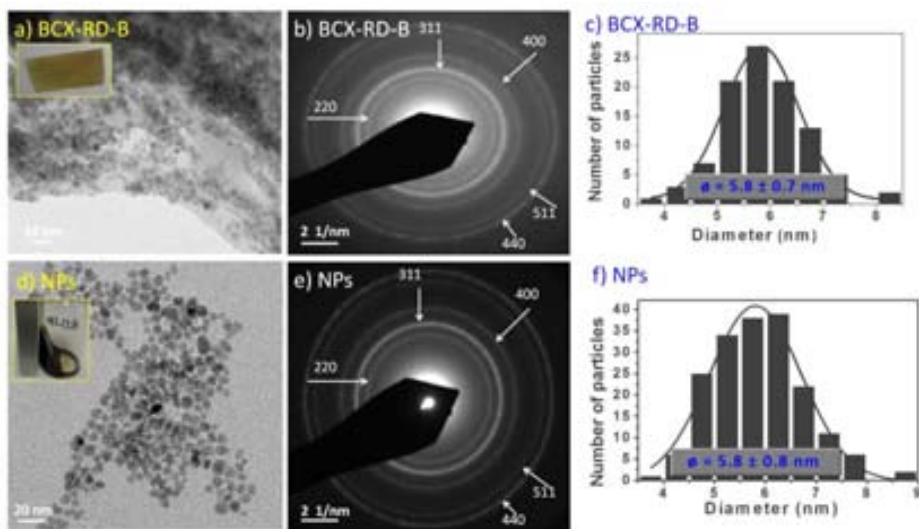


**Figure 3.14** a) TEM images and the selected area electron patterns of BCX-RD-B film. b) TEM images and the selected area electron patterns of NPs from its mother solution. Cellulose fibres and individual NPs are here clearly observed in BCX-RD-B. Low insets: particle size histograms and mean particle size values.

Furthermore, I have used dynamic light scattering (DLS) measurements to determine the averaged hydrodynamic diameter and to study the stability of the colloidal dispersion (**Table 3.2**). The hydrodynamic diameter of our iron oxide NPs suspended in water was investigated with a Zetasizer Nano ZS from Malvern Instruments equipped with a He/Ne 633 nm laser. Care was taken that DLS peak position and width was the same after three consecutive runs of 15 scans each run for all the mother solutions (BCX-RD-B and BCX-Wet were shown). The hydrodynamic diameter, which includes the magnetic core and the electrostatic stabilizer (TMAOH), is in all cases larger than the diameter determined by TEM. The size distribution of all the NPs from mother solutions is around 11 nm except the BCX-Wet sample that is a little larger than the others, which was also confirmed by TEM measurement.

**Table 3.2** DLS results of NPs size from mother solutions. Two samples (BCX-RD-B and BCX-Wet) size distribution curves were shown. The rest have the same behaviour.

BC films	NPs size (DLS) from mother solution	BC films	NPs size (DLS) from mother solution
BCX-SCD	13 nm	BCX-RD-A	12 nm
BCX-FD	11 nm	BCX-RD-B	11 nm
BCX-RD	11 nm	BCX-RD-C	11 nm
BCX-Wet	15 nm	BCX-RD-D	11 nm

## Nanoparticles load

In all cases the magnetic fraction was calculated by weighting the pure BCFs before and after the synthesis of the magnetic NPs, as well as by thermogravimetric analysis measurement. In **Figure 3.15**, the magnetic cellulose films were heated by TGA from room temperature to 800 °C with a heating rate of 10 °C per minute under air. The residual weight for pristine BCX-RD cellulose is around 2 % wt. The residual weight of the magnetic cellulose for BCX-Wet, BCX-RD-A and BCX-RD-C was 39.8 %, 9.4 % and 4.8 %, respectively. The residual components in magnetic cellulose films are attributed to the iron oxide NPs. Therefore, compared to the pristine BCX-RD film, we can calculate the coating amount of iron oxide NPs. Both results of weighting cellulose before and after MW and the TGA measurements were coincident and gathered in **Table 3.3**. The decomposition temperature of the magnetic cellulose films slightly shifted to lower temperatures in comparison, suggesting that iron oxide-coating could reduce the thermal stability of cellulose to a certain extent. Similar results have been reported by previous researches when other metal oxides were immobilized in cellulose matrix.(26, 27)

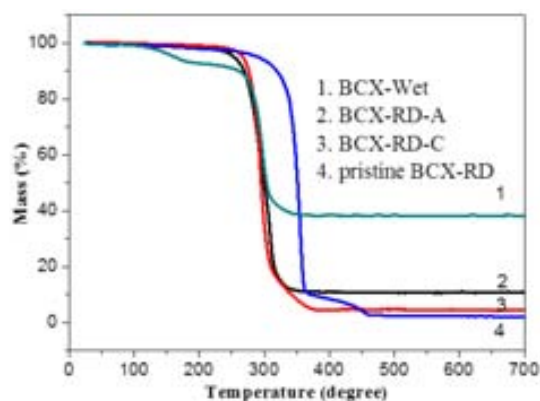


**Figure 3.15** TG curves of magnetic cellulose films (BCX-Wet, BCX-RD-A, BCX-RD-C) and pristine BCX-RD bacterial cellulose.

Magnetic coverage ranged from 4% wt of the BCX-RD-D material exposed to the lowest iron precursor concentration to up to 41 % wt for the never dried cellulose, magnetic BCX-Wet as determined by TGA. These values are depicted in **Figure 3.16** where the concentrations of the NPs recovered from the supernatant after the reactions are also included. **Figure 3.16** shows the major influence of the drying procedure of the BCFs in the magnetic loading of the final material. The never dried cellulose (BCX-Wet) and the supercritical dried (BCX-SCD) films allowed up to 40 % of magnetic coverage, while the room temperature dried film (BCX-RD) only 7 %. This can be related to the porosity of the starting material (90%, 80% and 60% for BCX-SCD-FD-RD respectively) and thus to the number of accessible hydroxyls. (28) Concentration of initial iron precursor can also be used to control the magnetic coverage, although to a lesser extent than the drying method. Increasing the initial concentration eight

times, results in only a factor two and half increase of the magnetic coverage (from 4% for 20 mmol/l to 9% for 160 mmol/l).

**Table 3.3** Coating amounts of iron oxide NPs

Sample	Fe precursor (M)	NPs coating (%)	Sample	Fe precursor (M)	NPs coating (%)
BCX-Wet	0.078	41	BCX-RD-A	0.156	9
BCX-SCD	0.078	38	BCX-RD-B	0.078	7
BCX-FD	0.078	20	BCX-RD-C	0.039	5
BCX-RD	0.078	7	BCX-RD-D	0.02	4

In all cases there was an excess of reagents available as can be seen by the resulting colloidal dispersions of the recovered NPs not attached to the cellulose. Therefore, we can conclude that the amount of accessible hydroxyls in the BCFs is a determining factor in order to control the magnetic load of the films.

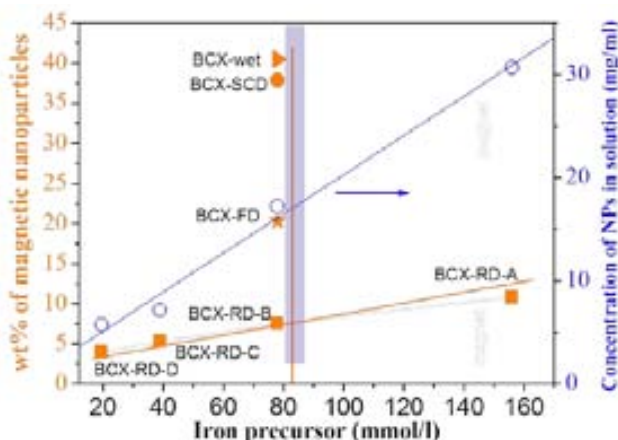


**Figure 3.16** Left y-axis represents the magnetic fraction of the magnetic films vs initial iron precursor concentration (full orange squares and orange line as a visual guide to show the linear dependence). Right y-axis represents the concentration of iron oxide nanoparticles in solution, recovered from the supernatant (empty symbols and blue line as a visual guide to show linear dependence). At 78 mM initial iron precursor concentration the magnetic fraction of the magnetic films is depicted for the several the drying routes used (full orange symbols: square, star, circle and triangle).

### Magnetic properties

The magnetic properties of the BCF-SPIONs composites for the RD series are summarized in **Figure 3.17**. Plots of magnetization *versus* field,  $M(H)$ , and field-cooled/zero-field-cooled (FC-ZFC) normalized to grams of iron oxide showed that all curves collapsed to a single one, which indicates all almost identical magnetic behaviour for the four samples despite their different magnetic loading fractions. The saturation magnetization value is approximately



30 emu/g  $\gamma$ -Fe<sub>2</sub>O<sub>3</sub>; a rather modest value for crystalline maghemite particles of 6 nm diameter. The lack of remanence and coercivity evidence the superparamagnetic behaviour of the films, which is also confirmed by the characteristic features of the FC-ZFC plots displayed in **Figure 3.17b**, which also allows us to point out three more features. Firstly, all four samples exhibit the same maximum for the ZFC curves that signals the blocking temperature ( $T_B \approx 50$  K), which thus indicates that the particle volume is the same in all the films. Secondly, the sharpness of the ZFC curves indicates that the particle assembly has a narrow particle size distribution, as already observed by the size histogram from the TEM images. Finally, the sharp increase of the FC curve at very low temperature could indicate a paramagnetic component in the system, which likely arises from Fe<sup>3+</sup> ions bonded to the cellulose, and which in turn may explain the rather moderate value of the saturation magnetization values.

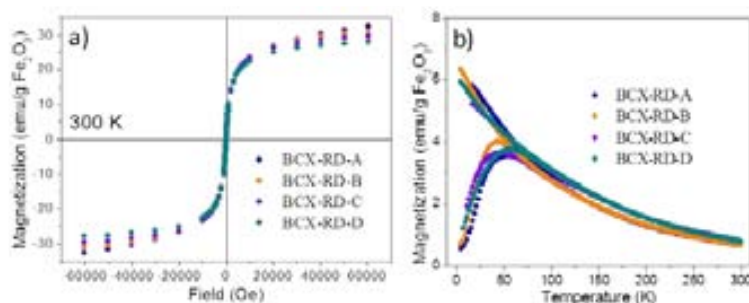


**Figure 3.17** (a) Magnetization (emu/g Fe<sub>2</sub>O<sub>3</sub>) vs. magnetic field at room temperature of the series of magnetic bacterial cellulose films with decreasing initial iron concentration. (b) Magnetization (emu/g Fe<sub>2</sub>O<sub>3</sub>) vs. temperature for the same series measured with a 50 Oe applied field.

**Figure 3.18** includes the magnetic characterization for the sample with the largest magnetic fraction, the BCX-Wet. Essentially the same magnetic behaviour as that described above can be recognized here also. In this case the NPs volume is slightly larger, as seen by the increase of the blocking temperature ( $T_B \approx 100$  K; see inset of **Figure 3.18**). The FC curve does not show a prominent increase at low temperature but rather levels off to a given value, which indicates that no paramagnetic component is present in this sample. These two features lead to a larger magnetization saturation value (ca. 60 emu/g Fe<sub>2</sub>O<sub>3</sub>) for this system than for the previously described ones. **Figure 3.18b**) includes a TEM image and size histogram of the NPs in suspension formed during the coating of BCX-Wet supporting a larger NPs mean size (8.7 nm) compared to the previously discussed system (5.8 nm). TEM investigation of magnetic BCX-Wet was not possible since the high magnetic load prevented electronic transmission through the film. Several repeats of this experiment were made and they confirmed the result that a large NP size was always found in BCX-Wet, however, at this point we do not have a plausible explanation for this phenomenon.

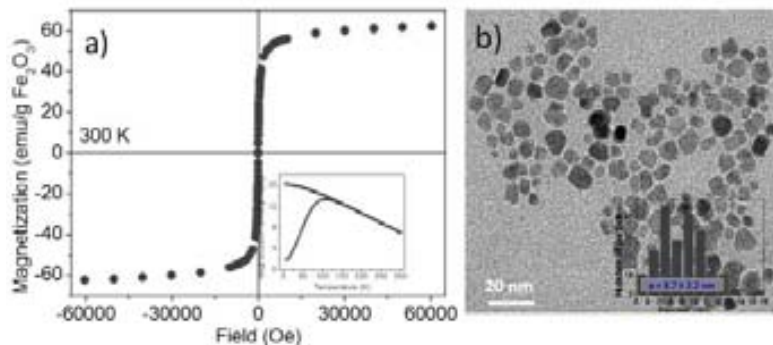


**Figure 3.18** (a) Magnetization (emu/g Fe<sub>2</sub>O<sub>3</sub>) vs. magnetic field at room temperature of magnetic BCX-Wet. Inset: Magnetization (emu/g Fe<sub>2</sub>O<sub>3</sub>) vs. temperature measured with a 50 Oe applied field. (b) TEM image of NPs in solution. Inset: particle size histogram and mean particle size value.

### Stability of the nanoparticles

In order to study the stability of BCF-SPIONs composites or to check the NPs leaching from the films, one piece of each sample was immersed in DI water for three months. **Figure 3.19** show a series of images of the magnetic cellulose films immersed in water where the water remained completely uncoloured even after three months thus, pointing to the lack of NPs leaching. Moreover, thermogravimetry of a BCX-RD-B film was performed after 3 months to confirm the lack of NPs leaching.

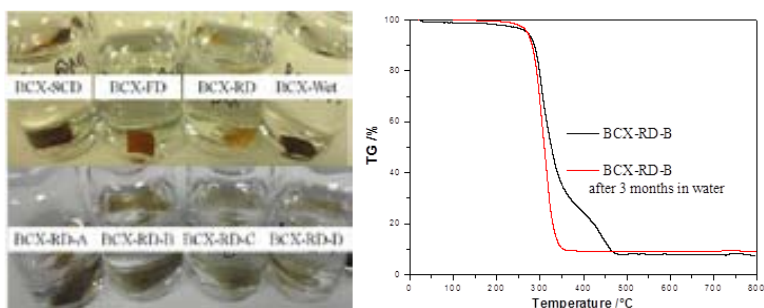


**Figure 3.19** Pictures of magnetic cellulose films immersed in water for about three months without leaching (left). TG curves of magnetic of an as-obtained BCX-RD-B film and the one performed after 3 months of soaking confirming the lack of NPs leaching (right).

### Mechanical properties

The mechanical properties of the BCF-SPIONs composites were determined by a manual bending test, as well as by nanoindentation measurements. **Figure 3.20** illustrates the hardness and flexibility of the magnetic films under applied

pressure/weight, two key properties of our films. The first row of pictures shows some digital images of the BCX magnetic films holding a solid wax droplet (approx. 25 mg), which indicate that the films do not break when weighted; the second row demonstrates the flexibility of the magnetic cellulose films when it is rolled over, while the ability to recover their original shape is shown in the third row. BCX-RD-B is also transparent, which is clearly depicted in the figure inset.

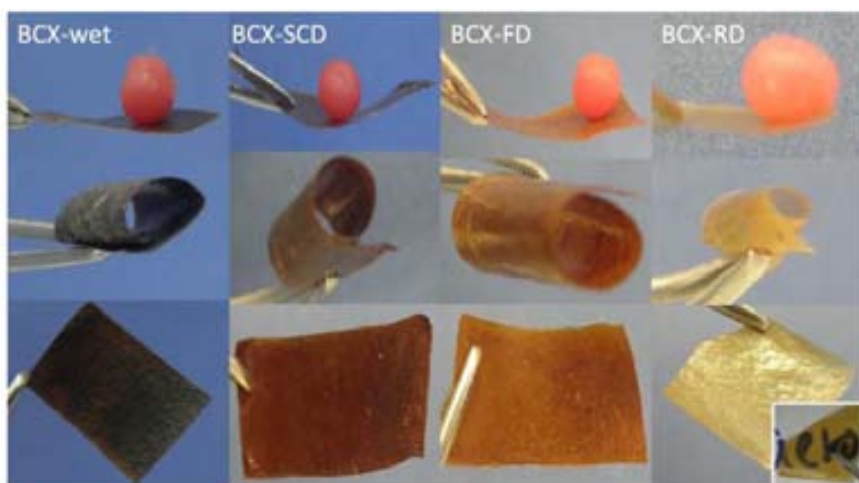


**Figure 3.20** Upper row: Images of the magnetic BCX-films holding a wax ball. Middle row: Flexibility of the magnetic cellulose films is illustrated by rolling them up. Lower row: Magnetic cellulose films recovered their initial flat shape after being rolled. Inset: BCX-RD-B film transparency is evidenced.

Furthermore, the mechanical properties of all the magnetic cellulose films were analyzed with a Nanoindenter XP system. The load-displacement curves of magnetic cellulose films obtained by nanoindentation show their elastic-plastic properties, which is similar to the pristine cellulose films (**Figure 3.21**). All the magnetic cellulose films have higher young modulus and hardness (**Table 3.4**) than the pristine cellulose, because the rigid iron oxide NPs contained in the BCFs. This is mainly due to the good dispersion of iron oxide NPs and their interconnection within the cellulose fibres to create a rigid network and to impart a great mechanical stability to the entire system.

It is especially interesting when I compared the mechanical behaviour of magnetic cellulose films with the rewet-dry cellulose films since the cellulose films have been rewetted during the microwave reaction, as they show the lower mechanical performance with less steep loading-unloading curves in **Figure 3.21**. It indicates that the magnetic cellulose films are softer or less stiff than the rewet-dry cellulose films, although the rigid  $\text{Fe}_2\text{O}_3$  NPs were contained in the films. As shown in **Table 3.4**, the Young's modulus and hardness of BCX films (BCX-SCD, BCX-FD and BCX-RD) are become similar after the rewet-dry cycle, which are around 1600 MPa and 100 MPa, respectively. Furthermore,

**Figure 3.22** shows that not only their structures were turning similar, but also their thicknesses were getting closer.

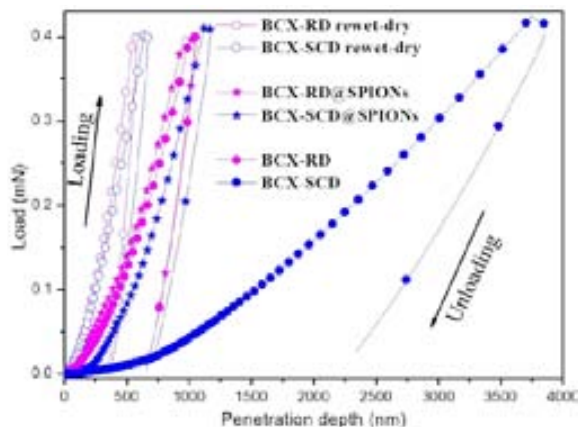


**Figure 3.21** Representative loading-unloading curve for pristine BCX-SCD, RD films, magnetic cellulose (BCX-SCD and BCX-RD were coated with iron oxide NPs) and the rewet-dry BCX-SCD, RD films obtained using the nanoindenter under a load of 0.4 mN. (BCX-FD films have a similar behaviour to the others, which were not seen.)

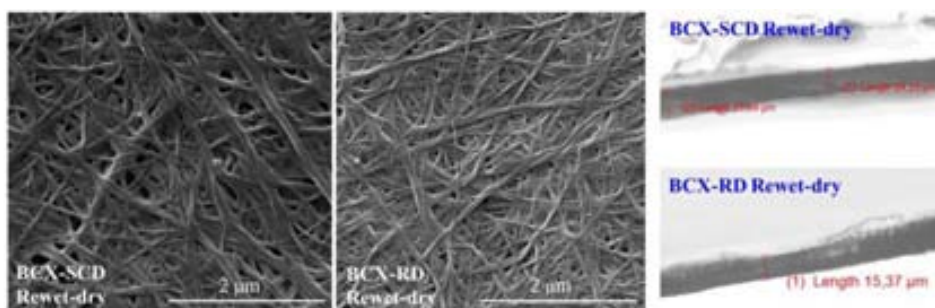


**Figure 3.22** After rewet-dry cycle, BCX-SCD and BCX-RD films became similar: SEM images of their structures, and the optical microscopy images of their thickness (25 I 0.7 µm and 16 I 1.4 µm, respectively).

Magnetic cellulose films show the increased trend of mechanical parameters from BCX-SCD to BCX-RD, which depends on the different drying methods that affected the structure and porosity of the pristine cellulose films. For instance, the BCX-SCD aerogel films which are the softer ones with the largest porosity (about 90 %) have the smallest young modulus and hardness values. Therefore, the topological arrangement of nano-fibres and their interactions play a significant role in the mechanical behaviour of magnetic cellulose composites.

**Table 3.4** Mechanical parameters (young modulus and hardness) of the pristine cellulose, magnetic cellulose films and rewet-dry cellulose films.

Sample	Young's modulus E (MPa)	Hardness H (MPa)
Pristine BCX-SCD	198±34	19±21
Pristine BCX-FD	601±155	26±12
Pristine BCX-RD	659±85	39±9
Magnetic BCX-SCD	708±310	62±23
Magnetic BCX-FD	769±169	76±17
Magnetic BCX-RD	1028±666	88±74
Rewet-dry BCX-SCD	1683±346	97±41
Rewet-dry BCX-FD	1593±352	108±49
Rewet-dry BCX-RD	1685±675	98±49

### Water capacity ability

Untreated BCFs are hydrophilic, and have high water absorption capacity (WAC) that has been evaluated in Chapter 2. The contact angle measurements were performed with a Kruss DSA 100 instrument from Drop Shape Analysis System. The pristine and magnetic cellulose films were fixed flat on the top of a glass slide. A droplet of distilled water (5  $\mu$ L) was placed on top of the BCX films. The droplet is illuminated from the side, contact angles were calculated using ImageJ analysis software (**Figure 3.23**). For instance, the pristine BCX-RD film has a WAC value of 34, meaning that it can hold water up to 34 times its own weight. Magnetic cellulose film, BCX-RD, presents a less hydrophilic character than the pristine one; this is likely to be associated with an increase of surface roughness provided by the NPs while the WAC value has diminished to 7 from an initial value of 34. These results were also confirmed by the contact angle measurement. The contact angles values of pristine cellulose films (BCX-SCD, BCX-FD and BCX-RD) are almost zero, while the magnetic cellulose films are much higher after being coated with iron oxide NPs. They are 17 $^{\circ}$ , 31 $^{\circ}$  and 45 $^{\circ}$ , respectively.

Pristine Cellulose	WAC	Contact angle	Magnetic cellulose	WAC	Contact angle
BCX-SCD	45	=0	BCX-SCD	6	17
BCX-FD	20	8	BCX-FD	5	31
BCX-RD	34	11	BCX-RD	7	45

**Figure 3.23** The WAC and contact angles values of pristine BCX films and magnetic BCX films in the left table. A) contact angle image of pristine BCX-RD film, B) contact angle image of magnetic BCX-RD film, and C) picture of magnetic BCX-RD film with one drop of distilled water on the top.

## Conformal coating

To further show the flexibility of the BCFs I constructed a small origami figure with a square piece of 1.5 cm x 1.5 cm (**Figure 3.24**). Interestingly the cellulose swan could be conformally and homogeneously nanocomposited with superparamagnetic NPs using MW method allowing the fabrication of intricate magnetic light objects.

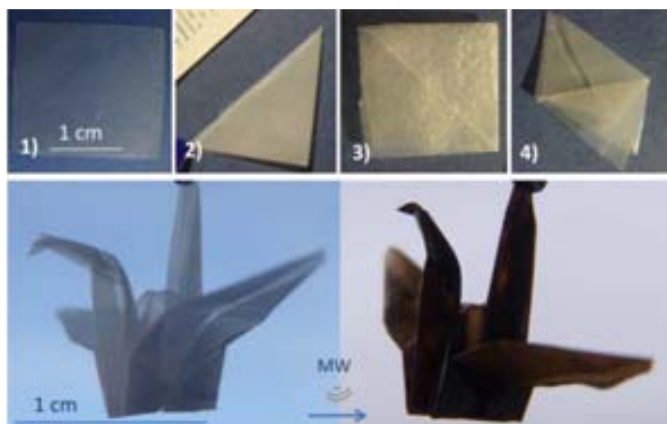
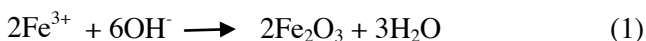


**Figure 3.24** Upper row show several folding steps to construct an origami swan out of bacterial cellulose (BCX-RD), final result is depicted in the lower row which also includes the “magnetic origami” after being treated in a microwave oven for five minutes with the iron precursor.

## Proposed mechanism

It has been explained in Chapter 1 and 2 that BC is formed by the polymerization of a glucose monomer yielding a large number of surface accessible polar hydroxy groups that facilitate the chemical modification of BC, including the modification of the hydrophilicity character of the original BC or incorporate NPs.(29) The hydroxy terminated surfaces of BC are more susceptible to absorb microwave energy than the bulk of the material activating in this way on the BC surface and promoting the nucleation and growth of the Fe<sub>2</sub>O<sub>3</sub> NPs on those sites as represented in **Figure 3.25A**.

According to previous researchers(30), the chemical reaction of iron oxide formation may be written as shown in equation 1(**Figure 3.25A**), which is made in several steps.



1. Step 1 Fe(OH) monomers(**Figure 3. 25B**): It begins with the formation of Fe(OH) monomers from the iron precursors and the benzyl alcohol. The mechanism of the formation of Fe(OH) monomer is assumed to be similar to the one proposed by Idalia Bilecka et al.(31) for the zinc oxide synthesis from

the zinc (III) acetate precursor. In our case, the precursor is iron (III) acetylacetonate ( $\text{Fe}(\text{acac})_3$ ) and the mechanism is an aldol condensation(32) instead of an ester elimination reaction.

2. Step 2 ( $\text{C}_6\text{H}_{10}\text{O}_5$ )-Fe (**Figure 3.25C**): Similar to step 1, a nucleophilic attack of cellulose repeat unit on the acetylacetonate group of the iron precursor leads to benzyl acetate and enolate groups.
3. Step 3  $\text{Fe}_2\text{O}_3$  NPs: In a final step, one  $\text{Fe}(\text{OH})$  monomers from step 1 can react with one ( $\text{C}_6\text{H}_{10}\text{O}_5$ )-Fe from step 2 by a condensation reaction. At this step,  $\text{Fe}_2\text{O}_3$  NPs were formed. During ageing time, further growth can occur by the Ostwald ripening process: small particles are dissolved in the bigger ones, which narrows the distribution of particle size.(8)

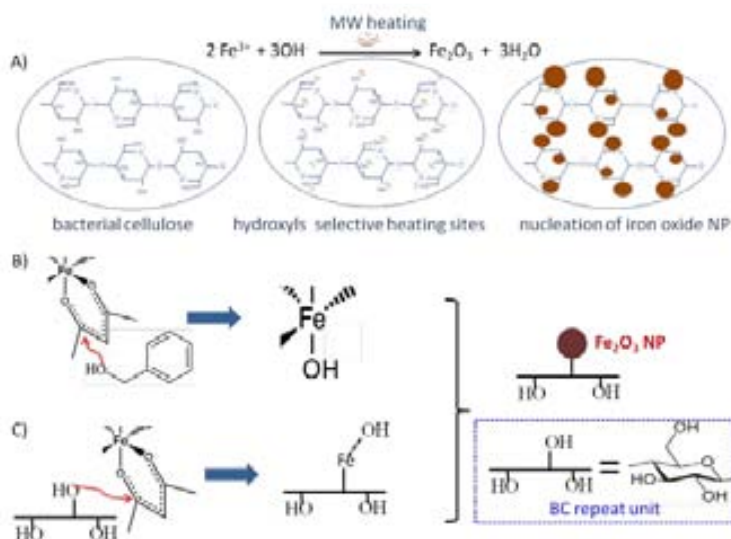


**Figure 3.25** Proposed mechanism of the bacterial-iron oxide nanocomposites.

### Synthesis of BCF-Au composites

BCF-Au composites were also prepared via one-step microwave-assisted method in aqueous suspension. Au NPs were successfully embedded into the 3D nano-network structure of BCFs while the amount of NPs can be controlled by choosing different types of our BCX films as the same synthesis of magnetic cellulose films. The same synthesis procedure was used successfully for BCF-Au composites in four different types: BCX-SCD, BCX-FD, BCX-RD and BCX-Wet films. These BCX films were firstly immersed into the gold precursor solution before the MW reaction, which followed the same process as magnetic cellulose films. In **Figure 3.26**, the BCX films present uniform and incremental purple colour (BCX-Wet > BCX-SCD > BCX-FD > BCX-RD), which indicate the macroscopic homogenous coverage of Au NPs.

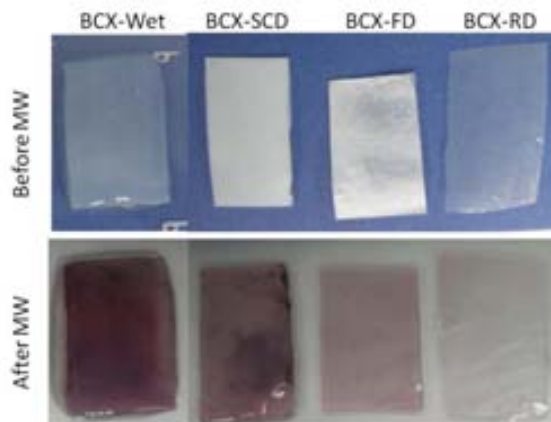


**Figure 3.26** Digital images of BCX films before and after MW. Au NPs were successfully coated on the BCX-SCD, BCX-FD, BCX-RD and BCX-Wet films by using microwave-assisted one step method.

**Figure 3.27** includes the UV-vis absorption spectra of Au NPs from the mother solutions and the dry BCX-Au films. The absorption spectra of Au NPs from mother solutions show the same peaks at 530 nm, due to the surface plasmon resonance of Au NPs, which was also confirmed by the TEM images in **Figure 3.28**. Well-defined Au NPs (10 ± 2 nm) from BCX-RD-Au film were observed. Moreover, the sharp peak suggested a narrow size distribution of Au NPs. The absorption peak of Au NPs in the BCF-Au composites became broader, and slightly red-shifted because of the surface plasmon coupling between closely spaced NPs(33). It was reported in one of the previous work(10), which is also similar to the absorption of silica nano-fibres-Au NPs hybrid nanostructure (34).

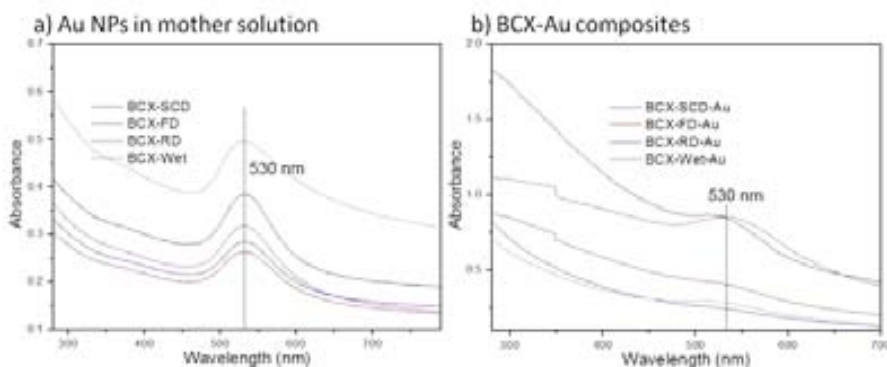


**Figure 3.27** UV-vis of gold NPs of mother solutions and BCX-Au films. Peaks are clearly seen for BCX-SCD-Au and BCX-Wet-Au. BCX-FD-Au and BCX-RD-Au films do not present clearly distinguishable bands due to their low Au content.

Meanwhile, as shown in **Figure 3.27b**, no additional peaks were observed indicating there are not any aggregated Au NPs. The obtained Au NPs in BCX films are very stable and we hypothesize it could be the existence of strong



hydrogen bonding between the Au NPs and the cellulose fibres. Interestingly, the coating amount of Au NPs can be also calculated by UV-vis, which was following the same trend as the one observed in the case of iron oxide nanoparticles: BCX-Wet > BCX-SCD > BCX-FD > BCX-RD.

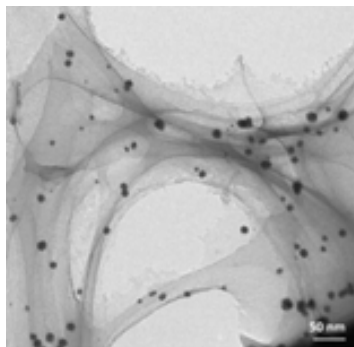


**Figure 3.28** TEM images of Au NPs embedded in the BCX-RD films.

### 3.3 Synthesis of functional and complex BCF-NPs composites

#### Synthesis of patterned BCF-SPIONs composites

In addition, we were interested in investigating the possibility of producing patterned BCFs by inducing selective nucleation of magnetic NPs in these films. In this way we could obtain biodegradable magnetic micromeshes that, once magnetized, allow the creation of complex field patterns and attract magnetic nano-objects or magnetized cells to the spots with the highest field gradient. A demand for this type of material was clearly stated by Fu et al., (35) who used a highly toxic nickel mesh to enhance cancer targeting in living subjects and mentioned the need for biocompatible micromeshes for clinical implementation of the technology.



**Figure 3.29** *First column;* Scheme of hydrophobic (blue) and hydrophilic (white) patterns in a BCX-RD-1 film. *Second column;* BCX-RD-2 film with patterned hydrophobic/hydrophilic zones. A water droplet with large contact angle is displayed in the hydrophobic region. *Third column;* depicts the patterned BCF-SPIONs composites. It can be seen that darker areas, higher iron oxide load, correspond to the hydrophilic zones of the patterned BCFs.

---

Following our hypothesis, we collaborated with the Karlsruhe Institute of Technology (KIT, Germany). They patterned pristine BCX-RD samples with 4-pentynoic acid (hydrophilic zones) and hydrophobic zones with non-polar terminated 1H,1H,2H,2H-perfluorodecanethiol, patterns shown **Figure 3.29**. Two pieces of BCX-RD film in rectangular shape (aprox 1 cm x 2 cm) were immersed into 25 mL of a dichloromethane solution containing 4-pentynoic acid (120 mg, 1.23 mmol) and catalyst 4-(dimethylamino)pyridine (56 mg, 0.46 mmol). Then, the coupling reagent N,N'-diisopropylcarbodiimide (190  $\mu$ L, 1.23 mmol) was added to the solution cooled to about 0 °C, and the solution was stirred at room temperature for 4 h. The films were then washed extensively with ethanol, followed by drying. Next, the 4-pentynoic acid modified BCX-RD film was placed on a glass substrate, wetted with acetone solution containing 10 vol% 1H,1H,2H,2H-perfluorodecanethiol, covered by a quartz slide, and irradiated by UV light (260 nm, 8.0 mw/cm<sup>2</sup>) through a quartz photo mask for 60 s. After removing the photo mask, washing with acetone and drying, the film was wetted with 1:1 ethanol: water solution containing 15 wt% cysteamine hydrochloride and irradiated by UV light for another 60 s. Finally, the film was washed extensively with ethanol and dried with a nitrogen gun gently. The parts of the film irradiated by UV turned hydrophobic while the parts protected from UV irradiation by the photo-mask remain hydrophilic with 4-pentynoic acid with available hydroxyls similar to the pristine films.

We hypothesized that the nucleation and growth of iron oxide NPs will be mostly favoured on the hydrophilic part of the BCX film. Preliminary results showed that indeed hydrophilic parts are darker indicating a larger fraction of NPs, which can be seen in both types of patterned BCFs (**Figure 3.29**). TGA was used to determine the weight percentage of iron oxide NPs on different areas of the patterned BCF-SPIONs composites (**Figure 3.30**). It can be concluded that, there is 50% larger magnetic load on the hydrophilic zone than in the hydrophobic one (BCX-RD-1 type).

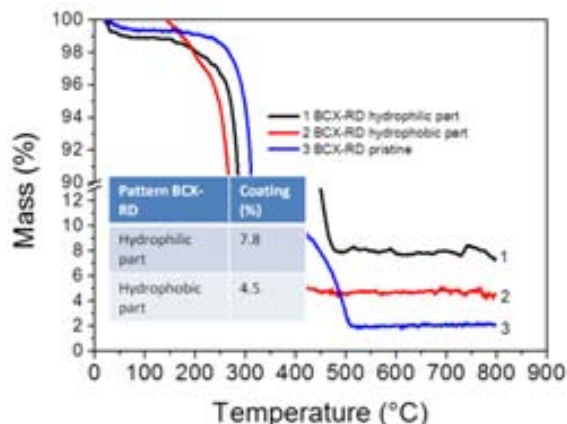


**Figure 3.30** TG curves of magnetic of pristine BCX-RD-1 bacterial cellulose and of the magnetic cellulose from the hydrophilic and hydrophobic parts, the second one display only 50% of the magnetic load.

Moreover, TEM images (**Figure 3.31**) showed that the  $\text{Fe}_2\text{O}_3$  NPs have been dispersed around the cellulose fibres. Compared with the hydrophobic areas, there were more NPs coated on the hydrophilic part (**Figure 3.31a**). They were homogeneously coating around the cellulose fibres, presenting darker colour than the another part (hydrophobic part).

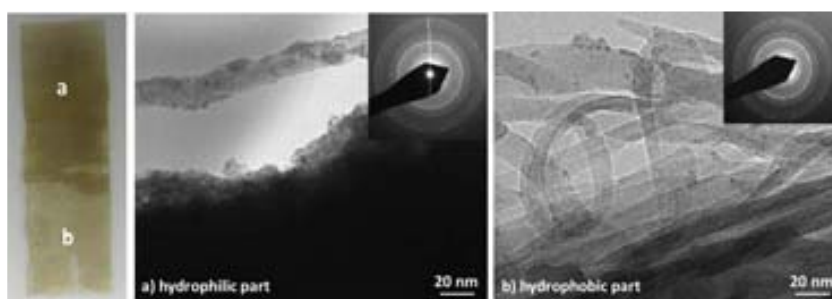


**Figure 3.31** TEM images of magnetic patterned BCX-RD-1 films: hydrophilic part (a) and hydrophobic part (b). Upper Insets: selected area electron diffraction pattern, which confirmed that both of them are iron oxide NPs.

Some  $\text{Fe}_2\text{O}_3$  NPs were also observed on the hydrophobic parts of BCF-SPIONs composites, which were coated with cellulose fibres, as seen **Figure 3.31b** and **Figure 3.32**. The reason is probably that not all of the hydroxy groups reacted with 4-pentynoic acid in the esterification step and both hydrophobic and hydrophilic areas contained residual hydroxy groups. Moreover, benzyl alcohol partially hydrolyzes the hydrophobic groups and thus some  $-\text{OH}$  groups from the patterned BCFs were exposed and then coated with  $\text{Fe}_2\text{O}_3$  NPs during the MW reaction. So some magnetic coating is also visible in the hydrophobic part.

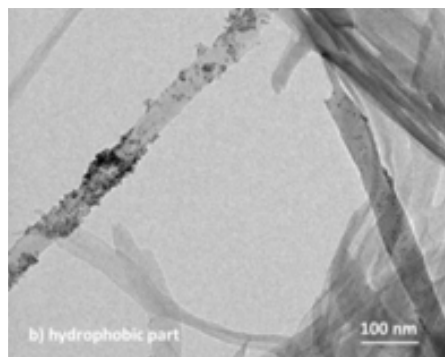


**Figure 3.32** TEM image of magnetic patterned BCX-RD-1 hydrophobic part.

A second approach to hydrophobize the bacterial cellulose was by using polydimethylsiloxane (PDMS) to pattern cellulose films since PDMS does not dissolve in benzyl alcohol. As shown in **Figure 3.33**, one piece of BCX-RD films was partly patterned with PDMS. One drop of distilled water was imaged on the patterned area, showing the hydrophobic property. Exactly following the same MW process, the magnetic BCX-RD-PDMS films were harvested. The colour of the hydrophilic parts of cellulose was changed after the MW reaction, indicating  $\text{Fe}_2\text{O}_3$  NPs were coated on these areas.



**Figure 3.33** BCX-RD-PDMS film, one drop of distilled water on top of the hydrophobic part, which was patterned by PDMS. Then it was cut into rectangular shaped pieces ( $\sim 2 \times 1$  cm) for MW reaction. After the clean process, iron oxide NPs were observed coating only the hydrophilic parts where there are free  $-\text{OH}$  groups.

TEM was performed on both hydrophilic and hydrophobic parts of the cellulose (**Figure 3.34**). One area of the hydrophilic part was named b, and another hydrophobic part was called a. There was no NPs observed on the hydrophobic part, in contrast, there are lots of  $\text{Fe}_2\text{O}_3$  NPs on the hydrophilic part. As expected, the  $\text{Fe}_2\text{O}_3$  NPs were only coated on the hydrophilic parts since the  $-\text{OH}$  groups of cellulose were not covered by PDMS.

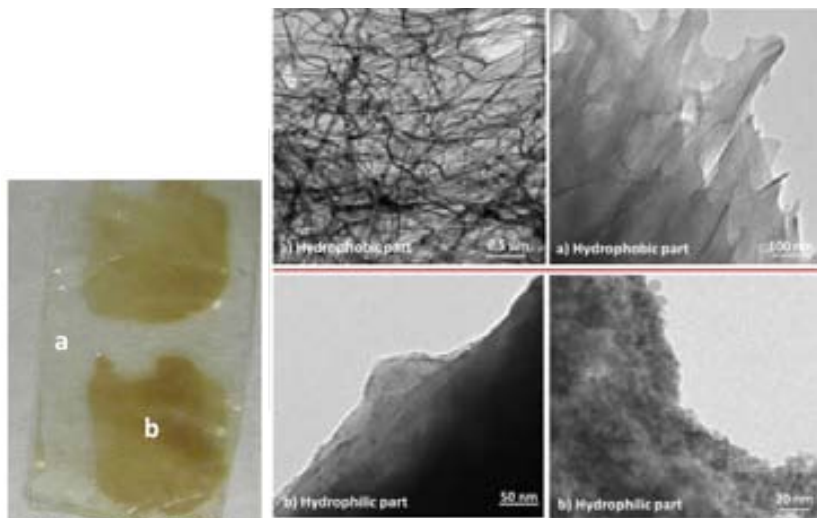


**Figure 3.34** One picture of patterned BCF-PDMS-SPIONs composite (a is the hydrophobic area, and b is the hydrophilic part.). Upper: TEM images of the hydrophobic part where  $\text{Fe}_2\text{O}_3$  NPs were not observed. Lower: TEM images of the hydrophilic part with  $\text{Fe}_2\text{O}_3$  NPs coated.

### Synthesis of BCF-Au-SPIONs composites

BC-NPs composites containing two or more different nanoscale functionalities are attractive candidates for advanced nanomaterials. With controlled amount, size and structure of different types of NPs, these nanocomposites can exhibit novel physical and chemical properties that could be essential for future applications. However, the controllable incorporation of more than one type of NPs in the BC implies a more complex synthetic pathway. Until now, no published studies were identified in the direction of using microwave-assisted method to prepare homogeneous and controllable BC-NPs composites with different metal or metal oxide NPs.

Here, I presented a possible method to synthesis BC-NPs composites with two different NPs:  $\text{Fe}_2\text{O}_3$  and Au NPs. As shown in **Figure 3.35**, the mode of processing used for BCF-Au-SPIONs composites is similar to the BCF-SPIONs composites synthesis, but including two steps synthesis instead of one. First of all, pristine cellulose of BCX-Wet, BCX-FD and BCX-RD coated with Au NPs (middle row). Then these purple, clean and dried BCF-Au composites were immersed in the iron precursor solution (0.078 M) about 30 minutes and followed the second coating of  $\text{Fe}_2\text{O}_3$  NPs by the MW method.

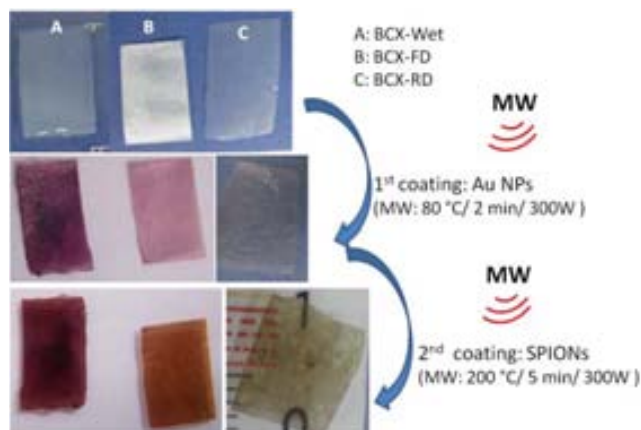


**Figure 3.35** Upper row: pristine cellulose of BCX-Wet, BCX-FD and BCX-RD. Middle row: BCF-Au composites after first coating of gold NPs. Lower row: BCF-Au-SPIONs films after second coating of iron oxide NPs.

TEM was used to distinguish these two NPs. The images and the selected area electron patterns obtained from the BCF-Au-SPIONs composites are shown in **Figure 3.36**. It is easy to identify that the darker particles are gold NP and the rest are iron oxide NPs due to the different density of particles, while it was also confirmed by the electron diffraction pattern. This investigation opens a new field that it is possible to manipulate different types of NPs to synthesize functional BC-NPs composites, even the size, structure and loading amount of NPs can be controlled.

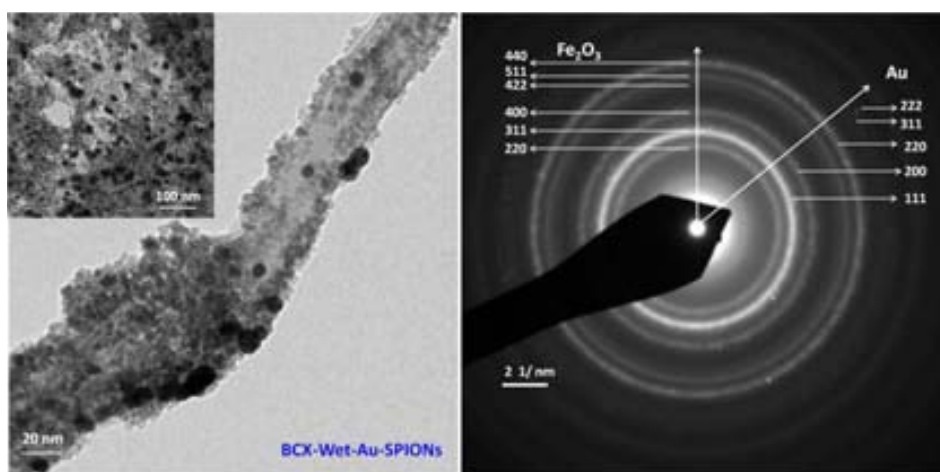


**Figure 3.36** TEM images and selected area electron pattern of BCX-Wet-Au-SPIONs films.

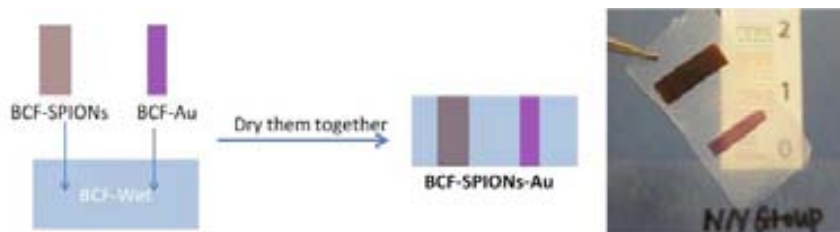


**Figure 3.37** BCF-SPIONs-Au composite was prepared by “block building” method.

Furthermore, an easy method of preparing BCF-SPIONs-Au composites is also depicted here, which we named “block building” method (**Figure 3.37**). Two pieces of functional bacterial cellulose films (BCF-SPIONs and BCF-Au) were added on the surface of BCF-Wet film, and then followed the drying process (Room temperature drying in this case). This method is the most likely cause of composite being unstable due to the weak connection between functional BCF-NPs composites with the pure BCFs. However, it is somewhat surprising that this BCF-SPIONs-Au composite was not separated after more than 5 minutes of sonicating in water (**Figure 3.38a**). In addition, it is difficult to remove the functional BCF-NPs films from the BCF-SPIONs-Au composite. This may suggest strong links exist between the functional BCF-NPs film and the pure film. A possible explanation might be that there are hydroxyl condensations between the two adjacent cellulose layers (**Figure 3.38d**). From the preliminary SEM image (**Figure 3.38e**) we can see that two layers of cellulose were tightly connected, which seems to confirm our hypothesis of hydroxyl condensation. However, more investigation is required. With the control of functionalities and stable interactions, the “block building” method could be the ideal and easiest model system for studying more complex BC-NPs composites with different NPs, and may evolve as useful nano-scale building blocks for future applications.

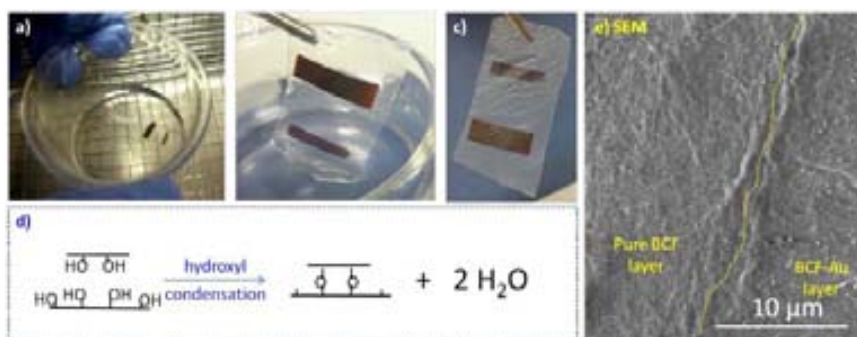


**Figure 3.38** a) The BCF-SPIONs-Au composite was immersed in distilled water and sonicated about 5 min. b) The BCF-SPIONs-Au composite was not destroyed or separated after the sonication. c) Rewet-dry BCF-SPIONs-Au composite. d) Proposed “chemical reaction” of hydroxyl condensation between the adjacent cellulose layers. e) SEM image of BCF-SPIONs-Au composite: the conjunction of pure BCF layer and BCF-Au layer.

---

### 3.4 Conclusions

Microwave heating represents an attractive non-traditional energy source to perform chemical synthesis due to the high acceleration and yield of the chemical reaction obtained.(7, 31, 36, 37) In comparison to other conventional heating methods (heating plates, oil bath), the microwave radiation avoids temperature gradients within the vessel, decreasing the possibility of an asynchronous nucleation and heterogeneous nano-crystals growth. Microwaves produce a rapid, intense heating of polar substances permitting to use them as selective heating modes. In addition, microwave induces molecular vibration and a subsequent temperature increase causing a greater movement of the molecules, higher diffusivity and collision probability. Based on heating selectivity and the increase of the molecular motion, complex nano-structured materials can be fabricated, as for instance conformal coating of porous materials by an in-situ synthesis of a secondary phase.(38, 39)

Here, we presented a microwave-assisted thermal decomposition method for BC-NPs composites with superparamagnetic maghemite NPs within only 5min and without the need for post-synthetic treatment. The NPs are crystalline, less than 10 nm in size, with a narrow particle size distribution. The NPs coat the BCFs conformally and uniformly, even when the films are folded into complex shapes, and they do not leach when immersed in water for a long time (up to three months). Control over the magnetic fraction was achieved either by employing never-dried cellulose, BCFs dried by different methods, or by adjusting the initial iron concentration. All films react easily to an external magnetic field, present superparamagnetic behaviour at room temperature, and are flexible enough to be bent, even those with the largest magnetic fraction (up to 40 %). Interestingly, the films with the lowest magnetic fraction are also transparent. Moreover, this effective approach was successfully expanded to gold NPs and even two types NPs.

It is worth noting that BCFs allow multiple patterning with several materials. For instance, they were patterned with hydrophobic/hydrophilic domains and selectively anchor the magnetic NPs allowing us to create magnetic patterns in the cellulose, which is promising to pave the way to new uses of functional bacterial cellulose. We believe that our newly designed material could have ground breaking features that may tremendously expand the applications of the BCF-based nanocomposites in tissue engineering and cell culture applications.



---

### 3.5 References

1. W. Hu, S. Chen, J. Yang, Z. Li, H. Wang, Functionalized bacterial cellulose derivatives and nanocomposites, *Carbohydrate polymers*, **101**, 1043, (2014).
2. N. Shah, M. Ul-Islam, W. A. Khattak, J. K. Park, Overview of bacterial cellulose composites: a multipurpose advanced material, *Carbohydrate polymers*, **98**, 1585, (2013).
3. R. T. Olsson, M. A. Samir, G. Salazar-Alvarez, L. Belova, V. Ström, L. A. Berglund, O. Ikkala, J. Nogues, U. W. Gedde, Making flexible magnetic aerogels and stiff magnetic nanopaper using cellulose nanofibrils as templates, *Nature nanotechnology*, **5**, 584, (2010).
4. D. Fragouli, I. S. Bayer, R. Di Corato, R. Brescia, G. Bertoni, C. Innocenti, D. Gatteschi, T. Pellegrino, R. Cingolani, A. Athanassiou, Superparamagnetic cellulose fiber networks via nanocomposite functionalization, *Journal of Materials Chemistry*, **22**, 1662, (2012).
5. J. Cheng, R. Roy, D. Agrawal, Radically different effects on materials by separated microwave electric and magnetic fields, *Material Research Innovations*, **5**, 170, (2002).
6. P. Lidström, J. Tierney, B. Wathey, J. Westman, Microwave assisted organic synthesis—a review, *Tetrahedron*, **57**, 9225, (2001).
7. O. Pascu, E. Carena, M. Gich, S. Estradé, F. Peiró, G. Herranz, A. Roig, Surface Reactivity of Iron Oxide Nanoparticles by Microwave-Assisted Synthesis; Comparison with the Thermal Decomposition Route, *The Journal of Physical Chemistry C*, **116**, 15108, (2012).
8. O. Pascu, Synthes Magnetic Nanoparticles and Strategies towards Magneto-Photonic materials, *Doctoral thesis*, (2012).
9. M.-C. Daniel, D. Astruc, Gold nanoparticles: assembly, supramolecular chemistry, quantum-size-related properties, and applications toward biology, catalysis, and nanotechnology, *Chemical reviews*, **104**, 293, (2004).
10. T. Zhang, W. Wang, D. Zhang, X. Zhang, Y. Ma, Y. Zhou, L. Qi, Biotemplated Synthesis of Gold Nanoparticle-Bacteria Cellulose Nanofiber Nanocomposites and Their Application in Biosensing, *Advanced Functional Materials*, **20**, 1152, (2010).
11. E. Boisselier, D. Astruc, Gold nanoparticles in nanomedicine: preparations, imaging, diagnostics, therapies and toxicity, *Chemical Society reviews*, **38**, 1759, (2009).
12. T. Maneerung, S. Tokura, R. Rujiravanit, Impregnation of silver nanoparticles into bacterial cellulose for antimicrobial wound dressing, *Carbohydrate polymers*, **72**, 43, (2008).
13. A. Stoica-Guzun, M. Stroescu, S. I. Jinga, I. M. Jipa, T. Dobre, Microwave assisted synthesis of bacterial cellulose-calcium carbonate composites, *Industrial Crops and Products*, **50**, 414, (2013).
14. A. R. Silva, G. Unali, Controlled silver delivery by silver-cellulose nanocomposites prepared by a one-pot green synthesis assisted by microwaves, *Nanotechnology*, **22**, 315605, (2011).
15. S.-M. Li, N. Jia, M.-G. Ma, Z. Zhang, Q.-H. Liu, R.-C. Sun, Cellulose–silver nanocomposites: Microwave-assisted synthesis, characterization, their thermal stability, and antimicrobial property, *Carbohydrate polymers*, **86**, 441, (2011).

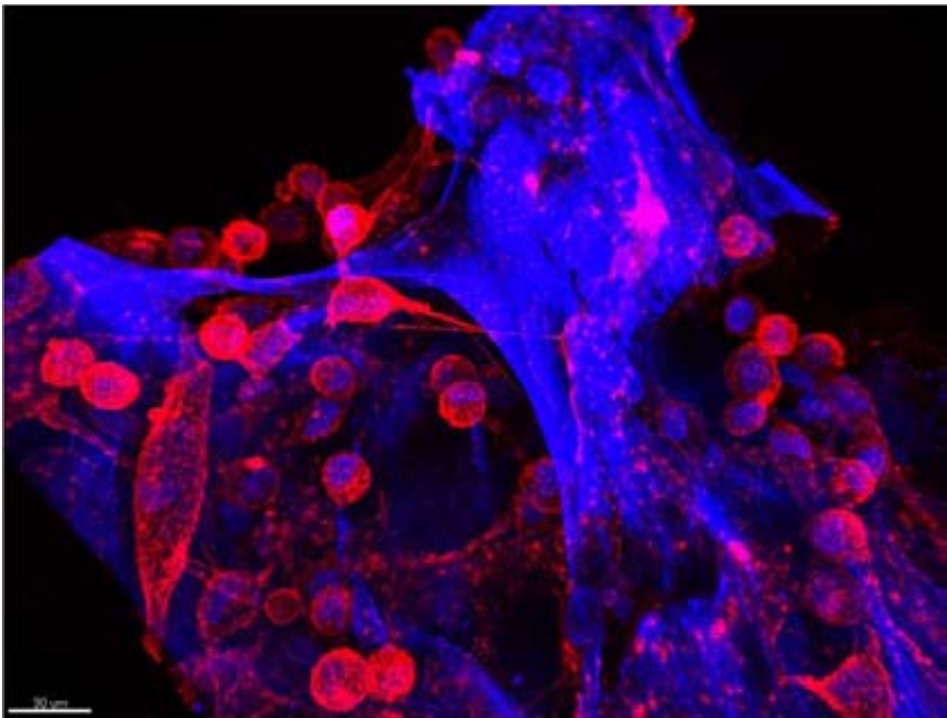
- 
16. C. H. Chia, S. Zakaria, K. L. Nguyen, V. Q. Dang, T. D. Duong, Characterization of magnetic paper using Fourier transform infrared spectroscopy, *Materials Chemistry and Physics*, **113**, 768, (2009).
  17. P. R. a. L. R. R. H. Marchessault, Magnetic cellulose fibres and paper: preparation, processing and properties, *Polymer*, **33**, (1992).
  18. S. Liu, X. Luo, J. Zhou, Magnetic Responsive Cellulose Nanocomposites and Their Applications, (2013).
  19. S. Galland, R. L. Andersson, M. Salajková, V. Ström, R. T. Olsson, L. A. Berglund, Cellulose nanofibers decorated with magnetic nanoparticles – synthesis, structure and use in magnetized high toughness membranes for a prototype loudspeaker, *Journal of Materials Chemistry C*, **1**, 7963, (2013).
  20. W. Zhang, S. Chen, W. Hu, B. Zhou, Z. Yang, N. Yin, H. Wang, Facile fabrication of flexible magnetic nanohybrid membrane with amphiphobic surface based on bacterial cellulose, *Carbohydrate polymers*, **86**, 1760, (2011).
  21. D. Faivre, Multifunctional materials: Dry but flexible magnetic materials, *Nature nanotechnology*, **5**, 562, (2010).
  22. X. Yu, S. Tong, M. Ge, J. Zuo, C. Cao, W. Song, One-step synthesis of magnetic composites of cellulose@iron oxide nanoparticles for arsenic removal, *Journal of Materials Chemistry A*, **1**, 959, (2013).
  23. Y. Zheng, J. Yang, W. Zheng, X. Wang, C. Xiang, L. Tang, W. Zhang, S. Chen, H. Wang, Synthesis of flexible magnetic nanohybrid based on bacterial cellulose under ultrasonic irradiation, *Materials science & engineering. C, Materials for biological applications*, **33**, 2407, (2013).
  24. C. Katepetch, R. Rujiravanit, Synthesis of magnetic nanoparticle into bacterial cellulose matrix by ammonia gas-enhancing in situ co-precipitation method, *Carbohydrate polymers*, **86**, 162, (2011).
  25. M. Zeng, A. Laromaine, W. Feng, P. A. Levkin, A. Roig, Origami magnetic cellulose: controlled magnetic fraction and patterning of flexible bacterial cellulose, *Journal of Materials Chemistry C*, (2014).
  26. H. Y. Zhu, Y. Q. Fu, R. Jiang, J. H. Jiang, L. Xiao, G. M. Zeng, S. L. Zhao, Y. Wang, Adsorption removal of congo red onto magnetic cellulose/Fe<sub>3</sub>O<sub>4</sub>/activated carbon composite: Equilibrium, kinetic and thermodynamic studies, *Chemical Engineering Journal*, **173**, 494, (2011).
  27. J. Zeng, S. Liu, J. Cai, L. Zhang, TiO<sub>2</sub> Immobilized in Cellulose Matrix for Photocatalytic Degradation of Phenol under Weak UV Light Irradiation, *The Journal of Physical Chemistry C*, **114**, 7806, (2010).
  28. M. Zeng, A. Laromaine, A. Roig, Bacterial Cellulose Films: Influence of bacterial strain and drying route on film properties, *Submitted*, (2013).
  29. H. Jin, M. Kettunen, A. Laiho, H. Pynnonen, J. Paltakari, A. Marmur, O. Ikkala, R. H. Ras, Superhydrophobic and superoleophobic nanocellulose aerogel membranes as bioinspired cargo carriers on water and oil, *Langmuir : the ACS journal of surfaces and colloids*, **27**, 1930, (2011).
  30. S. Laurent, D. Forge, M. Port, A. Roch, C. Robic, L. Vander Elst, R. N. Muller, Magnetic iron oxide nanoparticles: synthesis, stabilization, vectorization, physicochemical characterizations, and biological applications, *Chemical reviews*, **108**, 2064, (2008).
  31. I. Bilecka, P. Elser, M. Niederberger, Kinetic and thermodynamic aspects in the microwave-assisted synthesis of ZnO nanoparticles in benzyl alcohol, *ACS nano*, **3**, 467, (2009).

- 
32. M. Niederberger, G. Garnweitner, Organic reaction pathways in the nonaqueous synthesis of metal oxide nanoparticles, *Chemistry*, **12**, 7282, (2006).
  33. K. H. Su, Q. H. Wei, X. Zhang, J. J. Mock, D. R. Smith, S. Schultz, Interparticle Coupling Effects on Plasmon Resonances of Nanogold Particles, *Nano Letters*, **3**, 1087, (2003).
  34. S. Zhang, W. Ni, X. Kou, M. H. Yeung, L. Sun, J. Wang, C. Yan, Formation of Gold and Silver Nanoparticle Arrays and Thin Shells on Mesostructured Silica Nanofibers, *Advanced Functional Materials*, **17**, 3258, (2007).
  35. R. J. W. Aihua Fu, Bryan R. Smith, Joyce Mullenix, Chris Earhart, Demir Akin, Samira Guccione, Shan X. Wang,\* and Sanjiv S. Gambhir\*, Fluorescent Magnetic Nanoparticles for Magnetically Enhanced Cancer Imaging and Targeting in Living Subjects, *ACS Nano*, **6**, 6862, (2012).
  36. D. Monti, A. Ponrouch, M. Estruga, M. R. Palacín, J. A. Ayllón, A. Roig, Microwaves as a synthetic route for preparing electrochemically active TiO<sub>2</sub> nanoparticles, *Journal of Materials Research*, **28**, 340, (2013).
  37. M. Baghbanzadeh, L. Carbone, P. D. Cozzoli, C. O. Kappe, Microwave-Assisted Synthesis of Colloidal Inorganic Nanocrystals, *Angewandte Chemie International Edition*, **50**, 11312, (2011).
  38. O. Pascu, M. Gich, G. Herranz, A. Roig, 2D Magnetic Frames Obtained by the Microwave-Assisted Chemistry Approach, *European Journal of Inorganic Chemistry*, **2012**, 2656, (2012).
  39. O. Pascu, J. M. Caicedo, M. Lopez-Garcia, V. Canalejas, A. Blanco, C. Lopez, J. Arbiol, J. Fontcuberta, A. Roig, G. Herranz, Ultrathin conformal coating for complex magneto-phonic structures, *Nanoscale*, **3**, 4811, (2011).



# Chapter 4

## Biocompatibility of Bacterial cellulose films



---

## Chapter Index

Chapter summary .....	97
4.1 Biocompatibility of bacterial cellulose films.....	98
Bacterial cellulose films in biological medium and cell culture medium .....	98
Bacterial cellulose films with cells .....	101
MTT assays .....	102
Live/dead fluorescence viability testing- calcein AM staining.....	104
Confocal microscopy.....	105
4.2 3D bacterial cellulose scaffold .....	107
Production of 3D bacterial cellulose scaffold .....	107
3D bacterial cellulose scaffold with cells.....	110
Confocal microscopy.....	110
4.3 Conclusions .....	113
4.4 References .....	114

---

## Chapter summary

As mentioned in Chapter 1, biocompatibility is a major requirement for the use of bacterial cellulose in biological and medical applications such as: artificial skin, wound care materials, dental implants, scaffolds for tissue engineering and cell studies. Although BC is generally considered a non-cytotoxic material, its biocompatibility has not been so far fully evaluated. A recent review from Petersen and Gatenholm states that cell-BC interactions are complex and will yet require further *in vitro* and *in vivo* studies.(1)

In this chapter, I present a comprehensive investigation of the *in vitro* biocompatibility of our BCFs. Firstly, the BCFs were evaluated in cell culture medium and then in the presence of MDA-MB 231 and HepG2 cells. Secondly, experiments were conducted to study the cytotoxicity of BCFs and cell viability for BCFs as 2D scaffolds. Optical and confocal microscopes were used to visualize and characterize the cell distribution.

Since the cell environment is a factor, which can influence cell behaviour and migration,(2, 3) it is necessary to find new scaffolds which more realistically real cell environment. Here, I also present a method for producing BCFs with bigger pores, in order to mimic a 3D environment of living tissues.

The work presented in this chapter has been done in collaboration with other group members Dr. Maria Milla and Ilargi Napal, MSc student.

---

## 4.1 Biocompatibility of bacterial cellulose films

Bacterial cellulose, as a novel scaffold material, is being actively studied. The use of biocompatible BC scaffolds in wound care or tissue engineering is essential in order to support cell proliferation and remain in contact with living tissue without causing any toxic or allergic side-effects(4).

The present section is focused in the study of BCFs biocompatibility with cells, carried out using MDA-MB 231 and HepG2 cell lines, but also in the behaviour of BCFs in biological medium and in the cell culture. These investigations constitute an important step towards the use of bacterial cellulose in medical devices such as implants for tissue engineering.

### Bacterial cellulose films in biological medium and cell culture medium

#### Materials

Phosphate buffered saline (PBS), minimum essential medium (MEM) and MEM enriched with 10 % of fetal bovine serum (FBS) were purchased from Sigma Aldrich. BCX and BCE films dried by three methods (SCD, FD and RD) were used (see Chapter 2).

All experiments concerning cytotoxicity have to be performed under sterile conditions. Thus a suitable method for sterilizing BCFs had to be identified in the first place. We evaluated two sterilization methods: UV radiation and autoclaving.

We added two pieces of BCX-RD films under the germicidal ultraviolet lamp, which was emitting high intensity ultraviolet radiation concentrated around the wavelength of 253.7 nm (UV-C radiation) and also happened to be in the region of maximum germicidal effectiveness. One film was irradiated for 2 hours (called BCX-RD-1) and another for 6 hours (called BCX-RD-2). Sterilized BCX-RD films were cut to fit into a 6-well plate. Each well was filled with 5 mL of MEM medium. All the samples well incubated statically for 6 days, at 37 °C. As control, we prepared one sample with only MEM medium without cellulose films. **Figure 4.1**, presents the first trial experiment were done with BCX-RD-1 and BCX-RD-2 films, which were irradiated with UV light for 2h and 6h, respectively.

We also sterilized one more piece of BCX-RD film by autoclaving, at 120 °C for 30 mins. The autoclave method involves the immersion of the films in water, following previous protocols, and we disregarded this method because it could change the initial properties of BCFs (such as porosity, thickness).



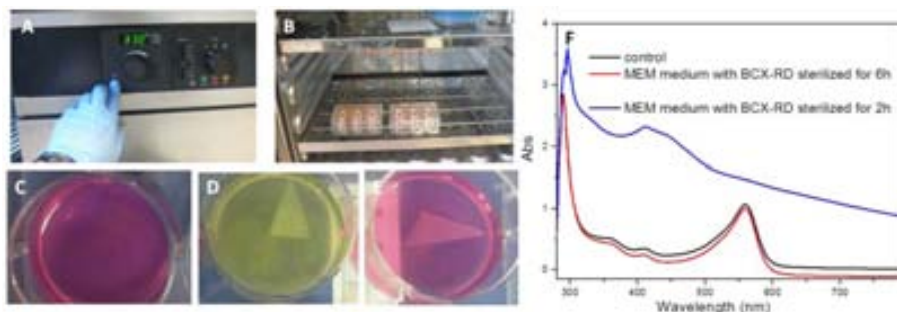


**Figure 4.1** A) incubator at 37 °C; B) 6-well plates were incubated inside the incubator; C) MEM medium without BCF as control; D) BCX-RD-1 was incubated in MEM medium for 6 days; E) BCX-RD-2 was incubated in MEM medium for 6 days; F) UV-vis spectra of C, D and E medium after 6 days incubation.

After 4 days incubation, the medium of BCX-RD-1 started to change the colour from pink to yellow, showing the medium was contaminated, indicating that 2h of UV radiation was not enough to sterilize BCX-RD-1 film. Cell medium were analysed by ultraviolet visible spectroscopy (Shimadzu UV/VIS UV-2102 spectrometer). As is seen in **Figure 4.1F**, the medium of BCX-RD-2 show the same peaks as the control medium. Therefore, 6 hours irradiation under UV light was our selected method to sterilize BCFs.

In order to analyse the BCFs behaviour in biological medium and cell culture medium, PBS, MEM and MEM enriched with 10% of FBS (MEM + 10% FBS) were used. All the sterilized BCFs were cut to fit into a 6-well plate, which were filled with three mediums. All the samples were incubated statically for 6 days, at 37 °C. In **Figure 4.2**, two pieces of each film including BCX-SCD, FD, RD and BCE-SCD, FD, RD films were immersed in the medium and incubated for 6 days.

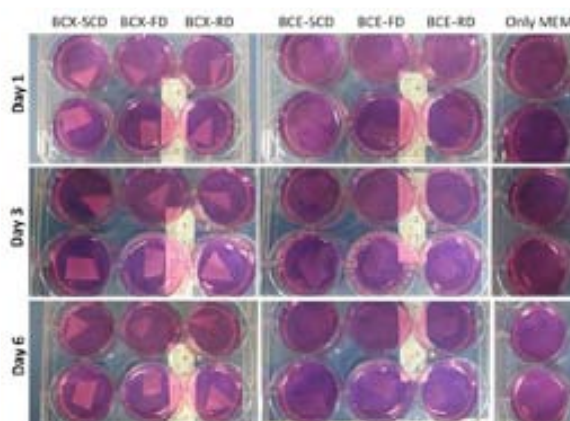


**Figure 4.2** Images of MEM medium were incubated with BCFs from both GX and GE strains for 1, 3 and 6 days. Images of PBS medium and MEM+10% FBS medium incubated with BCFs are not seen.

After 6 days, the pink colour of each medium was unaltered, giving a preliminary indication that mediums were not contaminated by the BCFs. In addition, the control medium and the MEM medium incubated with BCFs were also analysed by ultraviolet visible spectroscopy. The result is shown in **Figure 4.3**. All the spectra showed the same peaks, confirming that BCFs did not affect the characteristics of the medium after 6 culture days. So it is safe to say that BCFs are stable and are not affecting the cell medium after being incubated in it for 6 days.

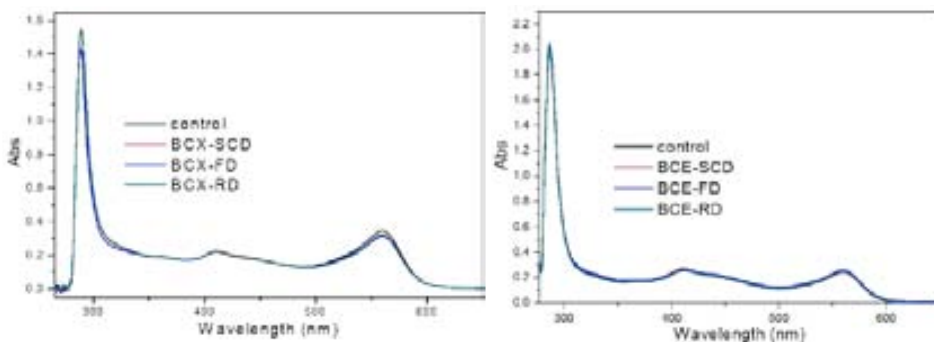


**Figure 4.3** UV-vis spectra of MEM cell culture medium incubated 6 days with BCFs. In comparison of the control medium, all the mediums maintain the same indicating the BCFs did not affect the medium without degradation.

Additionally, we weighed the BCFs before and after the incubation with cell cultures. Each BCF almost maintained the same weight as before the incubation. Furthermore, we were also interested to check the BCFs stability in the mediums. Therefore, these BCFs were kept in the medium for another 15 days (21 days in total). After this period, BCFs were cleaned with distilled water and dried at room temperature. In **Figure 4.4**, the pictures of each film before and after being incubated with PBS, MEM and MEM (MEM + 10% FBS) are presented. BCE films were too difficult to manipulate after the incubation with the three different mediums. Some of the films were broken during the cleaning and drying processes. In comparison to BCE films, BCX films are more robust to any manipulation. They maintained almost the same shape as before, including SCD, FD and RD as can be seen in **Figure 4.4**.

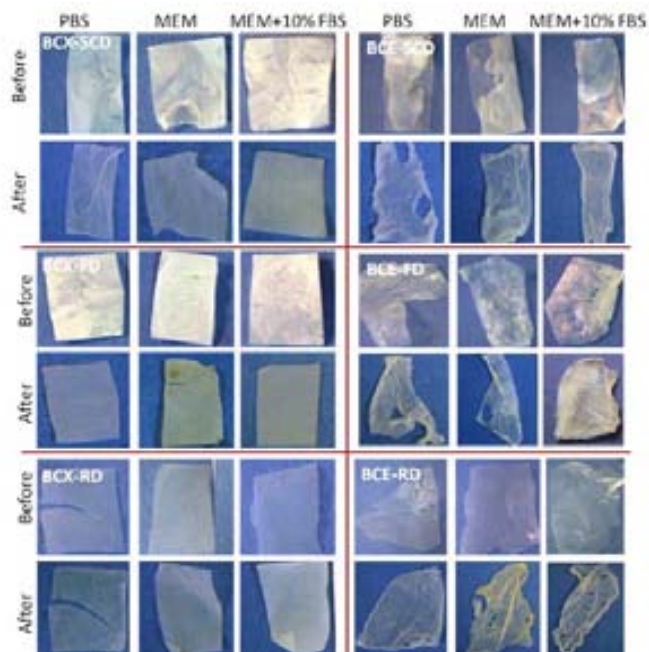


**Figure 4.4** Images of BCX and BCE films before and after being incubated in PBS, MEM and MEM+FBS for 21 days.

The medium used after the treatment with BCFs were also analysed by dynamic light scattering (DLS). As we expected, cellulose fibres dispersed in the medium were not identified because BC can hardly degrade without the presence of enzymes.

So it is safe to conclude that BCFs are stable and their characteristics are not affected when immersed in cell mediums nor the films have a deleterious effect on the medium.

### **Bacterial cellulose films with cells**

In order to check the biocompatibility of BCFs with cells, BCX films were chosen because they are much easier to manipulate than the BCE films. Here, we used MDA-MB 231 cells to analyse the cytotoxicity of the BCX films by viability assays. Moreover, we also investigated the metabolic activity of cells cultured with cellulose films by performing live/dead viability assay.

### **Materials**

MDA-MB 231 cell line was obtained from American Type Culture collection (ATCC, Manassas, VA). GlutaMax and PBS were obtained from Life-Technologies (Invitrogen). Cells were grown in RPMI medium, containing 10 % FBS and 6 mM GlutaMax.

## MTT assays

MDA-MB 231 cells were detached from growth flasks by using treatment with trypsin-EDTA (1 min); re-suspended with supplemented medium and pelleted by centrifugation at 1400 rpm (Eppendorf Centrifuge 5702). Cells were plated at a concentration of  $0.2 \times 10^6$  cells/mL in a 24 well-plate and incubated for 24 h at 37 °C and an atmosphere of 5 % CO<sub>2</sub>. The following day, the media was replaced with a fresh one containing 1 % antibiotic-antimycotic agents. Pieces of the same size of BCX films were added and immersed in the cultures during 24 h, as shown in **Figure 4.5a**. Plates were incubated for another 24 h. Finally, MTT reactive (Bio-medica) was added up to 10 % volume and plates were incubated at 37 °C for 2-5 hours and were read in a micro plate reader (Victor3, Perkin Elmer) at 450 nm, and 620 nm as reference.

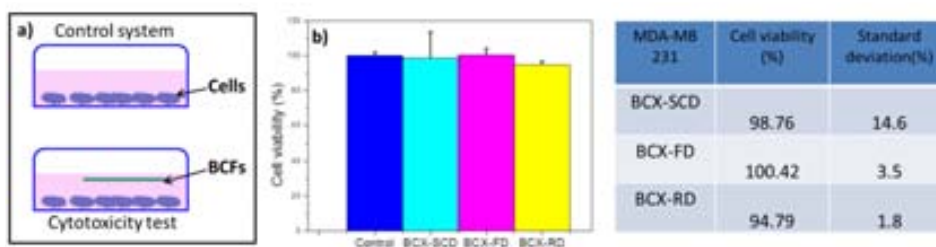


**Figure 4.5** a) Schematic images of control system and MDA-MB 231 cells grown with BCX films immersed in the culture medium; b) The viability of cells grown in the presence of the films. The data from the table represent the mean  $\bar{I}$   $\sigma$  (standard deviation) for three independent repeats.

Viability of MDA-MB 231 cell line cultured in the presence of different types of BCX films was studied with MTT assay (**Figure 4.5**). As expected, after 24 h of incubation, all the BCX films showed high cell viability indicating these films can be supposed not cytotoxic and allow the growth of the cells.

Optical microscopy images of cultured cells were obtained by inverted optical microscopy (Nikon Eclipse TS100). As is can be seen in **Figure 4.6**, all BCX films were observed. After 1 week in culture, MDA-MB 231 cells proliferated and spread on the surface of all the well-plates with or without BCX films immersed. Cells showed the same morphological properties in all cases analysed. There were no differences in cell growth and in cell behaviour.

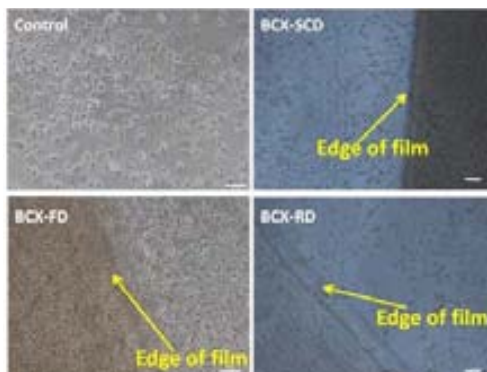


**Figure 4.6** MDA-MB 231 cultures (optical microscopy), after 1 week of incubation. Cells proliferated and spread on the surface of all samples, showing the same morphological properties. Bars: 20  $\mu\text{m}$ .

We also evaluated the cell viability when the cells were spotted on each BCX film as a scaffold. The system can be seen in **Figure 4.7a**. 4  $\mu\text{L}$  of a suspension of  $10^7$  cell/mL were spotted on the film surface with a Gilson P10 pipette. Spotted films were placed into a Petri dish filled with warm growth media and cultured for 48 h in an incubator at 37  $^{\circ}\text{C}$  and an atmosphere of 5 %  $\text{CO}_2$ . Specially, we used one piece of chromatography paper to grow cells as a control in this case, which has been reported by Derda et al.(5)

As shown in **Figure 4.7b**, the result of cell viability confirms that our BCX films are not cytotoxic and capable of maintaining the cell growth. Interestingly, the proliferation speed of cells is faster when compared to the cells cultured on the chromatography paper (as plant cellulose). It is worth mentioning the functional magnetic cellulose films (see Chapter 3) can also provide a safety environment for cells growth, which can be used as a novel functional BC composite in biological field.(6, 7) The investigation of BCX-RD-SPIONs with cells is the preliminary result, which deserved further research and not presented in the thesis.

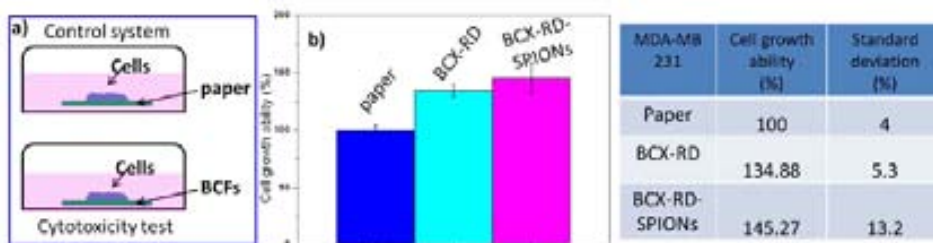


**Figure 4.7** a) Schematic images of the control system and MDA-MB 231 cells grown on the surface of one chromatography paper (plant cellulose), BCX-RD film and BCX-RD-SPIONs composite film. b) Cell viability of each sample. The data from the table represent the mean  $\bar{I}$   $\sigma$  (standard deviation) for three independent repeats.

---

As shown in **Figure 4.8**, optical microscopy images of cells grown in BCX films were presented. After 1 week in culture, MDA-MB 231 cells proliferated and spread on the surface of BCX-SCD, BCX-FD and BCX-RD films. Cells showed the same morphology as they cultured in petri dishes (**Figure 4.6**). Moreover, the homogeneous distribution of cells in each film could also indicate good cell function and viability.



**Figure 4.8** MDA-MB 231 cultures (optical microscopy), after 1 week of incubation. Cells proliferated and spread on the surface of all samples, showing the same morphological properties. A) BCX-SCD; B) BCX-FD and C) BCX-RD film.

#### **Live/dead fluorescence viability testing- calcein AM staining**

Live/dead assay can be used to qualitatively and quantitatively indicate the viability of the cells within the BCFs scaffold. This assay consisting of calcein-AM and propidium iodide (PI) was performed. Calcein-AM is a non-fluorescent dye that is converted to a green-fluorescent calcein after its hydrolysis by cell metabolic activity. PI is a fluorescent molecule that can be used to stain cells and DNA. PI can enter the membrane of dead cells and bind to DNA, showing a red colour. Samples were protected from light. All the BCX films were washed 2 times with HBSS and then stained with a 0.5 µg/mL PI and 1 µg/mL calceinAM solution (in HBSS) for 15 min at 37 °C. Films were washed twice with HBSS, fixed with cold paraformaldehyde (PFA) for 5 min and then washed twice again with HBSS.

After 7 days culture, we counted the number of cells in the contrast images and the number of alive cells in the fluorescent images (green). As shown in **Figure 4.9**, cells were alive with all the BCX films: RD, FD and SCD. Moreover, we did not observe any dead cells that should be dyed with PI showing red colour (**Figure 4.9GHI**).

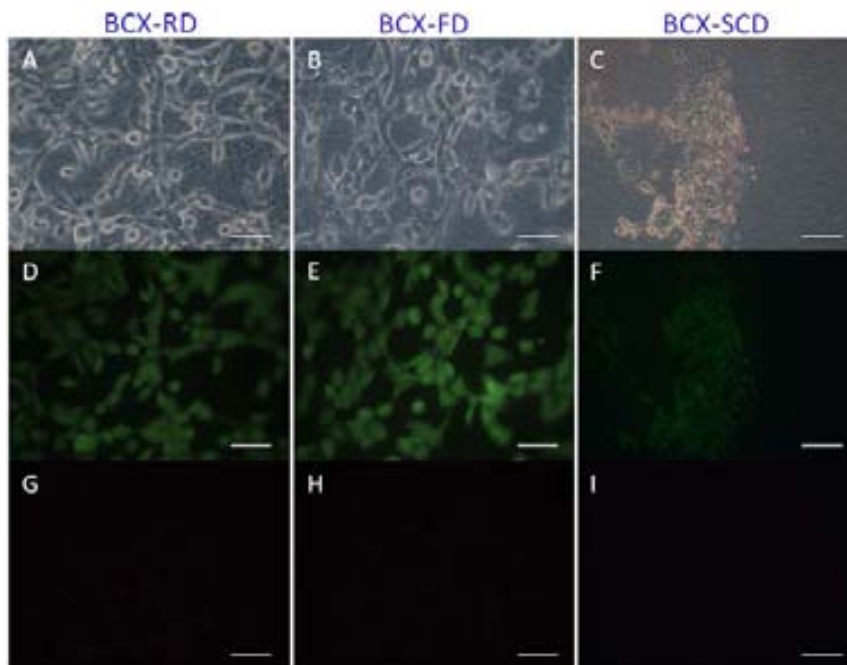


**Figure 4.9** Live/dead fluorescence viability testing: MDA-MB 231 cells were alive in all the BCFs scaffold including BCX-RD, FD and SCD. A-C: Phase contrast images of cells within BCX-RD, FD and SCD films; D-F: Fluorescence images (Calcein-AM staining) of living cells- green; G-I: Fluorescence images (PI staining) of dead cells- red. Bars: 200  $\mu\text{m}$  (C, F, I); 50  $\mu\text{m}$  (rest).

### Confocal microscopy

After the MTT assay and live/dead viability assay, it is clearly that BCX films are suitable for growing cells as a biocompatible scaffolds. Besides, it is also desirable to utilize our cellulose film as a scaffold having the adequate porosity to support cell in-growth like in a 3D environment similar to the human tissues. For the analysis of cell diffusion into the BCX films, we have chosen confocal microscopy. The microscope is an optical imaging technique used for the reconstruction of 3D structures and it is commonly used in cell culture field. Cells were imaged with Leica SP5 and Zeiss LSM 700 confocal microscopes. Firstly, samples were washed twice with PBS. Cells were fixed with cold PFA for 5 min and washed twice with PBS. Prior to their observation, cells were stained with 10  $\mu\text{g}/\text{mL}$  Hoechst and 5  $\mu\text{g}/\text{mL}$  Cell Mask<sup>TM</sup> for 5 min at room temperature and washed twice with PBS. We have also stained cells with calcein AM (4  $\mu\text{g}/\text{mL}$ ) for 15 seconds at 37  $^{\circ}\text{C}$ . 3D reconstructions were processed with Imaris software.

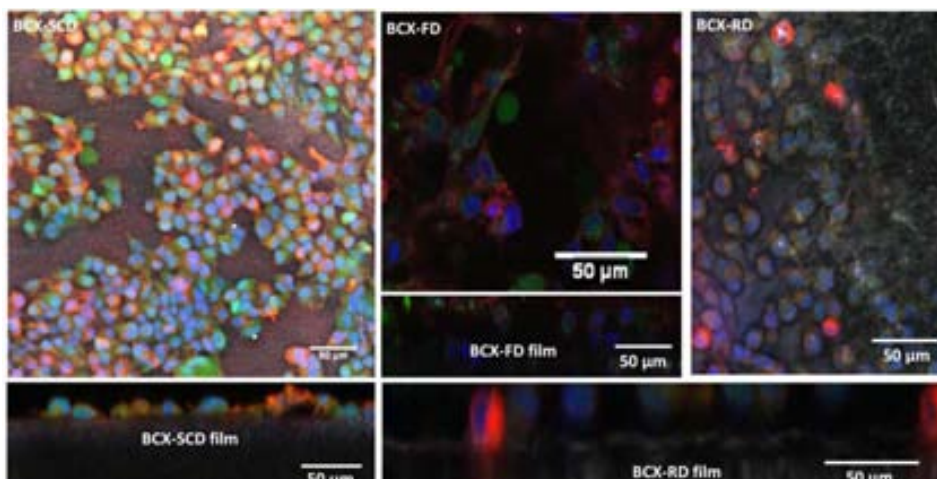


**Figure 4.10** MDA MB-231 cells were growing on the surface of BCX films (upper and lateral views of confocal microscopy). Nucleus, membranes and cytoplasm were stained with Hoechst, Cell mask and calcein AM, in blue, red and green, respectively. BCFs appear in grey by reflection.

Cell cultures growth in BCX films were analysed by confocal microscopy. In order to visualize changes in cell structure as well as the distribution through the films, cell nucleus, membranes and cytoplasm were stained with Hoechst, Cell Mask and calcein AM, respectively. From the upper views of confocal images shown in **Figure 4.10**, cells proliferated and spread in each films indicating the good cell function and viability. From the lateral views, cells were growing on the surface of BCX films but cannot migrate inside the cellulose film.

Even though our cellulose films have shown ultra-fine 3D structure with high porosity especially BCX-SCD films, which has been described in Chapter 2, cells did not migrate into the cellulose films. It is thought that the size of MDA-MB 231 cells is big, preventing to enter the cellulose pores. Therefore, HepG2 cells (smaller than MDA-MB 231 cells), were used and grown with BCX-SCD films.

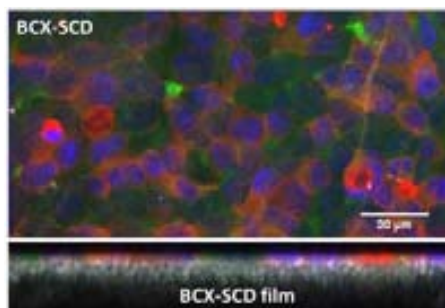


**Figure 4.11** HepG2 cells were growing on the surface of BCX films (upper and lateral views of confocal microscopy). Nucleus, membranes and cytoplasm were stained with Hoechst, Cell mask and calcein AM, in blue, red and green, respectively. BCX film appears in grey by reflection.



---

From the upper view image in *Figure 4.11*, we can observe that HepG2 cells were proliferating on the cellulose film with good distribution and cell activity. From the lateral image, however, cells could not in-growth inside the film even for those smaller cells and the highest porous BCX-SCD films. Even though both two types of cells did not migrate into the cellulose films, the comprehensive investigations of BCFs biocompatibility are very important and useful. It showed that our cellulose films are biocompatible scaffold materials which can be used in wound healing and artificial skin fields. Moreover, these 2D BCX scaffolds have tensile strength and extensibility similar to human skin, especially when hydrated with saline water prior to use.(8)

## **4.2 3D bacterial cellulose scaffold**

As I explained above, the final goal of this chapter is to use our BCF as 3D scaffolds for cell culture studies. Creating a suitable and comfortable 3D environment for cells is highly sought, since the primitive 2D system (such as petri dishes) does not reproduce the real physiology of a tissue or human for informative or useful study. In contrast, 3D scaffolds offer a more realistic representation of the micro-environment of living tissues for evaluating cell migration, which is a key step during physiological processes, such as tissue repair, inflammatory responses, embryonic development and metastasis of cancer cells(9-11). Moreover, the pore size and structure of BC network might influence the cell growth. In order to analyse the influence of the bacterial cellulose network geometry in the cells, further studies are required.

Except the reason of cell size, another reason why cells did not migrate into the cellulose films is that the nano-pores of BCX films are probably too small to allow cell migration inside the films. Here, a method to prepare 3D bacterial cellulose network scaffolds with controlled micro porosity has been developed.

### **Production of 3D bacterial cellulose scaffold**

Several research groups have tried to alter the pore size and overall porosity of BC networks. For instance, Serafica et al.(12) have used solid particles such as aluminium, iron, silica gel and glass beads, which were incorporated into the film while BC culture was incubated in a rotating disk reactor. They reported that there was no effect on the rate of BC formation. Porogen/particle-leaching techniques have been also used for scaffold fabrication. Different porogen materials have been used, including salt(13), paraffin(14, 15), ice(16), gelatin and sugar(17, 18). Normally, these porogens are placed in a mould and a polymer is cast moulding it, following a leaching step to remove the porogens from the system leaves a porous scaffold of the cast polymer.

In order to obtain porous structures for cell culture experiments and taking into account the studies previously described, a homemade method was created. Ideal porogenic particles should not contain toxic products that could

contaminate the cellulose films, light density to keep float on the culture media, and should be easy to remove after the fermentation. By using homemade wax microspheres in the growing culture of GX bacteria, 3D bacterial cellulose scaffolds with bigger pores were prepared.

### Preparation of wax microspheres

Homemade wax microspheres with sizes of 200  $\mu\text{m}$  and 0.2 cm can be produced by three steps (**Figure 4.12**). Firstly, I used a candle to get melted wax. Secondly, absorbing liquid wax with a syringe and dropping it onto ice cold water in a glass beaker, generating solid shaped beads. Finally, wax microspheres were dried and sterilized by UV radiation for 6 hours as the same condition of BCFs sterilization. The diameter of the wax microspheres can be controlled by changing the size of needle.

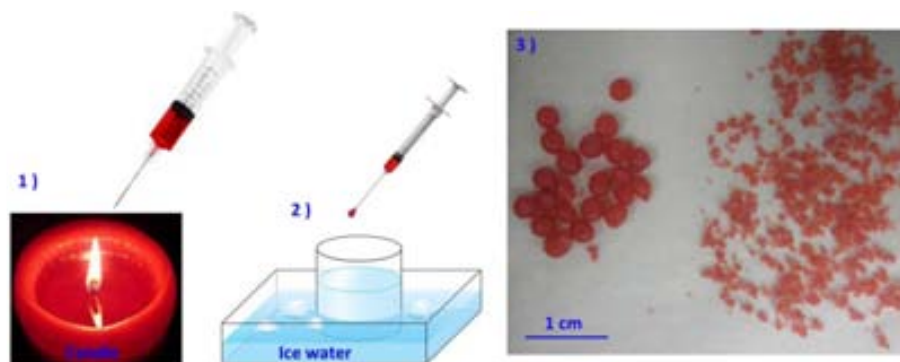


**Figure 4.12** Steps of making wax microspheres: 1) using syringe to take hot wax liquid; 2) pushing the liquid wax onto the ice cold water; 3) different sizes of wax microspheres.

As explained in Chapter 2 (production of bacterial cellulose section), 8 mL medium with re-grown GX bacteria were transferred aseptically to a glass tube of 50 mL with 12 mL liquid medium. Wax microspheres were added and floated on the surface of the liquid medium. As is shown in **Figure 4.13**, two sizes of wax beads (A:  $\sim 0.2$  cm and B:  $\sim 200$   $\mu\text{m}$ ) were used to produce cellulose films. In order to immerse the wax beads inside the medium, a PDMS layer was used (**Figure 4.13** a and b). Under such set-up, the bacteria can have both oxygen and carbon source as food (medium) for producing cellulose fibres which will be altered with wax microspheres. With this system, the pore size and the porosity of the film can be controlled by changing the sizes of the wax microspheres. Finally, the bacteria cultures were incubated in static conditions for 14 days, at 26  $^{\circ}\text{C}$ . Additionally, we also prepared one sample as a control (**Figure 4.13** I). After 2 weeks fermentation, a layer of cellulose pellicles appeared. As expected, the wax microspheres were entrapped in the bacterial cellulose films as shown in **Figure 4.13** II and III. It can be clearly seen in **Figure 4.14A**, the thickness of control sample is thinner than the one grown with the wax microspheres under the same conditions, which conforming the wax beads were wrapped by the cellulose fibres.

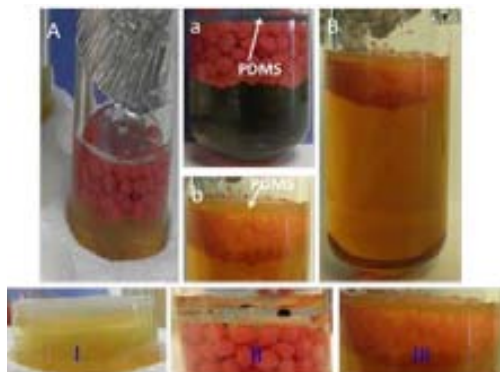


**Figure 4.13** Homemade wax microspheres (A:  $\sim 0.2$  cm diameter and B:  $\sim 200$   $\mu\text{m}$  diameter) were added and floated on the surface of the liquid medium in the glass tubes; PDMS layers were used to press the wax microsphere into the medium (a and b). After 2 weeks fermentation, wax microspheres were entrapped in the bacterial cellulose shown in II and III, labelled as BCX-B-II and BCX-B-III, respectively. I is the control sample without wax microspheres, labelled as BCX-B-I.

Keeping the same clean process, these bacterial cellulose pellicles were boiled with DI water, and treated with a 0.1 M NaOH solution to remove organic residues. After the alkali treatment, they were soaked in 97 % ethanol for at least 8 h in a 75 °C shaking water bath to completely remove the wax (**Figure 4.13**). BCX-B-II sample showed dark colour due to the contamination during the culture process. Moreover, we realized that the pores of BCX-B-II were too big for the cells. Therefore, we only targeted BCX-B-III sample for further use in cell growth. Finally, we used the supercritical CO<sub>2</sub> method (SCD) to dry the BCX-B-III samples because this method can help us to maintain the original pores. These dry samples were labelled as BCX-B-SCD.

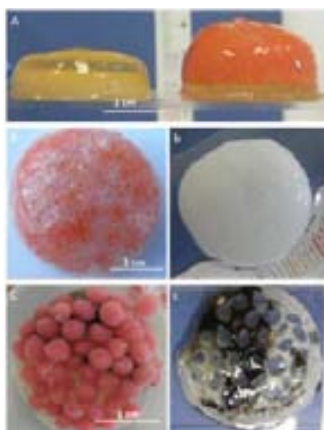


**Figure 4.14** A) pictures of BCX wet pellicles harvested from BCX-B-I and BCX-B-III sample after 2 weeks fermentation. Wax microspheres were wrapped by the cellulose fibres, showing a thicker thickness than the control sample. Images of BCX-B-III layer before (B) and after (b) the cleaning process. Images of BCX-B-II layer before (C) and after (c) the cleaning process.

---

## Characterization of 3D bacterial cellulose scaffold

The characterization of the big pores and the micro-structure of BCX-B-SCD scaffolds were performed by SEM using the same conditions as previously described in Chapter 2. **Figure 4.15** shows the morphology of BCX-B-SCD samples.

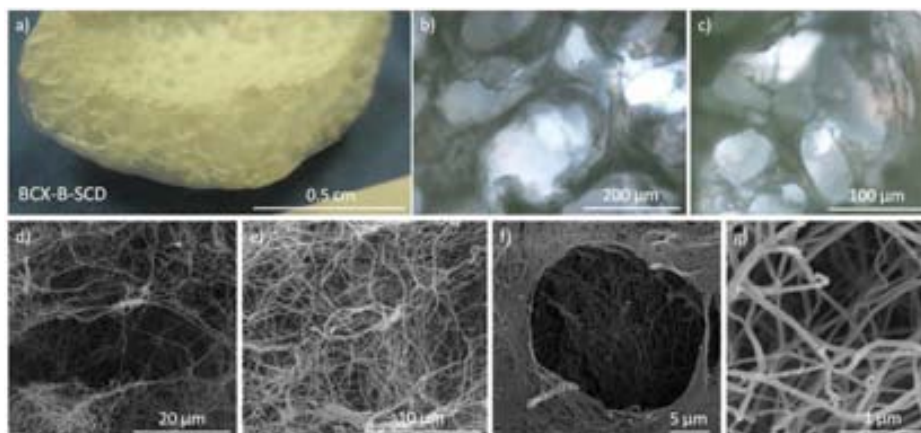


**Figure 4.15** BCX-B-SCD scaffold: a) optical image; b) and c) optical microscopy images to image the bigger pores; d, e, f and g) SEM images to image the smaller pores in different magnifications.

The main aim of this procedure was to produce a 3D cellulose scaffold in size range suitable for cell growth inside the film. As shown in **Figure 4.15**, BCX-B-SCD presents an open porous structure with ultra-fine cellulose fibres. From the optical images, big and individual macro pores were observed. The micro and nano pores were also presented by SEM. The incorporation of wax microspheres resulted in large pores and evidenced the pore interconnectivity which could allow cell presence and migration.

## 3D bacterial cellulose scaffold with cells

### Confocal microscopy

After 3 days of culturing cells in the 3D BCX-B-SCD scaffolds, they were washed twice with PBS. Cells were stained directly with 10  $\mu\text{g}/\text{mL}$  Hoechst and 5  $\mu\text{g}/\text{mL}$  Cell Mask<sup>TM</sup> for 5 and 10 min, respectively, at room temperature and washed twice with PBS. Samples were observed with a Leica SP5 confocal microscope and a Zeiss LSM 700 confocal microscope. 3D reconstructions were processed with Imaris software.

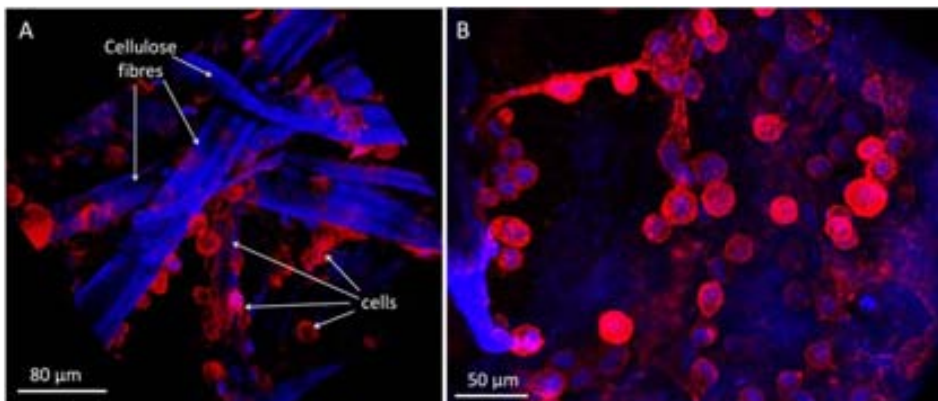


**Figure 4.16** Confocal microscopy images of MDA-MB 231 cells seeded inside the BCX-B-SCD scaffold, after 3 days of culture. Cell membranes were stained with Cell Mask (red) and nucleus with Hoechst (blue).

As is shown in **Figure 4.16**, the confocal images of BCX-B-SCD scaffold with MDA-MB 231 cells grown are presented. From these images, it is clearly seen that cells were growing across the cellulose fibres within the cellulose pores. During the staining treatment, the cellulose fibres were also dyed (blue), which are identified in **Figure 4.16A**. Thus, the blue of cell nuclei is not well seen. The difference in the two scaffolds (BCX-B-SCD as 3D and BCX-SCD as 2D) was the micro-structure introduced by the wax microspheres provided additional bigger pores for cell to enter and permitted that the cells accumulated as clusters within the pores. These BCX-B-SCD films with macro pores allowed cells to grow in a 3D environment.

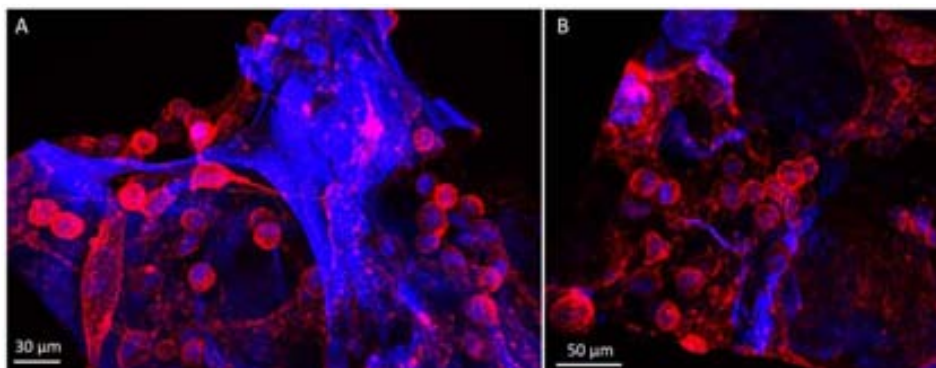


**Figure 4.17** Confocal microscopy images of MDA-MB 231 cells inside BCX-B-SCD films, after 3 days of culture. Cell membranes were stained with Cell Mask (red) and nucleus with Hoechst (blue).

Two more independent repeats demonstrated that, we were capable to produce cellulose films with big pores and grow cells inside the cellulose films. From the upper view images of the two samples in **Figure 4.17**, cells were both growing on the surface as well as inside the porous BCX-B-SCD scaffolds.

---

Furthermore, as shown in *Figure 4.17A*, cells proliferated and migrated around the cellulose fibres within the pores, from the top of BCX-B-SCD scaffold to the bottom. Especially, due to the good mechanical properties and high water absorption capacity of bacterial cellulose, the cells in the 3D cellulose films are not limited by mass transport in their access to nutrients and oxygen, or in their loss of metabolic by-product. Importantly, these BCX scaffold are easy to sterilize, very stable in cell culture medium and facile to manipulate.

---

### 4.3 Conclusions

The present chapter evaluated the potential of BCFs to function as a scaffold for cell culture *in vitro*. First of all, we have investigated the behaviour of BCFs when incubated in biological medium and cell culture medium. After 21 days incubation, all the BCFs were still stable keeping the same weight and shape as the initial dry cellulose. Especially important was the finding that BCX films were easier to manipulate than BCE films after those have been immersed in biological medium. Moreover, we also analysed these mediums after the incubation period and they were not affected by the addition of BCFs during the culture process. Secondly, we used MDA-MB 231 cells to study BCFs biocompatibility. MTT assay and live/dead fluorescence viability test were performed to calculate the cell viability and cell metabolic activity. Both assays confirmed that our cellulose films are a biocompatible material and allow the correct growth of cells. Confocal microscopy was used to check the cell distribution in BCFs. Cells only proliferated on the surface of BCFs and they did not migrate into the cellulose films; even we have tried to use another type cell line (HepG2), which are smaller than MDA-MB 231 cells.

In order to create a 3D scaffold, which provides *in vivo* like environment(19) for cell differentiation and proliferation,(20) we improved the production of porous bacterial cellulose films. 3D bacterial cellulose scaffolds with bigger pores were obtained by incorporating homemade paraffin wax microspheres into the bacterial cellulose synthesis. Using confocal microscopy, we observed that cells penetrated into these scaffolds and aggregated in clusters following the cellulose fibres. A 3D culture environment can enable higher cell density;(21) allow cell-cell contact and cell-matrix interaction.(22) Although the current study has only examined the biocompatibility and cell distribution of the 3D BCFs scaffold, the findings suggest that controllable porosity in various shapes of bacterial cellulose can be achieved, which is attractive as a future scaffold for tissue engineering.

---

## 4.4 References

1. N. Petersen, P. Gatenholm, Bacterial cellulose-based materials and medical devices: current state and perspectives, *Applied microbiology and biotechnology*, **91**, 1277, (2011).
2. R. A. Pértile, S. Moreira, R. M. Gil da Costa, A. Correia, L. Guãrdao, F. Gartner, M. Vilanova, M. Gama, Bacterial cellulose: long-term biocompatibility studies, *Journal of Biomaterials Science, Polymer Edition*, **23**, 1339, (2012).
3. M. Zaborowska, A. Bodin, H. Backdahl, J. Popp, A. Goldstein, P. Gatenholm, Microporous bacterial cellulose as a potential scaffold for bone regeneration, *Acta biomaterialia*, **6**, 2540, (2010).
4. W. K. Czaja, D. J. Young, M. Kawecki, R. M. Brown, The future prospects of microbial cellulose in biomedical applications, *Biomacromolecules*, **8**, 1, (2007).
5. R. Derda, A. Laromaine, A. Mammoto, S. K. Tang, T. Mammoto, D. E. Ingber, G. M. Whitesides, Paper-supported 3D cell culture for tissue-based bioassays, *Proceedings of the National Academy of Sciences*, **106**, 18457, (2009).
6. A. Fu, R. J. Wilson, B. R. Smith, J. Mullenix, C. Earhart, D. Akin, S. Guccione, S. X. Wang, S. S. Gambhir, Fluorescent magnetic nanoparticles for magnetically enhanced cancer imaging and targeting in living subjects, *ACS nano*, **6**, 6862, (2012).
7. M. Zeng, A. Laromaine, W. Feng, P. A. Levkin, A. Roig, Origami magnetic cellulose: controlled magnetic fraction and patterning of flexible bacterial cellulose, *Journal of Materials Chemistry C*, (2014).
8. Y. Hu, J. M. Catchmark, In vitro biodegradability and mechanical properties of bioabsorbable bacterial cellulose incorporating cellulases, *Acta biomaterialia*, **7**, 2835, (2011).
9. S. A. Erik Kupperman, Nick Osborne, Steven Waldron and Didier Y. R. Stainier, A sphingosine-1-phosphate receptor regulates cell migration during vertebrate heart development, *Nature*, **406**, 192, (2000).
10. J. Condeelis, J. E. Segall, Intravital imaging of cell movement in tumours, *Nature reviews. Cancer*, **3**, 921, (2003).
11. S. P. Palecek, J. C. Loftus, M. H. Ginsberg, D. A. Lauffenburger, A. F. Horwitz, Integrin-ligand binding properties govern cell migration speed through cell-substratum adhesiveness, *Nature*, **385**, 537, (1997).
12. G. Serafica, R. Mormino, H. Bungay, Inclusion of solid particles in bacterial cellulose, *Applied microbiology and biotechnology*, **58**, 756, (2002).
13. A. G. Mikos, A. J. Thorsen, L. A. Czerwonka, Y. Bao, R. Langer, D. N. Winslow, J. P. Vacanti, Preparation and characterization of poly (L-lactic acid) foams, *Polymer*, **35**, 1068, (1994).
14. H. Backdahl, M. Esguerra, D. Delbro, B. Risberg, P. Gatenholm, Engineering microporosity in bacterial cellulose scaffolds, *Journal of tissue engineering and regenerative medicine*, **2**, 320, (2008).
15. P. X. Ma, J.-W. Choi, Biodegradable polymer scaffolds with well-defined interconnected spherical pore network, *Tissue engineering*, **7**, 23, (2001).
16. G. Chen, T. Ushida, T. Tateishi, Development of biodegradable porous scaffolds for tissue engineering, *Materials Science and Engineering: C*, **17**, 63, (2001).



- 
17. Q. Zhou, Y. Gong, C. Gao, Microstructure and mechanical properties of poly (L - lactide) scaffolds fabricated by gelatin particle leaching method, *Journal of Applied Polymer Science*, **98**, 1373, (2005).
  18. J. Capes, H. Ando, R. Cameron, Fabrication of polymeric scaffolds with a controlled distribution of pores, *Journal of Materials Science: Materials in Medicine*, **16**, 1069, (2005).
  19. C. Provin, K. Takano, T. Yoshida, Y. Sakai, T. Fujii, R. Shirakashi, Low O<sub>2</sub> metabolism of HepG2 cells cultured at high density in a 3D microstructured scaffold, *Biomedical microdevices*, **11**, 485, (2009).
  20. G. H. Heppner, F. R. Miller, The cellular basis of tumor progression, *International review of cytology*, **177**, 1, (1997).
  21. J. Vukasinovic, D. K. Cullen, M. C. LaPlaca, A. Glezer, A microperfused incubator for tissue mimetic 3D cultures, *Biomedical microdevices*, **11**, 1155, (2009).
  22. J. El-Ali, P. K. Sorger, K. F. Jensen, Cells on chips, *Nature*, **442**, 403, (2006).



# Chapter 5

## Conclusions and Future work

	Pag.
5.1 General conclusion	118
5.2 Prospective of future work	121

---

## 5.1 General conclusions

The main objectives of the PhD thesis presented were the following:

- 1) Synthesis and characterization of bacterial cellulose films.
- 2) Coating of the bacterial cellulose films with nanoparticles to fabricate functional bacterial cellulose nanocomposites.
- 3) Evaluating the biocompatibility of bacterial cellulose films prior to their use as 2D and 3D cellular scaffolds.

### 1) Synthesis and characterization of bacterial cellulose films

A lab set-up for producing bacterial cellulose from two strains of bacteria (*Gluconacetobacter Xylinum* and *Gluconacetobacter E uropeaus*) was put in place. Bacterial cellulose pellicles were harvested from the air/liquid interfaces of culture medium. To get pure bacterial cellulose, they were cleaned by two steps: boiling with distilled water and treating with alkali media.

The wet cellulose films were dried by three different methods: room temperature drying, freeze drying and supercritical drying. The as-obtained materials were investigated by an array of characterization techniques. Fourier transform infrared spectroscopy was used to check the chemical structure and purity of the different series. Their crystallinity and polymorphs were evaluated by the measurement of X-ray diffraction. The open porous structure, the individual cellulose fibres and the films thickness could be observed by scanning electron microscopy. Their density and porosity was also calculated. Moreover, their mechanical properties were comprehensively investigated by nanoindentation. The differences of their water absorption capacity, transparency and stability were also carefully compared and analysed. Even after 10 days of culturing, BCE films are lighter, independently of the drying method, than BCX films harvested after 5 days. GX strain affords BC films with higher crystallinity (up to 91 %) suggesting that the biosynthesis of the cellulose fibrils for the two strains could have some differences. The use of supercritical drying slightly increases the crystallinity of the BC films for both strains.

We conclude that the properties of the cellulose produced from *Gluconacetobacter Europeaus* strain are only slightly dependent on the selection of the drying method. From this strain, when supercritical dried, we obtained mechanically robust and extremely light (0.05 g/mL) films with up to 96 % of porosity, and with a water absorption capacity up to 110 times their dried weight. *Gluconacetobacter Xylinum* offered denser films, which were more sensitive to the drying method with density values almost four times larger for RD films (0.59 g/mL) than for the SCD one (0.16 g/mL). In that

---

series, BCX films dried by supercritical method presented the most open structure and a higher porosity (90 %) and crystallinity (96 %). Moreover, the used drying methods allowed to obtain broader range of mechanical properties for BCX films.

The load-displacement curves obtained by nanoindentation are representative of materials with elastoplastic properties. The young modulus values are around 200 MPa, except for BCX-RD and BCX-FD that have ~600MPa. After water absorption capacity measurement, all BC films improved their optical transmittance. BCE films are more transparent than BCX films; therefore BCE films could be used in applications where visualization through the film is necessary. BCE-SCD shows the highest water absorbance capacity that allows us to suggest BCE films as a suitable candidate for applications such as absorbents, removal of contaminants or wound healing dressings.

BC films from GX source offer a more versatile platform since we can control the porosity, mechanical properties and water absorption capacity by only selecting the appropriate drying method. These films could be good candidates to interface with tissues since their mechanical properties could be tailored to mimic the final tissue replacement and their mechanical properties are not hampered in aqueous medium.

## **2) Coating of bacterial cellulose films with nanoparticles to fabricate functional bacterial cellulose nanocomposites**

Superparamagnetic Fe<sub>2</sub>O<sub>3</sub> and Au nanoparticles were successfully synthesized by one-step microwave-assisted thermal decomposition method. The nanoparticles were crystalline with a narrow particle size distribution. Functional bacterial cellulose nanocomposites (BCF-NPs) including (BCF-SPIONs and BCF-Au) were prepared using the same microwave method without the need of any post-synthetic treatment. Such method allowed us the fabrication of homogeneous and conformal coating of the bacterial cellulose films with nanoparticles, even when the films were folded into complex origami shapes. The load of nanoparticles could be tuned by the drying method used to obtain the cellulose as well as by the initial precursor concentration, although in this case to a lesser extent. A mechanism of particle nucleation and growth has been proposed based on the selective heating of the cellulose hydroxyl groups and their accessibility, which depends on the drying method to nucleate the particles under the microwave heating.

BCF-SPIONs composites were thoroughly characterized including their microstructure, magnetic properties, nanoparticles loading and anchoring stability, water absorption capacity, and mechanical properties. All the films react easily to an external magnetic field, present superparamagnetic behaviour at room temperature, and are flexible enough to bend them, even those with the

---

largest magnetic fraction (up to 40 %). Interestingly, the films with the lowest magnetic fraction are also transparent.

We further showed preliminary results in a strategy to selectively pattern the bacterial cellulose films with iron oxide nanoparticles. This approach is based on the prior hydrophobization of selected zones of the films.

Finally, an initial proof of concept that composites with two types of nanoparticles could also be fabricated has been described.

### **3) Evaluating the biocompatibility of bacterial cellulose films prior to their use as 2D and 3D cellular scaffolds**

The evaluation of the performance of bacterial cellulose films incubated in biological medium and cell culture medium was carefully assessed. After 21 days incubation with three different mediums, all the films were stable without presenting degradation. Moreover, the mediums were not affected by the addition of cellulose films during the process. In this case, bacterial cellulose films from *Gluconacetobacter Xylinum* (BCX films) were more stable and stiffer than *Gluconacetobacter Europeaus* films (BCE films), thus easy to manipulate, which is suitable for cell culture studies as a scaffold material.

Biocompatibility of BCX films was investigated with MDA-MB 231 cell line. Firstly, MTT assay was carried out to check the cytotoxicity of cellulose films in two cases. In the first case, cells grew with the cellulose films immersed in the culture medium, and in the second one with cells spotted and cultured on the surface of the cellulose film as a 2D scaffold. In both cases, cells proliferated and showed the same morphological shape without large differences of cell growth and cell behaviour. All BCX films showed high cell viability, their cell metabolic activities were also analysed.

In order to provide 3D *in vivo* like environment for cell culture studies, we improved the production of bacterial cellulose films with large pore size structures. 3D bacterial cellulose scaffolds with micro pores were obtained by incorporating homemade paraffin wax microspheres into cellulose synthesis medium. These cellulose films were cleaned by three steps: boiling with distilled water, treating with alkali media and shaking them with hot ethanol. The wax microspheres were completely removed after the cleaning process. In order to maintain the big pores, wet cellulose films were dried by supercritical drying method and monitored by SEM characterization. Finally, cells were spotted on these 3D scaffolds. Performing confocal microscopy, we were able to observe that cells penetrated into the 3D bacterial cellulose scaffolds and showed good distribution within the cellulose fibres and the pores. With three independent experiments, we were successful and able to repeat the production of 3D bacterial cellulose scaffolds and grow cells inside the films.

---

## 5.2 Prospective for future work

Regarding prospective for future work the results presented in this thesis allow us for further research in two directions. First, concerning the functional bacterial cellulose nanocomposites, we expect that this fast and facile microwave-assisted method could be extended as a general model to synthesis uniform bacterial cellulose nanocomposites. It is worth expanding different nanoparticles coating with cellulose films, which promise in a great number of applications. Moreover, the size and morphology of nanoparticles could also be controlled by modifying the microwave conditions.

Secondly, regarding the investigations of bacterial cellulose scaffolds biocompatibility; this work shows that 3D bacterial cellulose is a promising biomaterial for tissue engineering applications. However, the cell-cell and cell-cellulose film interaction still needs further research. Tissue engineering is a strategy to create new tissue substitutes, which promote the regeneration of new tissue. It is necessary that these substitutes or scaffolds are not only biocompatible but also biodegradable. Therefore the biodegradability investigation of our bacterial cellulose scaffolds is also required. Furthermore, due to the hydroxy groups and high water absorption capacity of bacterial cellulose, the incorporation of drugs into scaffolds could open many doors in the future of medical applications.





# Chapter 6

	Pag.
Curriculum vitae of the author	124
List of publications	127

# Curriculum Vitae

## Personal information:

Name: Muling

Surname: Zeng

Date of birth: 10/12/1986



## Academic records:

Degree of B. Sc. in Chemistry with grade honour at “Yunnan University”, China

Date: Sep. 2004 to Jul. 2008

Degree: M. Sc. in Inorganic Chemistry at “Yunnan University”, China.

Date: Sep. 2008 to Jul. 2011

## Languages:

Chinese: mother tongue

English: fluent spoken, fluent written

Spanish: fluent spoken, basic written

## Current position:

PhD candidate in Material Science at the Institute of Materials Science of Barcelona (ICMAB-CSIC) [www.icmab.es](http://www.icmab.es), Nanoparticles and Nanocomposites group [www.icmab.es/nn](http://www.icmab.es/nn).

Supervisors: Dr. Anna Roig and Dr. Anna Laromaine (ICMAB-CSIC)

Title of the Thesis: “Bacterial cellulose: fabrication, characterization and biocompatibility studies”

## Awards and honours:

- 2008-2009 First Prize Scholarship of Yunnan University, China (Top 1%)  
First Prize of Excellent Graduate Scholarship of Yunnan University  
Outstanding Student Cadre Scholarship of Yunnan University  
Outstanding Student Cadre of Yunnan University
- 2009-2011 First Prize Scholarship of Yunnan University, China (Top 1%)  
First Prize of Excellent Graduate Scholarship of Yunnan University  
Outstanding Student Cadre Scholarship of Yunnan University  
Outstanding Student Cadre of Yunnan University  
“Wu Dagan” Scholarship of Yunnan University  
Excellent All-round Student of Yunnan University  
Merit Student of Yunnan Province (Only 10 each year)

2011-2014 Scholarship from Chinese Scholarship Council (CSC) 3 years  
CEICS- Southern Catalonia Nobel Campus- Spain 2012  
(Only 100 young researchers have been selected all over Europe.)  
Science program of TV3- Spain <http://blogs.tv3.cat/quequicom>

#### List of publications:

1. **M. Zeng**, A. Laromaine\*, W. Feng, P. A. Levkin, A. Roig\* Origami magnetic cellulose: controlled magnetic fraction and patterning of flexible bacterial cellulose, *Journal of Materials Chemistry C* (2014), DOI: 10.1039/c4tc00787e
2. **M. Zeng**, A. Laromaine\*, A. Roig\* Bacterial Cellulose Films: Influence of bacterial strain and drying route on film properties, submitted
3. C. García-González, E. Carenza, **M. Zeng**, A. Roig\* Design of biocompatible magnetic pectin aerogel monoliths and microspheres, *RSC Advances* 2 (2012) 9816–9823 DOI: 10.1039/C2RA21500D
4. Y. Ma, **M. Zeng**, J. He, L. Duan, J. Wang, J. Wang\* Synthesis, characterizations of cobalt doped mesoporous alumina prepared using natural rubber latex as template and its catalytic oxidation of tetralin to tetralone, *Applied Catalysis A: General* 396 (2011) 123–128
5. J. Yan, H. Tao, **M. Zeng**, J. Tao, S. Zhang, Z. Yan, W. Wang, J. Wang\* PVP-Capped Silver Nanoparticles as Catalyst for Oxidative Coupling of Thiols to Disulfides *Chinese. J. Catal.*, 30 (2009) 856-858
6. J. Wang, **M. Zeng**, N. Xu, J. Wang\* The effect of transition metal ions on morphology of actadecyl silane polymerized by bismuth sulfide, *Journal of Molecular Catalysis*, 21(2007) 325-330
7. Systematic study of several cell lines response to 2D and 3D growth environment in bacterial cellulose scaffold, in preparation
8. The effect of templates on the morphology of CuS and their catalytic polymerization of alkylsilanes, in preparation

#### Patent:

1. J. Wang\*, J. Yan, J. He, **M. Zeng** Developed synthesis method of polysiloxane by using silver bismuth sulfide nanocomposite as catalyst (Application No. 200910218225.3) China

#### Technical knowledge:

- Self-use: Dynamic Light Scattering (DLS), Spectrophotometry (UV-vis, FTIR), Scanning Electron Microscopy (SEM), Optical Microscopy, Nanoindenter XP, Microwave Oven, Contact Angle Measurement, Supercritical fluid autoclave and Freeze-drying equipment.
- Transmission electron microscopy (TEM), Thermo gravimetric analysis (TGA), Superconducting quantum interference device (SQUID), X-ray Diffraction (XRD).

- Synthesis of inorganic nanoparticles (iron oxide magnetic nanoparticles and gold nanoparticles) by microwave-assisted method
- Experience in bacteria culture, production and characterization of bacterial cellulose films; basic cell culture experiment

### Conferences:

1. XVII International Sol-Gel Conference, 25-30<sup>th</sup> August 2013, (Madrid-Spain).  
Contributed 1 **poster**: M. Zeng, A. Laromaine\*, A. Roig\*  
Title: Tailoring Bacterial cellulose films properties using different drying method
2. Chunhui Science Conference, 26<sup>th</sup> June to 2<sup>nd</sup> July 2013, (Dalian- China)
3. 1<sup>st</sup> Scientific Meeting of ICMA-B-ICN-CIN2 students, 13-14<sup>th</sup> May 2013, (Barcelona- Spain)  
Contributed 1 **oral**  
Title: Preparation and characterization of Bacterial Cellulose Films
4. Southern Catalonia Nobel Campus CEICS, 1<sup>st</sup>-4<sup>th</sup> July 2012, (Tarragona-Spain)  
Contributed 1 **oral** and 1 **poster**: M. Zeng, A. Laromaine\*, A. Roig\*  
Title: 3D porous scaffolds platforms to evaluate nanoparticles and cells
5. Jornades Doctorals- 2012 (The 2<sup>nd</sup> Jornades Doctorals on Chemistry), 6-8<sup>th</sup> June 2012, (Barcelona- Spain)

### Workshops:

6. Material Characterization Techniques for XRD and XRF, 19<sup>th</sup> May 2014, (Barcelona- Spain)
7. nanoLCA 2013- Health and Environmental Impact of Nano-Enabled Products Along Their Life Cycle, 6<sup>th</sup> May 2013, (Terrasa- Spain)
8. International Magnifyco Workshop, 20- 22<sup>th</sup> February 2013, (Barcelona-Spain)  
Contributed 1 **poster**: M. Zeng, A. Laromaine\*, A. Roig\*  
Title: Characterization of Bacterial Cellulose Films
9. Rethinking Nano Workshop, 8<sup>th</sup> November 2012, (Barcelona- Spain)  
Contributed 1 **poster**: M. Zeng, A. Laromaine\*, A. Roig\*  
Title: 3D Bacterial Cellulose Bio-films
10. First Workshop on Nano-medicine, 5<sup>th</sup> June 2012, (Barcelona- Spain)